"ROLE OF MAGNETIC RESONANCE SPECTROSCOPY IN THE EVALUATION OF INTRACRANIAL SPACE OCCUPYING LESIONS DIAGNOSED BY CONVENTIONAL MAGNETIC RESONANCE IMAGING"

By

Dr. KEERTHI. M

DISSERTATION SUBMITTED TO SRI DEVARAJ URS ACADEMY OF HIGHER EDUCATION AND RESEARCH, KOLAR, KARNATAKA

In partial fulfilment of the requirements for the degree of

DOCTOR OF MEDICINE

IN

RADIODIAGNOSIS

Under the Guidance of

Dr. AHANTHEM NABAKUMAR SINGH, M.D., D.M.R.D.
ASSOCIATE PROFESSOR, RADIO-DIAGNOSIS

DEPARTMENT OF RADIODIAGNOSIS,

SRI DEVARAJ URS MEDICAL COLLEGE,

TAMAKA, KOLAR – 563 101.

MAY 2018

SRI DEVARAJ URS ACADEMY OF HIGHER EDUCATION AND RESEARCH, TAMAKA, KOLAR, KARNATAKA

DECLARATION BY THE CANDIDATE

I hereby declare that this dissertation entitled **"ROLE OF MAGNETIC RESONANCE SPECTROSCOPY IN THE EVALUATION OF INTRACRANIAL SPACE OCCUPYING LESIONS DIAGNOSED BY CONVENTIONAL MAGNETIC RESONANCE IMAGING"** is a bonafide and genuine research work carried out by me under the guidance of **Dr. AHANTHEM NABAKUMAR SINGH** , Associate Professor, Department of Radiodiagnosis, Sri Devaraj Urs Medical College, Kolar, in partial fulfilment of University regulation for the award "**M.D. DEGREE IN RADIODIAGNOSIS**", the examination to be held in May 2018 by SDUAHER. This has not been submitted by me previously for the award of any degree or diploma from the university or any other university.

Dr. KEERTHI M
Postgraduate in Radiodiagnosis,
Sri Devaraj Urs Medical College,
Tamaka, Kolar.

Date:

Place: Kolar.

SRI DEVARAJ URS ACADEMY OF HIGHER EDUCATION AND RESEARCH, TAMAKA, KOLAR, KARNATAKA

CERTIFICATE BY THE GUIDE

This is to certify that the dissertation entitled **"ROLE OF MAGNETIC RESONANCE SPECTROSCOPY IN THE EVALUATION OF INTRACRANIAL SPACE OCCUPYING LESIONS DIAGNOSED BY CONVENTIONAL MAGNETIC RESONANCE IMAGING"** is a bonafide research work done by **Dr. KEERTHI M,** under my direct guidance and supervision at Sri Devaraj Urs Medical College, Kolar**,** in partial fulfilment of the requirement for the degree of "**M.D. IN RADIODIAGNOSIS"**.

Dr. AHANTHEM NABAKUMAR SINGH
Associate Professor,
Department Of Radiodiagnosis,
Sri Devaraj Urs Medical College,
Tamaka, Kolar.

Date:

Place: Kolar.

SRI DEVARAJ URS ACADEMY OF HIGHER EDUCATION AND RESEARCH TAMAKA, KOLAR, KARNATAKA

CERTIFICATE BY THE HEAD OF DEPARTMENT

This is to certify that the dissertation entitled "**ROLE OF MAGNETIC RESONANCE SPECTROSCOPY IN THE EVALUATION OF INTRACRANIAL SPACE OCCUPYING LESIONS DIAGNOSED BY CONVENTIONAL MAGNETIC RESONANCE IMAGING"** is a bonafide research work done by **Dr. KEERTHI M,** under direct guidance and supervision of **Dr. N. RACHEGOWDA**, Professor & H.O.D, Department of Radiodiagnosis at Sri Devaraj Urs Medical College, Kolar**,** in partial fulfilment of the requirement for the degree of "**M.D. IN RADIODIAGNOSIS"**.

Dr. N. RACHE GOWDA, M.D., D.M.R.D.
Professor & HOD
Department of Radiodiagnosis
Sri Devaraj Urs Medical College,
Tamaka, Kolar.

Date:

Place: Kolar.

SRI DEVARAJ URS ACADEMY OF HIGHER EDUCATION AND RESEARCH TAMAKA, KOLAR, KARNATAKA

ENDORSEMENT BY THE HEAD OF THE DEPARTMENT AND PRINCIPAL

This is to certify that the dissertation entitled **"ROLE OF MAGNETIC RESONANCE SPECTROSCOPY IN THE EVALUATION OF INTRACRANIAL SPACE OCCUPYING LESIONS DIAGNOSED BY CONVENTIONAL MAGNETIC RESONANCE IMAGING"** is a bonafide research work done by **Dr. KEERTHI M** under the direct guidance and supervision of **Dr. N. RACHEGOWDA,** H.O.D & Professor, Department of Radiodiagnosis, Sri Devaraj Urs Medical College, Kolar, in partial fulfilment of University regulation for the award "**M.D. DEGREE IN RADIODIAGNOSIS**"**.**

Dr. N. RACHE GOWDA,
Professor & HOD
Department Of Radiodiagnosis,
Sri Devaraj Urs Medical College,
Tamaka, Kolar.

Date:
Place: Kolar.

Dr. M. L. HARENDRA KUMAR,
Principal,
Sri Devaraj Urs Medical College,
Tamaka, Kolar.

Date:
Place: Kolar.

SRI DEVARAJ URS ACADEMY OF HIGHER EDUCATION

AND RESEARCH, TAMAKA, KOLAR, KARNATAKA

ETHICAL COMMITTEE CERTIFICATE

This is to certify that the Ethical committee of Sri Devaraj Urs Medical College, Tamaka, Kolar has unanimously approved

Dr. KEERTHI M

Post-Graduate student in the subject of

RADIODIAGNOSIS at Sri Devaraj Urs Medical College, Kolar

to take up the Dissertation work entitled

"ROLE OF MAGNETIC RESONANCE SPECTROSCOPY IN THE EVALUATION OF INTRACRANIAL SPACE OCCUPYING LESIONS DIAGNOSED BY CONVENTIONAL MAGNETIC RESONANCE IMAGING"

to be submitted to the

SRI DEVARAJ URS ACADEMY OF HIGHER EDUCATION

AND RESEARCH, TAMAKA, KOLAR, KARNATAKA,

Member Secretary,

Sri Devaraj Urs Medical College,

Kolar – 563 101.

SRI DEVARAJ URS ACADEMY OF HIGHER EDUCATION AND RESEARCH, TAMAKA, KOLAR, KARNATAKA

COPY RIGHT

Dr. KEERTHI M

Date:

Place: Kolar.

ACKNOWLEDGEMENT

I owe my debt and gratitude to my parents ***Shri. V MUNIYAPPA*** *and* ***Smt. JAYALAKSHMI N,*** *along with my beloved brother* ***KIRAN****, sister-in-law* ***YASHASWINI*** *and niece* ***AADYA*** *for their moral support and constant encouragement during the course of the study.*

With humble gratitude and great respect, I would like to thank my teacher, mentor and guide, ***Dr. AHANTHEM NABAKUMAR SINGH,*** *Associate Professor, Department of Radiodiagnosis, Sri Devaraj Urs Medical College and Research Institute, Kolar, for his able guidance and constant encouragement which went a long way in moulding and enabling me to complete this work successfully.*

I have great pleasure in expressing my deep sense of gratitude to ***Dr. N. RACHE GOWDA,*** *HOD & Professor, Department of Radiodiagnosis, Sri Devaraj Urs Medical College and Research Institute, Kolar. Without his initiative and constant encouragement this study would not have been possible.*

I would like to express my sincere thanks to ***Dr. PATTABHIRAMAN V.,*** *Professor, Department of Radiodiagnosis, Sri Devaraj Urs Medical College for his valuable support, guidance and encouragement throughout the study.*

*I would like to thank **Dr. SHIVAPRASAD G SAVAGAVE,** Assistant professor, Department of Radiodiagnosis, Sri Devaraj Urs Medical College and Research Institute, Kolar, for his constant guidance, immense help, valuable advices and encouragement during the study period.*

*I also would like to thank **Dr. NAVEEN G. NAIK, Dr. VINAY K. K** and **Dr. KUKU MARIAM SURESH**, former Assistant professors and all my teachers of Department of Radio diagnosis, Sri Devaraj Urs Medical College, Kolar for their support.*

I am extremely grateful to the patients and their families who volunteered to this study, without them this study would just be a dream.

*I am thankful to my fellow **postgraduates, especially Dr. Ramya, Dr. Ravindra, Dr.Rahul Deep G** and **Dr.Gowthami** with all other **postgraduates** for having rendered all their co-operation and help to me during my study.*

I would also like to thank my friends especially Dr. Ritesh, Dr. Deepthi, Dr. Vyshali, Dr.Jishnu and Dr. Vikas, for their constant encouragement.

*I am also thankful to **Mr. Ravi, Mr. Mateen** and **Mr. Srinivas** with other **technicians** of Department of Radio diagnosis, R.L Jalappa Hospital & Research Centre, Tamaka, Kolar for their help.*

*My sincere thanks to **Mrs. Veena, Mrs. Naseeba,** and **Mrs. Shobha,** along with rest of the computer operators.*

*I am also thankful to staff nurses **Mrs. Radha, Mrs. Saraswati,** helper **Mrs. Munivekatamma** and other **technicians** of Department of Radiodiagnosis, R.L Jalappa Hospital & Research Centre, Tamaka, Kolar for their help.*

*Last but not least I would be failing in my duty if I do not express my gratefulness to the **Almighty,** who helped me to successfully complete this study.*

Dr. KEERTHI M

LIST OF ABBREVIATIONS

↑	Hyperintense
↓	Hypointense
↔	Isointense
↕	Heterogenous
®	Right
Ш	Midline
A	Absent
ABS	Abscess
AC	Arachnoid cyst
Ala:	Alanine
APA	Aggressive pituitary adenoma
BEN	Benign
BLP	Broad Lipid Peak
BV	Blurring of vision
C	Carbon
CHESS	Chemical shift selective water suppression
Cho	Choline
CP	Craniopharyngioma
CPC	Choroid Plexus Carcinoma
Cr	Creatine
CSI	Chemical shift imaging
CSF	Cerebrospinal fluid

DVA	Developmental venous anomaly
DWI	Diffusion weighted image
E	Elevated
EA	Extra-axial
EC	Epidermoid cyst
F	Female
FDA	Food and Drug Administration
FDG	2-[fluorine-18]fluoro-deoxy-d-glucose
FLAIR	Fluid attenuated inversion recovery
GABA	Gamma amino butyric acid
GBM	Glioblastoma multiforme
Gd	Gadolinium
GJT	Glomus jugulare tumor
GLI	Glioma
Glx	Glutamate-Glutamine complex
GR	Granulomatous lesion
GRE	Gradient echo
GTCS	Generalised tonic clonic seizures
H	Hydrogen proton
HG	High grade glioma
Homo	Homogeneous enhancement
IA	Intra-axial
ICSOL	Intracranial space occupying lesion
K/c/o	Known case of

L	Left
Lac	Lactate
LG	Low grade glioma
Lip	Lipid
M	Male
MaE	Markedly elevated
MaR	Markedly reduced
ME	Mildly elevated
MEN	Meningioma
MET	Metastases
MI	Myo-inositol
MoE	Moderately elevated
MR	Mildly reduced
MRI	Magnetic resonance imaging
MRS	Magnetic resonance spectroscopy
N	No
Ñ	Normal
N/A	Not Applicable
Na	Sodium
NAA	N- acetyl aspartate
NAAG	N-acetyl-aspartyl glutamate
NCC	Neurocysticercosis
OVS	Outer-volume suppression
P	Phosphorus

PCA	Pilocytic astrocytoma
PIN	Pineoblastoma
PM	Pitutary macroadenoma
ppm	parts per million
PRESS	Pointed resolved spectroscopy
R	Reduced
RN	Radiation necrosis
RT	Radiotherapy
SCH	Schwannoma
SE	Subependymoma
STEAM	Stimulated echo acquisition mode
Suc	Succinate
SVS	Single voxel spectroscopy
T1 WI	T1 weighted image
T2WI	T2 weighted image
TB	Tuberculosis/ tuberculoma
TE	Time of Echo
VAPOR	Variable Pulse power and Optimized Relaxation
WET	Water suppression Enhanced Through T1 effects
Y	Yes

ABSTRACT

Background:

Magnetic resonance imaging (MRI) has revolutionized detection and characterization of ICSOL. Magnetic resonance spectroscopy (MRS) allows non invasive measurement of metabolic and biochemical processes occurring in the brain lesion and helps to narrow down the diagnosis.

Aims and objectives:

To determine if MRS findings are contributory to conventional MRI diagnosis of ICSOL. To correlate imaging diagnosis with histopathology or response to treatment or cerebrospinal fluid (CSF) analysis results, as applicable

Materials and Methods:

This study was carried out on 52 patients at department of Radio-Diagnosis, R. L. Jalappa Hospital and Research Centre, Tamaka, Kolar from January 2016 to June 2017, over a period of 18 months. Informed consent was taken from individuals for their willingness to participate in the study. Patients with space occupying lesions detected in routine MRI Brain study were included. Patients who had lesions close to the skull base or calvarium where it may not be technically feasible to acquire MRS data and patients in whom MR is contraindicated were excluded.

Results:

In this study out of 52 cases, 43 were intra-axial lesions and 9 were extraaxial. Majority of the lesions were to be infective in nature (n=26, 50%). followed by malignant (n=13) and benign (n=13) lesions constituting 25% each. MRS helped in arriving at a definitive diagnosis in 40 patients (76.9%), narrowed the diagnosis in seven patients (13.4%) and was not contributory in five patients (9.6%).

Conclusion:

MRS can be employed in evaluation of ICSOL in addition to helping in arriving at correct diagnosis, it may also help in ruling out potentially severe lesions such as metastasis and high-grade tumours, thus guiding appropriate treatment and management.

TABLE OF CONTENTS

Serial No.	TOPIC	Page No.
1	INTRODUCTION	1
2	AIMS AND OBJECTIVES	3
3	REVIEW OF LITERATURE	4
4	MATERIALS AND METHODS	59
5	RESULTS	63
6	DISCUSSION	88
7	CONCLUSION	100
8	SUMMARY	101
9	BIBLIOGRAPHY	103
10	ANNEXURES	115

LIST OF TABLES

Table No.	TABLES	Page No.
1	Normal brain metabolites	37
2	H-MRS changes in tumor characteristics and differential diagnosis	51
3	Contribution of MRS in final diagnosis of ICSOL	73

LIST OF FIGURES

Figure No.	FIGURES	Page No.
1	Embryological development of brain	5
2	Structures of cranial fossa	7
3	Image illustrating lobes of brain	8
4	Cerebral ventricular system	12
5	Vascular supply of brain at the level of basal ganglia and above	15
6	Vascular supply of brain at the level of basal ganglia and below	16
7	Vascular supply of brain at the level of temporal lobes, mid and hindbrain.	17
8	H-MRS signal after Fourier transformation to separate signal from different frequencies.	22
9	Normal spectra. Y axis corresponds to amplitude and X axis to the metabolites frequency	24
10	SVS. The intersection of the orthogonal planes, given by slice selection and phase gradients, results in the VOI	25
11	(a) PRESS and (b) STEAM MRS processing sequences.	26
12	Proton MRS from normal brain tissue using (A) long echo time (TE = 135 ms) PRESS and (B) short echo time (TE = 30 ms) STEAM techniques.	27
13	Use of OVS to minimize unwanted signal from outside the brain.	29
14	Water signal suppressing with CHESS. Spectrum before CHESS (a) and after CHESS (b).	31
15	Normal single voxel MR spectrum.	37
16	MRS for treatment monitoring Pre-treatment (A) and post-treatment	57
17	Age and gender distribution	63
18	Symptoms associated with ICSOL.	64
19	Location of ICSOL	65
20	Distribution of cases.	66
21	Side involvement of lesions.	67

Figure No.	FIGURES	Page No.
22	Location of lesions.	68
23	Distribution of lesions per patient.	69
24	Nature of lesions.	69
25	Demonstrating various metabolite activity in ICSOL	71
26	Usefulness of MRS in evaluation of ICSOL	73
27	Contribution of MRS in final diagnosis	74
28	(A) T2 axial (B) T1 FS post contrast, shows ring enhancing rounded cystic lesion in parieto-occipital region with perilesional edema (C) On MRS, there is acetate peak suggestive of pyogenic abscess.	78
29	(A) T2 axial (B) FLAIR axial images showing heterogeneously hyperintense mass lesion in right parieto-occipital region (C) On MRS, there is reduced NAA, increased Cho and Cho/creat ratio>2.3, suggestive of high grade glioma	79
30	(A) FLAIR sagittal (B) T1 postcontrast FS axial, shows subcentimetric ring enhancing lesion in left high parietal region and (C) MRS demonstrates mildly reduced Cho, absent lipid peak and Cho/creat ≤ 1, suggestive of neurocysticercosis	80
31	(A) T2WI axial (B) T1 FS post contrast axial sections show heterogeneously enhancing T2 hyperintense intraventricular mass lesion (C) MRS demonstrating decreased NAA, increased choline, Cho/creat >2.3, suggestive of high grade neoplasm.	81
32	(A) T2WI axial (B) FLAIR axial (C) T1FS post contrast shows a ring enhancing lesion in right periventricular occipital white matter region with T2 hypointense signal intensity (D) MRS demonstrating reduced NAA, and large lipid/lactate peak and Cho/creat > 1, suggesting a tuberculoma.	82
33	(A) T2WI axial (B) T1FS post contrast demonstrating heterogeneously enhancing T2 hyperintense lesion involving left parieto-occipital region. (C) MRS shows reduced NAA with predominant choline peak suggesting a recurrent lesion.	83

Figure No.	FIGURES	Page No.
34	(A) FLAIR axial (B) T1FS post contrast axial sections showing mild peripherally enhancing hypointense lesion in right frontal region with mild perilesional edema (C) MRS demonstrating normal NAA and Cho/creat ratios within the lesion and in perilesional edema, suggestive of radiation necrosis.	84
35	(A) T2 Axial (B) T1 FS post contrast sagittal images showing a large extra-axial homogenously enhancing mass lesion in midline frontal region (C) MRS shows reduced NAA and Alanine peak, suggestive of meningioma	85
36	(A) FLAIR axial (B) T2 coronal image showing revealed relatively hyperintense sellar SOL with supra-sellar extension (C) MRS shows predominant peak of Cho, reduced NAA and broad Lip peak, suggestive of craniopharyngioma	86
37	(A) FLAIR axial (B) T2WI coronal showing a hypointense mass lesion in high right fronto-parietal region with perilesional edema (C) mildly reduced NAA, lipid peak with Cho/creat=1.3, suggesting tubercular etiology.	87

INTRODUCTION

The term "intracranial space occupying lesions" (ICSOL) is defined as any neoplasm, benign or malignant, primary or secondary as well as any inflammatory or infective mass lying within the cranial cavity[1]**.** ICSOL constitute a wide range of differential diagnoses ranging from infections, vascular abnormalities, and benign & malignant neoplasms. Clinical history in patients with ICSOL may not be confirmatory in determining appropriate differential diagnoses. Imaging studies play a crucial role in localizing the lesion and arriving at provisional diagnosis[2].

Magnetic resonance imaging (MRI) has revolutionized detection and characterization of ICSOL. The detection rate of most types of brain lesions by MRI exceeds 90%, compared to 77% for computed tomography (CT)[3]. Added advantages of MRI are true multiplanar imaging capability, superior soft tissue characterization, and minimal distortion of images obtained by overlying bony structures without risk of ionizing radiation. However, conventional MRI does not provide functional or metabolic information, which may be helpful in narrowing the differential diagnosis. Magnetic resonance spectroscopy (MRS) allows non-invasive measurement of metabolic and biochemical processes occurring in the brain lesion and helps to narrow down the diagnosis[4].

In India, there is an increasing trend in incidence rates of brain tumors in both the sexes[5]. The purpose of this study is to evaluate the contribution of MRS to conventional MRI in diagnosing ICSOL in our patient population.

AIMS AND OBJECTIVES

The objectives of the study are as follows:

1. To determine if MRS findings are contributory to conventional MRI diagnosis of ICSOL.
2. To correlate imaging diagnosis with histopathology or response to treatment or cerebrospinal fluid (CSF) analysis results, as applicable.

REVIEW OF LITERATURE

EMBRYOLOGY

The central nervous system (CNS) appears at the beginning of the 3rd week as a slipper-shaped plate of thickened ectoderm, the neural plate. This plate is located in front of the primitive pit, in the mid-dorsal region. Soon its lateral edges become elevated to form the neural folds (Figure 1).These neural folds become more elevated, approach each other in the midline, and finally fuse, thus forming the neural tube[6]. By the fourth week of gestation, three vesicular dilatations develop at the rostral portion of the neural tube, thereby defining the forebrain (prosencephalon), midbrain (mesencephalon) & hindbrain (rhombencephalon). By the fifth week of gestation, the developing forebrain has divided into a cephalic telencephalon and a caudal diencephalon. The developing hindbrain has subdivided into a cephalic etencephalon and a caudal myelencephalon. The metencephalon later becomes the pons and cerebellum while the myelencephalon forms the medulla oblongata. Bilateral diverticula from the telencephalic end of the neural tube form the cerebral hemispheres. These hemispheres undergo complex expansion and folding with formation of permanent primitive fissures by the fourth month. Three major flexures, the midbrain, pontine and cervical flexures divide the developing brain into the cerebrum, cerebellum and spinal cord[7].

Early in development the cerebral hemispheres are smooth – surfaced (lissencephalic) and a germinal matrix of primitive cells surrounds each lateral ventricle. Cells from the germinal matrix proliferate, migrate outward to the cortex in an “inside out” sequence, and mature as neural and glial cells. The germinal matrix

forms at about 7 weeks gestational age and involutes at about 28 to 30 weeks, although it persists in the form of focal cell clusters upto weeks 36 through 39. During the sixth and seventh fetal months, the cerebral surfaces convolute to form primitive gyri and sulci. Thus, the adult pattern can already be recognized towards the end of gestation. Concomitant with cortical development is the formation of fiber tracts, including the commissures between the two cerebral hemispheres[7].

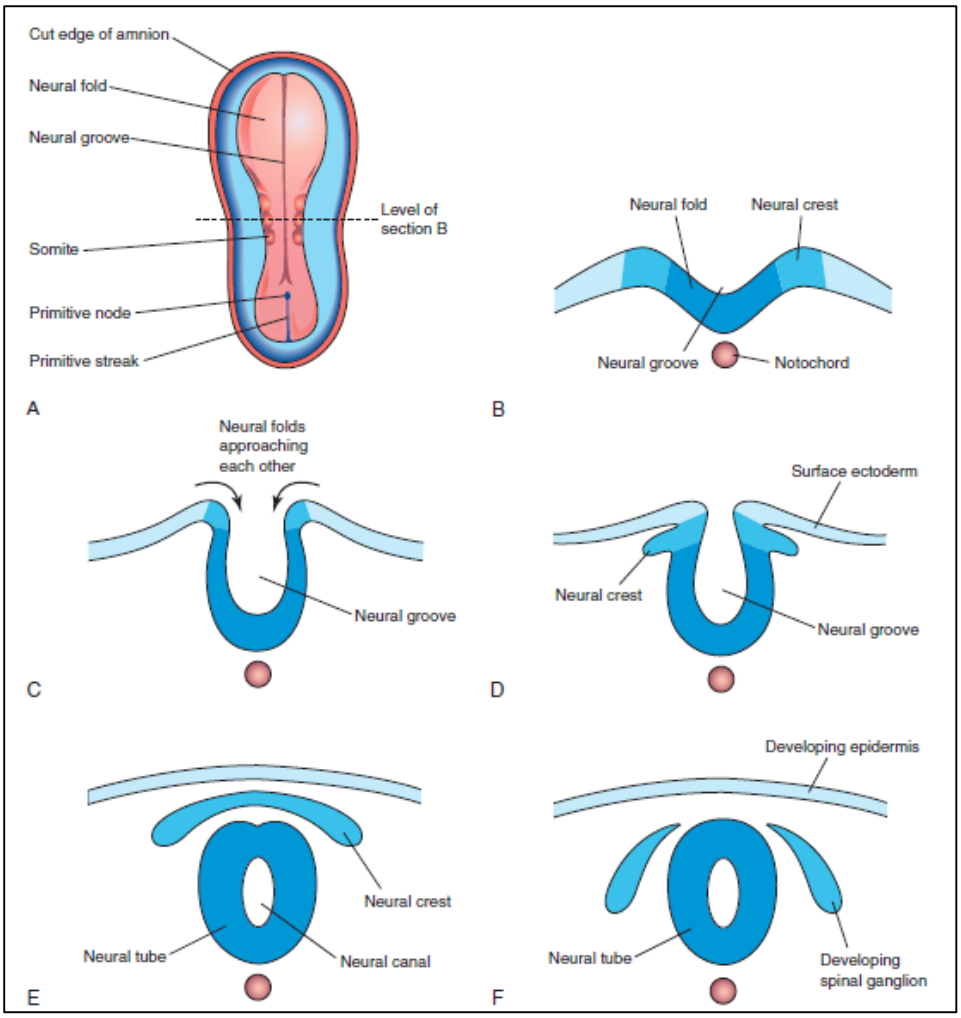

Figure 1. Embryological development of brain

ANATOMY

Anatomical Overview

The brain is supported by the skull base and enclosed within the skull vault. The cranial cavity is divided into the anterior, middle and posterior fossae (Figure 2). The anterior and middle cranial fossae contain the two cerebral hemispheres. The posterior fossa contains the brainstem, consisting of the midbrain, pons and, most inferiorly, the medulla, and the cerebellum[8].

Twelve paired cranial nerves arise from the brainstem, exit the skull base through a number of foramina, and innervate a variety of structures in the head proper. The largest of these foramina is the foramen magnum, through which the brainstem and spinal cord are in continuity[8].

The brain is invested by the meninges and bathed in cerebrospinal fluid (CSF), circulating in the subarachnoid space. Part of the meninges, the dura, forms an incomplete partition between the cerebral hemispheres, known as the falx and roofs the posterior fossa as the tentorium cerebelli. There is a gap in the tentorium, called the hiatus, through which the midbrain joins the hemispheres. Within the brain are a number of cavities, the lateral, third and fourth cerebral ventricles, which contain CSF produced by the choroid plexuses within the ventricles. CSF flows from the ventricles into the subarachnoid spaces over the cerebral surface and around the spinal cord.

Blood reaches the brain by the carotid and vertebral arteries and is drained by cerebral veins into a series of sinuses within the dura into the internal jugular veins[9].

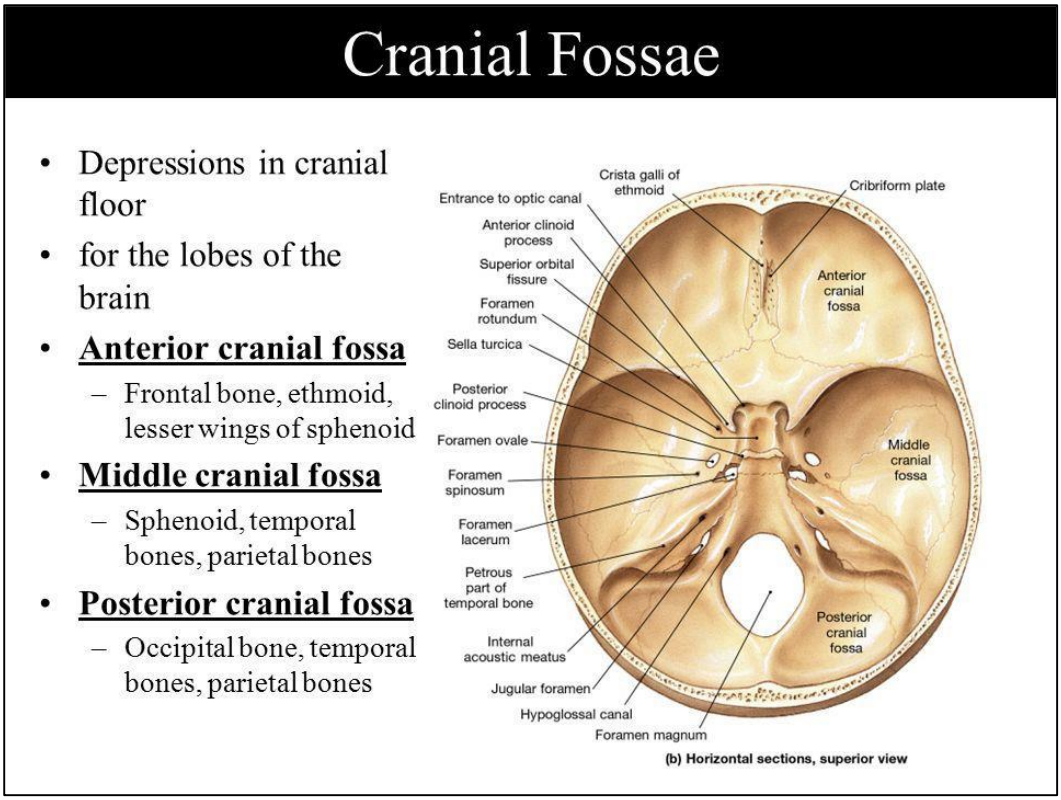

Figure 2: Structures of cranial fossa

The cerebral hemispheres

The cerebral hemispheres lie above the tentorium and are divided by fissures and sulci into frontal, parietal, temporal, and occipital lobes (Figure 3). The limbic system is also considered to be a lobe. The hemispheres are linked by the corpus callosum, the largest of the commissural tracts, which interconnect paired structures across the midline. Other examples of commissural tracts are the anterior, posterior, and habenular commissures. The anterior and posterior commissures are landmarks used in image-guided neurosurgical procedure[9].

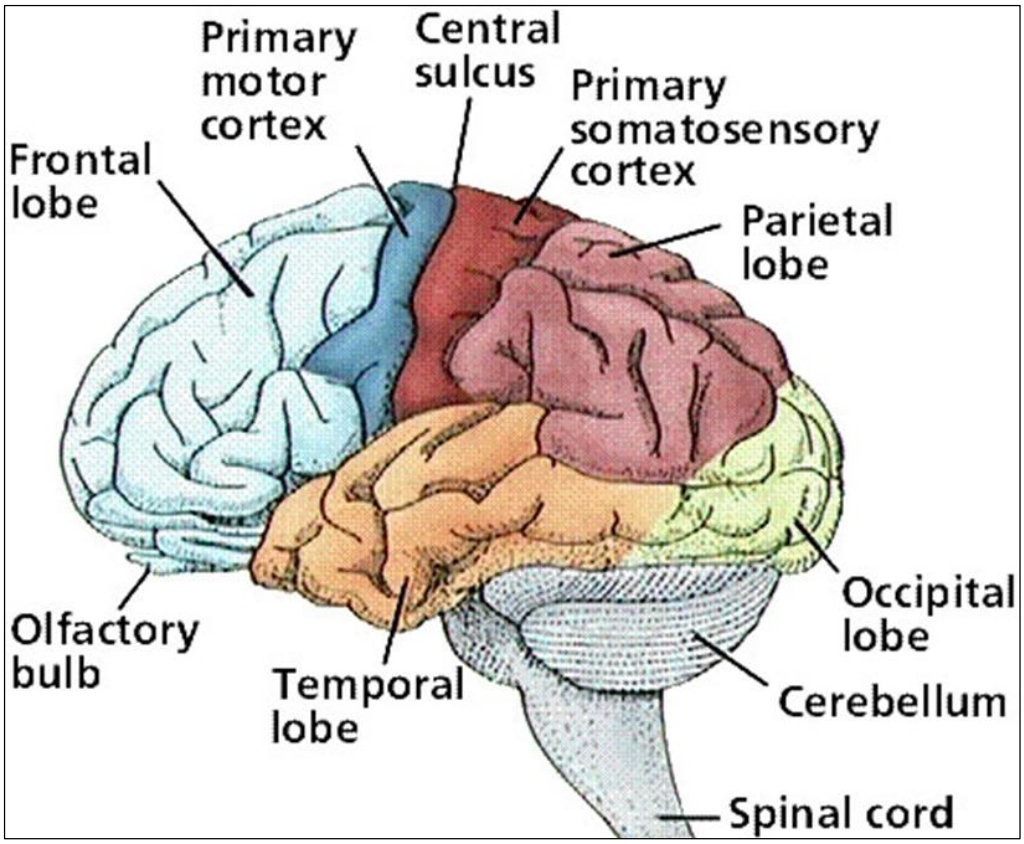

Figure 3: Image illustrating lobes of brain

The corpus callosum is a myelinated tract and appears curved in sagittal images. The anterior rostrum blends with the anterior commissure inferiorly. The curved genu (knee) leads posteriorly to the body hence the largest and most posterior part, the splenium. Fibers from the corpus callosum sweep anteriorly into the frontal white matter as the forceps minor and posteriorly into the occipital white matter as the forceps major.There is considerable individual variation in gyral anatomy. It is also important to appreciate that the relationship of function to structure may be variable and that speech, for example, may be represented over a number of gyri with intervening white matter. Equally, it may be difficult to identify the central sulcus and adjacent motor strip accurately[9].

The anatomical boundaries of the individual lobes may be indistinct, depending on the aspect. The frontal lobe is the largest of the anatomical lobes occupying the anterior cranial fossa and extending posteriorly to the central sulcus. In common with the temporal lobe, the frontal lobe has three major gyri, superior, middle, and inferior, which are oriented horizontally. The temporal lobe occupies the middle cranial fossa The anterior limit of the parietal lobe is the central sulcus, which, running in the coronal plane, separates the precentral (motor) gyrus of the frontal lobe from the postcentral (sensory) gyrus. The boundary between the parietal and temporal lobes laterally is indistinct but the parieto-occipital incisure medially defines the two lobes. The main cortical supply of the occipital lobe relates to vision[9].

The calcarine (visual) cortex can be seen to indent the posterior (occipital) horns of the lateral ventricles. The cortex here is deeply enfolded with little intervening white matter. Inferiorly and laterally, the temporo-occipital fissure marks the division between the two lobes[9].

The Sylvian or lateral fissure separates the superior surface of the temporal lobe from the inferior frontal lobe and the anterior parietal lobe. During development, the cortex overlying the basal ganglia is invaginated to form the insula. The cortex in front of, above, and below this depression expands to form covering folds termed the operculum. The Sylvian fissure is formed between these folds. On axial imaging it runs in the coronal plane on the lower cuts and in the sagittal plane on the higher slices. On coronal MRI, it resembles the shape of a T lying on its side[9].

The cerebellum

The cerebellum consists of two hemispheres joined by a central vermis. The cortical mantle of the cerebellum overlies the white matter core as in the cerebral hemispheres but the cerebellar cortical ridges, known as the folia, and the intervening sulci are approximately parallel to one another and are linked to the brainstem by the paired cerebellar peduncles. They are named logically. The inferior cerebellar peduncles join the medulla to cerebellum; the middle cerebellar peduncles (the largest), pons to cerebellum; the superior cerebellar peduncles, midbrain to cerebellum[8].

The brainstem

The brainstem consists of medulla, pons, and midbrain. The medulla, pons, and cerebellum together constitute the hindbrain.

The medulla commences at the foramen magnum as a continuation of the spinal cord. Initially it is “closed,” possessing a central canal like the spinal cord. More superiorly, it becomes “open” as the central canal leads into the fourth ventricle[9].

In the brainstem, the motor tracts are generally anterior to the sensory, hence the clinical usage of “anterior” columns meaning motor and “posterior” column, sensory. A number of decussations occur within the brainstem where both motor and sensory fibers cross the midline in accordance with the general principle that functional control of one-half of the body is largely exercised by the contralateral cerebral hemisphere. The sensory decussation is cranial to the motor, but both occur in the closed portion of the medulla. The medulla leads superiorly into the pons, which has an anterior “belly” and a posterior tegmentum[9].

The midbrain has two cerebral peduncles transmitting the motor tracts. Its posterior portion is pierced by the cerebral aqueduct (of Sylvius), to connect the third and fourth cerebral ventricles. The posterior portion is known as the tectum or tectal plate. It consists of four colliculi or quadrigeminal bodies concerned with auditory and visual reflexes.

The cerebral ventricular system cerebrospinal fluid spaces

The cerebral ventricular system consists of the paired lateral and single third and fourth ventricles. Cerebrospinal fluid (CSF) is produced in the choroid plexuses, and most of it is in the lateral ventricles, entering medially through the choroidal fissures. It flows from the lateral ventricles to the third ventricle through the foramen of Monro, in the anterior portion of the roof of the third and from the third to fourth via the cerebral aqueduct of the midbrain. From the fourth ventricle, the CSF enters the subarachnoid spaces, leaving through the paired foramina of Luschka, laterally and the midline, single foramen of Magendie (Figure-4). These foramina provide a potential route of spread for intraventricular tumors[9].

At the base of the brain, there are relatively large CSF spaces, the basal CSF cisterns, which are important both anatomically and in CT or MRI diagnosis. Although named individually, according to adjacent structures, they interconnect freely with each other and with the CSF spaces generally[9].

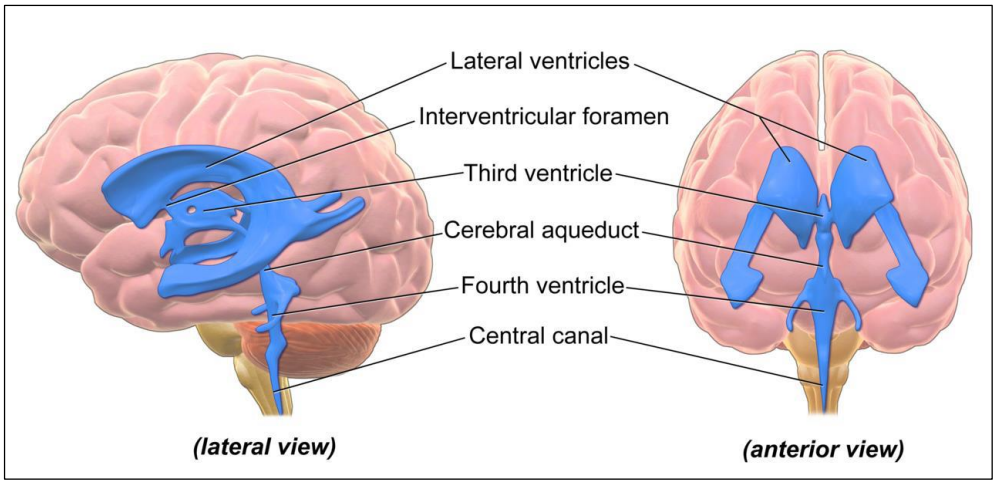

Figure 4: Cerebral ventricular system

The cerebral blood circulation

Cerebral arteries

The brain is supplied with oxygenated blood by the paired internal carotid and vertebral arteries. The common carotid artery in the neck divides at the approximate level of the upper border of the thyroid cartilage (C4) into its internal and external branches, the latter supplying the various craniofacial structures[8]. The internal carotid artery is the larger of the two branches, receiving 70% of the common carotid blood flow. It lies posterolateral to the external carotid near to the bifurcation and, neither common nor internal carotid arteries have cervical branches. The internal carotid artery enters the skull through the carotid canal, courses anteromedially and horizontally (the petrous segment) before turning superiorly into the cavernous sinus (Figure 5,6,7). In this position, the artery forms the shape of a siphon. Emerging from the cavernous sinus, the artery enters the subarachnoid space and divides into its terminal branches, the anterior and middle cerebral arteries[9].

The circle of Willis is situated in the suprasellar cistern and links the internal carotid arteries with each other and with the vertebrobasilar system, via the single anterior and paired posterior communicating arteries. It affords some protection in the event of occlusion of major arteries by facilitating “cross-flow.” Arising from the proximal anterior and middle cerebral arteries, a leash of small, perforating arteries (the lenticulostriates) supplies a variety of structures including the basal ganglia and internal capsule[9].

The vertebral arteries are the first branches of the subclavian arteries. They ascend vertically within the foramina transversaria of the 6th to the 2nd cervical vertebrae and posterolaterally through the foramen transversarium of the atlas, (first cervical vertebra). The arteries then travel superomedially to pass into the skull through the foramen magnum, piercing the dura and entering the subarachnoid space. At the level of the pontomedullary junction, the two arteries join to form the midline basilar artery, which runs anterior to the brainstem. The posterior inferior cerebellar arteries, arising from the vertebral arteries just before the confluence, and the anterior inferior- and superior cerebellar arteries, arising from the basilar artery, supply the cerebellum[9].

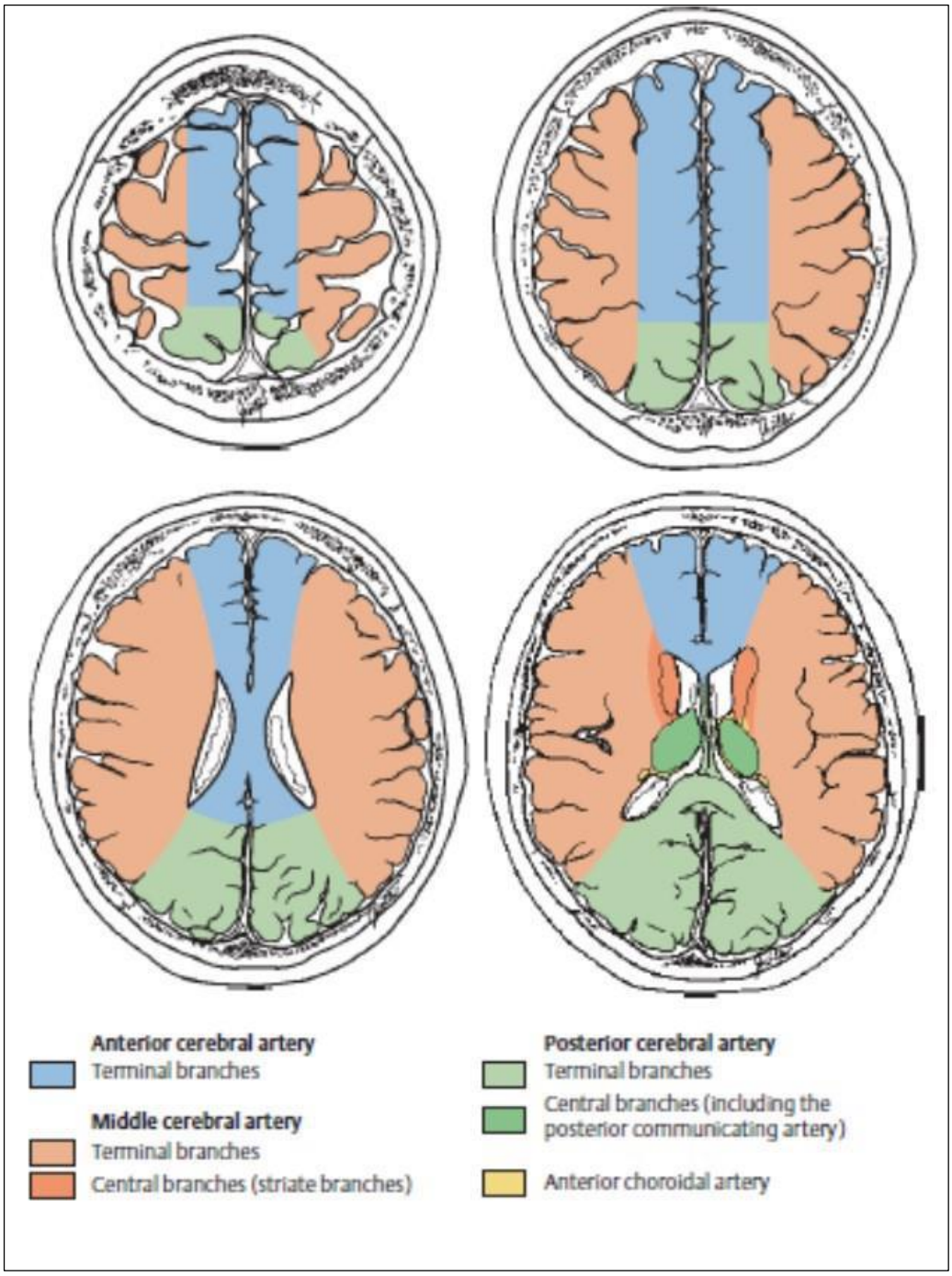

Figure 5: Vascular supply of brain at the level of basal ganglia and above

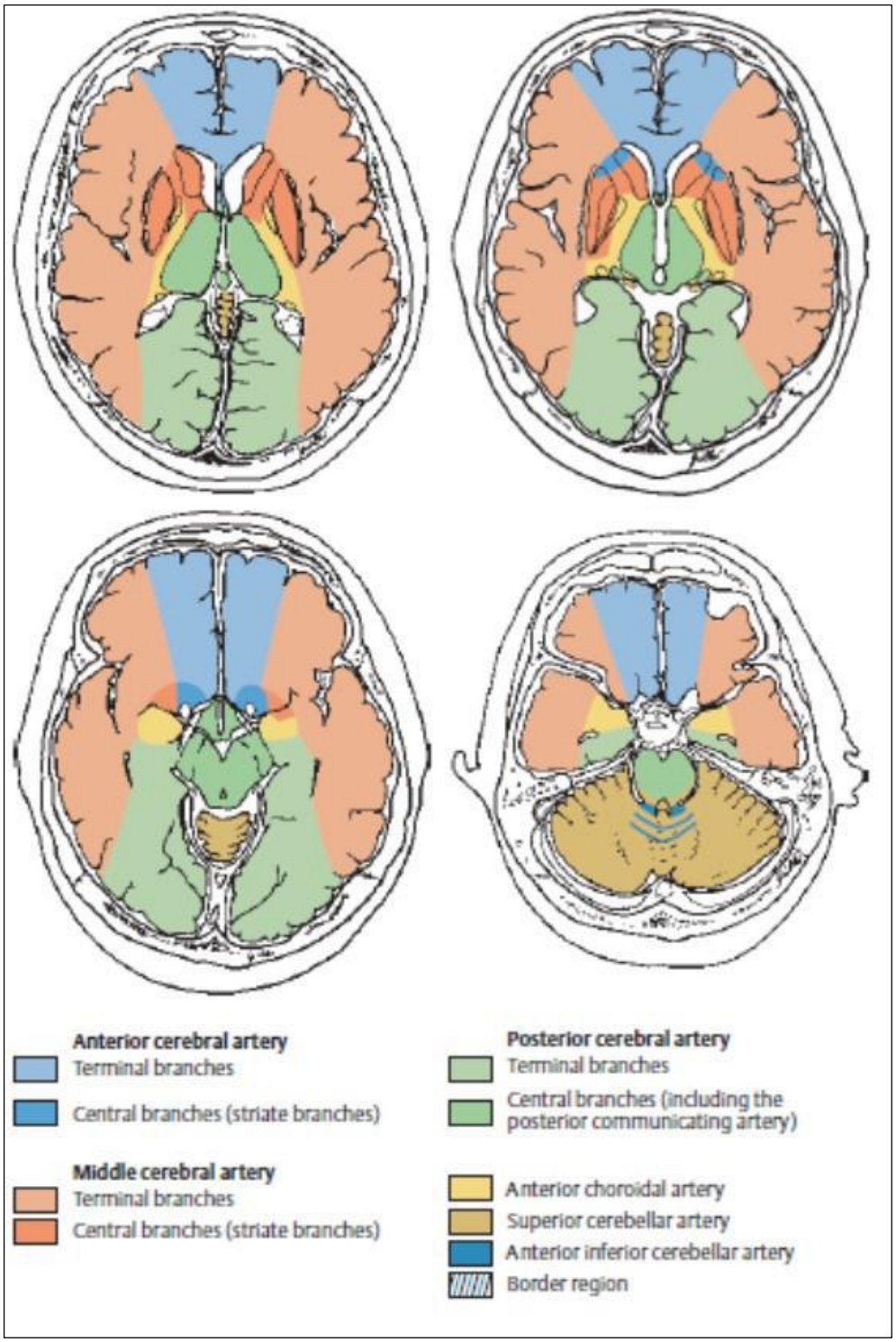

Figure 6 : Vascular supply of brain at the level of basal ganglia and below

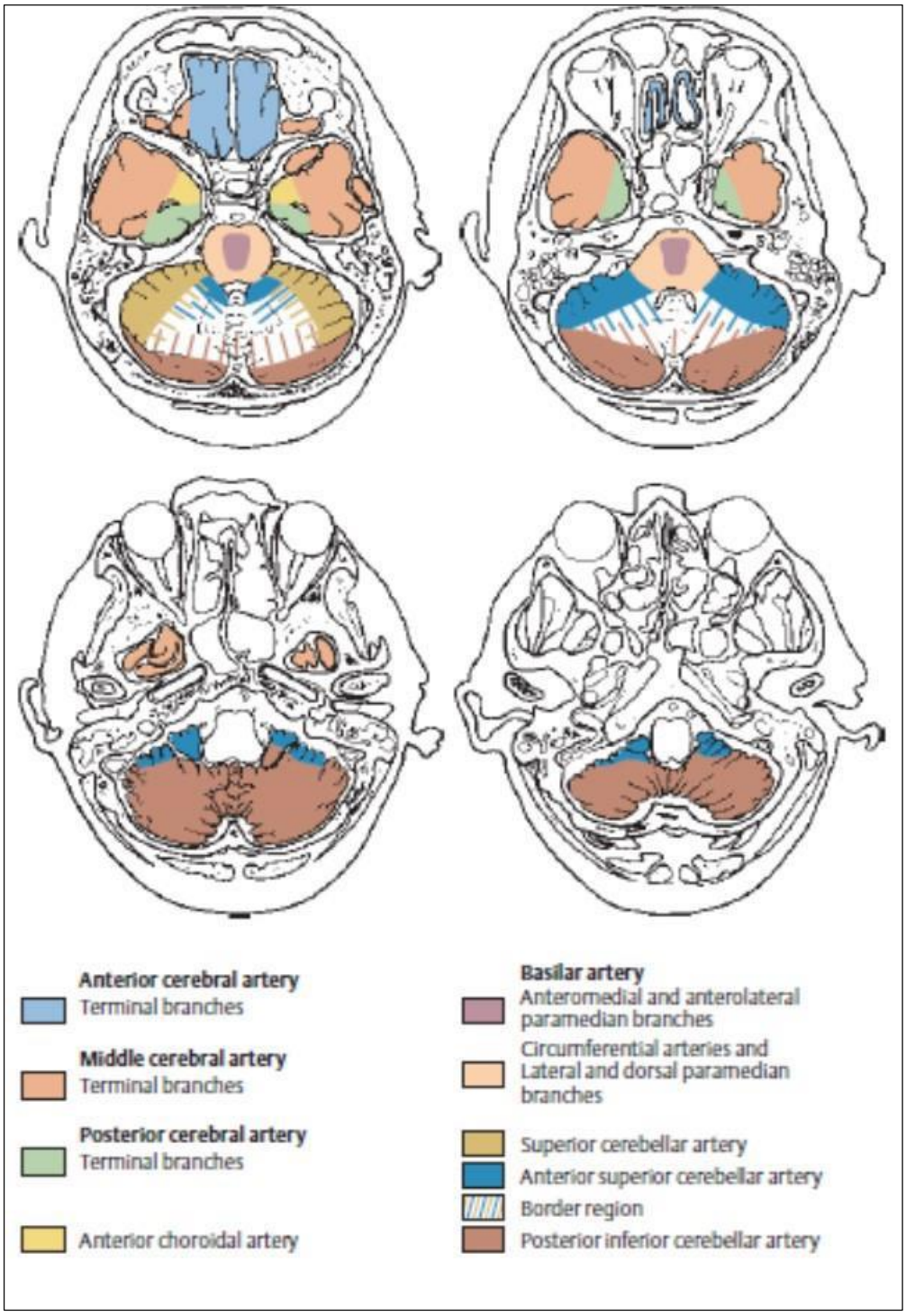

Figure 7 : Vascular supply of brain at the level of temporal lobes, mid and hindbrain.

HISTORICAL BACKGROUND

HISTORY OF MRI

The clinical field of magnetic resonance imaging (MRI) is comparatively new, yet its history spans more than a century and is renowned for several Nobel Prizes and key innovations in science and technology. The study of MRI launched in 1882 with a major breakthrough in Physics: namely, the discovery of the Rotating Magnetic Field by Nikola Tesla. In his honor, the "Tesla" became the international unit of magnetic flux density, which calibrates the strength of the magnetic field used in all MRI systems. The research and development of nuclear magnetic resonance spectroscopy by Felix Bloch of Stanford University and Edward Purcell of Harvard laid the foundation for nuclear magnetic resonance (NMR). Raymond Damadian of the State University of New York discovered a difference in relaxation times between normal and abnormal tissue (e.g., cancer). Paul Lauterbur utilized magnetic field gradients to produce the first nuclear magnetic resonance images. Meanwhile Peter Mansfield was working on improving the calculation used to process images in order to improve quality. Mansfield was successful and in 1978 presented the first cross-section images of both a finger and the abdomen[10].

Richard Ernst discovered a new reconstruction method for imaging. Ernst found that by altering the magnetic field, one could produce phase and frequency encoding, which continues to be the image reconstruction standard used today. In 2003 the Nobel Prize in Medicine or Physiology was shared by Lauterbur and Mansfield for their work.

The final step towards advancing the clinical use of MRI was to build a magnet scanner, which was accomplished in 1977 and approved for clinical use by the FDA (Food and Drug Administration) in 1984. In addition, gadolinium, an MRI contrast agent, was patented and approved by the FDA four years later. Clinical MRI is a rather young field that has yielded extraordinary achievements, most of which occurred in the United States[11].

The advent of CT and, more importantly, MR imaging revolutionized brain imaging. Brain and its surrounding structures could now be noninvasively visualized in detail. This has resulted in more rapid, more specific diagnosis, therapy, and improved outcomes. MRI provides excellent soft-tissue contrast[12].

MAGNETIC RESONANCE SPECTROSCOPY

Introduction

Magnetic resonance spectroscopy (MRS) is a means of noninvasive physiological imaging of the brain that measures absolute and relative levels of various brain tissue metabolites. MRS and MRI differ only in the manner in which the data are processed and presented. In MRI, the data is collected in the time domain of free induction decay [FID] signal to obtain information about the nuclear relaxation time namely T1 and T2, which is processed to generate an anatomic image. In MRS, time domain information is converted to frequency domain information via Fourier transformation of the FID time domain signal[13].

MRS receives a sum of individual metabolite signal amplitudes versus time in response to radiofrequency (RF) excitation similar to MR imaging. MRS presents the individual information as metabolite peak amplitude versus frequency, where frequency can be expressed in absolute values of hertz or relative units of parts per million. Its relative amount and chemical structure determine the amplitude and frequency of a particular metabolite peak. The phenomenon of chemical shift forms the basis of the MR spectroscopy. The relative resonance frequency position of each peak on the plot is dependent on the chemical environment of that nucleus and determines subtle chemical shifts in their absolute (Hz) or relative (ppm) resonance frequencies. An advantage of the ppm scale is that it allows relative chemical shifts to be expressed independently of the main magnetic field strength that is used[13].

In 1995, Food and Drug Administration (FDA) approved the use of fully automated MR spectroscopic sequences for clinical use in neuroradiology[13].

Physical Basis of MRS

Many nuclei such as phosphorus (31P), fluorine (19F), carbon (13C) and sodium (23Na) can be used to obtain MRS. Hydrogen protons (H1) are commonly used for MRS due to their natural abundance in organic tissues and high nuclear magnetic sensitivity compared with other magnetic nuclei.

The magnetic resonance frequency of an atomic nucleus is altered by its chemical environment, which causes a small change in the resonance frequency called chemical shift. Chemical shift is caused by the magnetic fields generated by circulating electrons surrounding the nuclei and shielding it from the main external magnetic field. The extent of this chemical shift depends on the number and type of adjacent atoms and molecular structures[14].

Fourier transformation converts information into the frequency domain; that is, a plot of signal intensity at each different possible resonance frequency (Figure 8). The horizontal axis is the chemical shift in ppm compared with a reference standard. The traditional reference standard, set as chemical shift of zero ppm, is a chemical compound called tetramethylsiline.

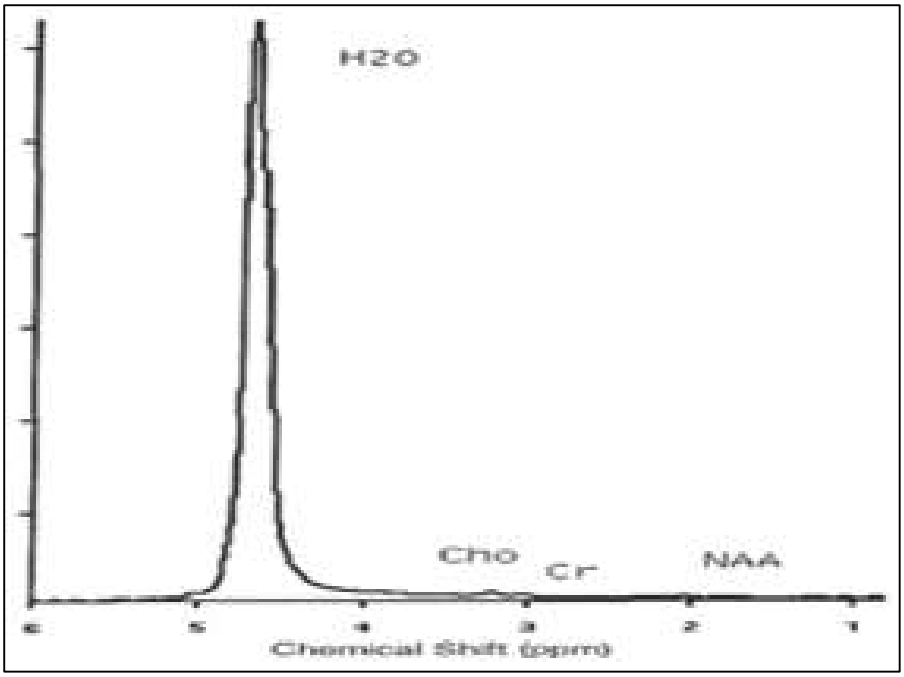

Figure 8: H-MRS signal after Fourier transformation to separate signal from different frequencies. X axis is parts per million (ppm) chemical shift, Y axis is signal intensity.

The vertical axis plots the signal amplitude at each possible resonance frequency. Parameters that characterize each peak include: resonance frequency, height, and width at half height. The baseline is composed of noise and non-resolvable metabolites. A homogenous magnetic field is required. Shimming the field in the region of interest obtains quality magnetic resonance spectra. After shimming, the water peak width at half the maximum intensity should ideally be less than 0.2 ppm[15].

The main objective of MRS is to detect weak signals from metabolites. Thus a higher strength field is required (1.5T or more) to produce higher signal-to-noise ratio (SNR), better resolution and shorter acquisition times. H-MRS is based on the chemical shift properties of the atom. When a tissue is exposed to an external magnetic field, its nuclei will resonate at a frequency (*f*) that is given by the **Larmor equation: $f = \gamma B0$**. Since the gyromagnetic ratio (γ) is a constant of each nuclear species, the spin frequency of a certain nuclei (*f)* depends on the external magnetic field (*B*0) and the local microenvironment.

The electric shell interactions of these nuclei with the surrounding molecules cause a change in the local magnetic field leading to chemical shift. The value of this chemical shift gives information about the molecular group carrying 1H and is expressed in parts per million (ppm).

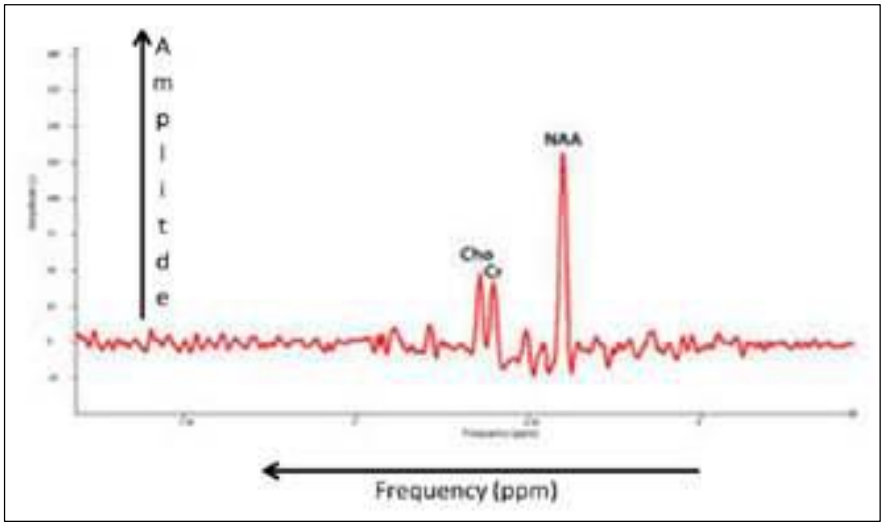

Figure 9. Normal spectra. Y axis corresponds to amplitude and X axis to the metabolites frequency

The chemical shift position of a nucleus is ideally expressed in ppm because it is independent of the field strength (Cho will be positioned at 3.22 ppm at 1.5T or 7T). The MR spectrum is represented by the x-axis that corresponds to the metabolite frequency in ppm according to the chemical shift and the y-axis that corresponds to the peak amplitude (Figure 9)[15].

Some metabolites such as lactate have doublets, triplets or multiplets instead of single peaks. These peaks are broken down into more complex peaks due to J-coupling (spin-spin) coupling. The J-coupling occurs when the molecular structure of a metabolite is such that protons are found in different atomic groups (for example CH3- and –CH2-). These groups have a slightly different local magnetic fields, thus each 1H resonates at a frequency characteristic of its position in the molecule resulting in a multiplet peak [15].

Techniques of MRS

Anatomical images are used to select a volume of interest (VOI) from where the spectrum will be acquired. Different techniques used are single- and multi-voxel imaging with long and short echo times (TE)[16].

Single-Voxel Spectroscopy (SVS)

The signal is obtained from a voxel previously selected. This voxel is acquired from a combination of slice-selective excitations in three dimensions in space, achieved when a RF pulse is applied while a field gradient is switched on. It results in three orthogonal planes and their intersection corresponds to VOI (Figure 10).

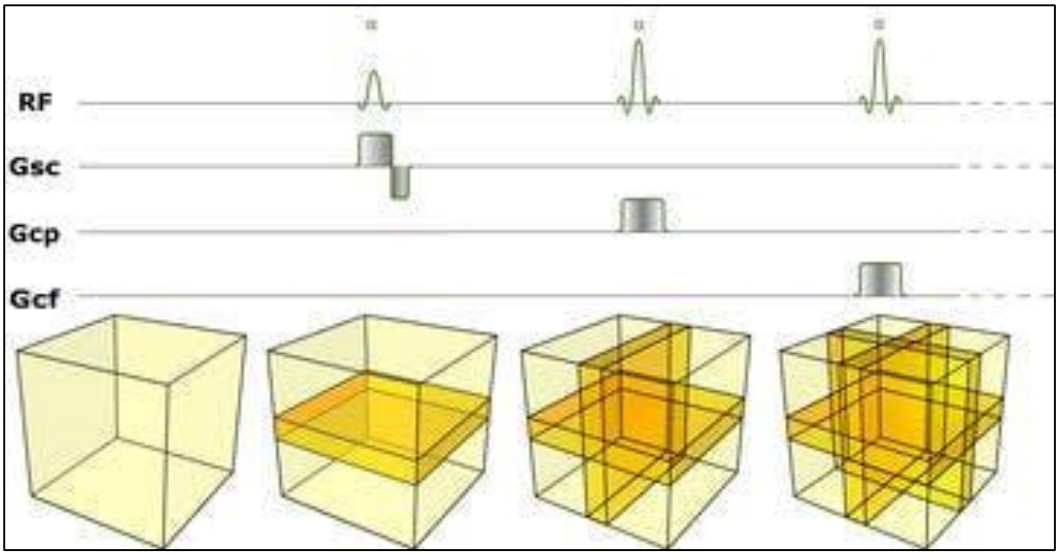

Figure 10: SVS. The intersection of the orthogonal planes, given by slice selection and phase gradients, results in the VOI

Two techniques used for acquisition of SVS H-MRS spectra are point resolved spectroscopy (PRESS) and stimulated echo acquisition mode (STEAM). The most used SVS technique is PRESS. The spectrum is acquired using one 90^{o} pulse followed by two refocusing 180o pulses. Each of them is applied at the same time as a different field gradient. Thus, the signal emitted by the VOI is a spin echo. The first 180^{o} pulse is applied after a time TE1/2 from the first 90o pulse and the second (180^{o}) pulse is applied after a time TE1/2+TE. The signal occurs after a time 2TE (Figure 11a).

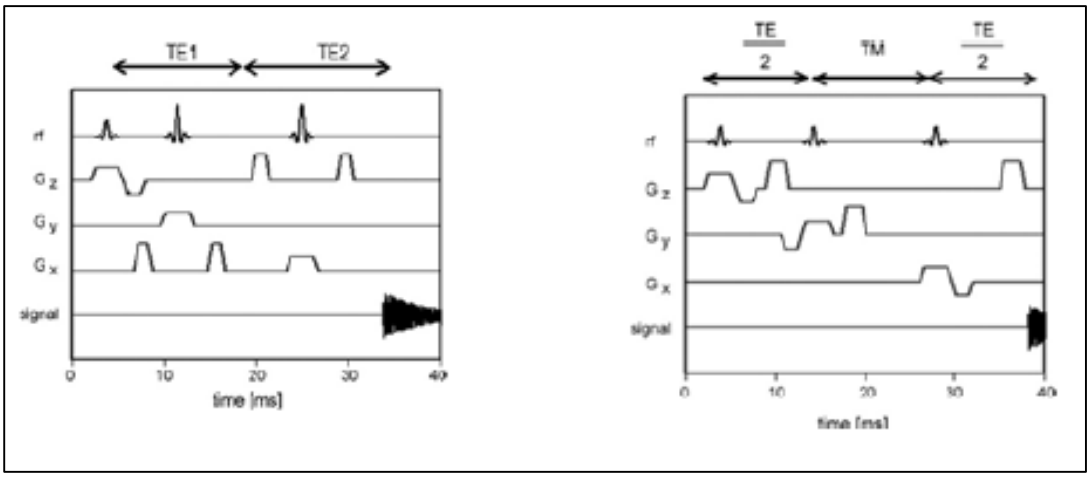

Figure 11. (a) PRESS (b) STEAM

Steam is the second most commonly used SVS technique. All the three pulses applied are 90o pulses. After a time TE1/2 from the first pulse, a second 90^{o} is applied. The time elapsed between the second and the third is called “mixing time” (MT) and is shorter than TE1/2. The signal is finally achieved after a time TE+MT from the first pulse (Figure 11b). Therefore, the total time for STEAM technique is shorter than PRESS[16].

A disadvantage of PRESS is the larger chemical shift displacement artifact. Hence STEAM is usually the modality of choice when a short TE and precise volume selection is needed. PRESS is more used than STEAM because it doubles the SNR ratio and is less sensitive to movement artifacts. Doubling of SNR by PRESS is an important factor leading to better spectral quality[17].

The most frequently evaluated metabolites by MRS are NAA, MI, Cho, Cr and Glx. With the appropriate factors considered, such as the number of protons and the relaxation times, a signal can be converted to a metabolite concentration by measuring the area under the curve[18]. Short TE allow for identification of other metabolites, such as Myoinositol (MI), glutamate, glutamine, and glycine (Glx) (Figure 12).

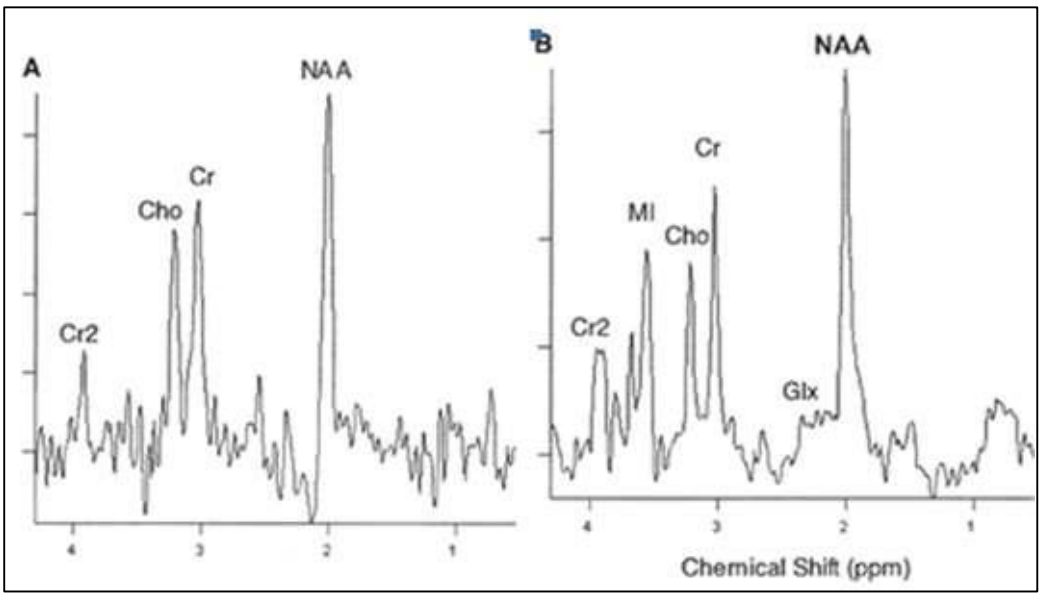

Figure 12: Proton MRS from normal brain tissue using (A) long echo time (TE = 135 ms) PRESS and (B) short echo time (TE = 30 milliseconds)

The term ‘voxel’ refers to a volume of tissue being sampled. The size of a voxel varies between 1 to 8 cm^3; with current equipment and STEAM it can be as small as 0.5 cm^3. Smaller voxels result in lower SNR and the number of signal averages may need to be increased. In the past, it was noted that the effects of Gadolinium (Gd) containing contrast agent might decrease the signal intensity of some important metabolites, such as Cho[15]. The other hand if Gd is given before the MRS studies and the magnetic field of the region of interest is reshimmed to 0.1 ppm before data acquisition, there will be no significant changes in resonance peak area, intensity, and line widths between pre- and post-contrast proton MRS studies[19]. Post-contrast proton MRS allows one to better localize and interrogate the MRS voxels to the region that is presumed to harbor active tumor (i.e., zones of contrast enhancement)[15].

Chemical shift imaging (CSI)

Chemical shift imaging is a multi-voxel technique in which simultaneously many voxels are interrogated. This technique uses phase-encoding gradients to encode spatial information after the RF pulses and the gradient of slice selection. It is acquired using only slice selection and phase encoding gradients, besides the spoiler gradients[16].

Suppression of unwanted signals from outside of the brain particularly from the subcutaneous fat is needed since lipids have a much higher signal than brain metabolites. Since an FOV has always a rectangular shape and the brain is oval shaped, the outer-volume suppression (OVS) technique is used as shown on the (Figure 13)[16].

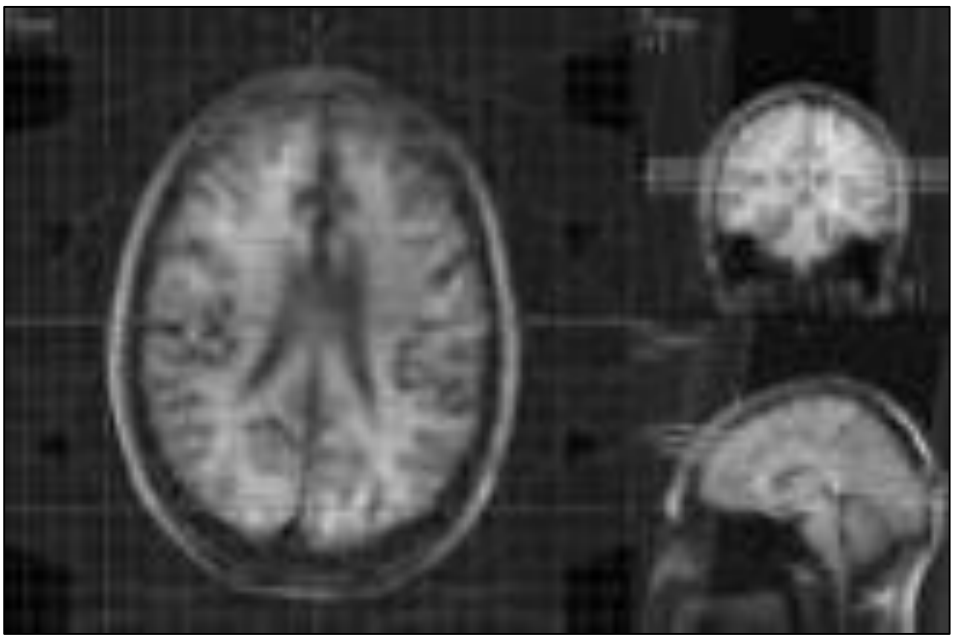

Figure 13: Use of OVS to minimize unwanted signal from outside the brain.

SVS vs CSI

SVS results in a high quality spectrum, a short scan time, and good field homogeneity. Thus, SVS technique is usually obtained with short TE since longer TE has decreased signal due to T2 relaxation. SVS is used to obtain an accurate quantification of the metabolites. SVS has the advantages of better spatial location, more homogeneity, better water suppression and quicker. However, we can get only one spectrum per acquisition. Until now, single voxel technique is still superior to MV technique on the grounds of reproducibility[20,21].

The main advantage of CSI is spatial distribution compared to SVS technique that only acquires the spectrum in a limited brain region. The grid obtained with MRSI allows voxels to be repositioned during post processing. But the quantification of the metabolites is not as precise because of voxel bleeding. Therefore, MRSI can be used to determinate spatial heterogeneity[22].

For SV studies, field homogeneity is performed with zero-ordered shimming. For CSI, field homogeneity in multiple regions requires higher order shimming. To have high-quality spectra, blood products, air, fat, necrotic areas, cerebrospinal fluid, metal, calcification and bone is to be avoided. In such areas differing magnetic susceptibility results in a non-homogenous field that hinders the production of diagnostic quality spectra[22].

Water Suppression

MRS-visible brain metabolites have a low concentration in brain tissues. Since water is the most abundant, its signal in MRS spectrum is 100,000 times greater than that of other metabolites. To avoid this high peak from water to be superimpose on the signal of other brain metabolites, water suppression techniques are needed (Figure. 14)[23].

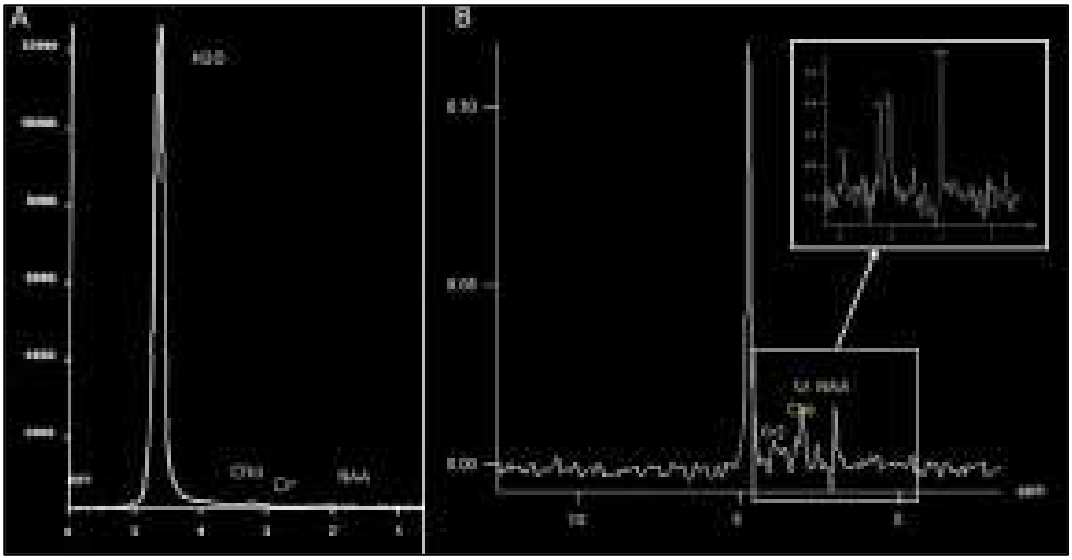

Figure 14: Water signal suppressing with CHESS. Spectrum before CHESS (a) and after CHESS (b).CHESS reduces signal from water by a factor of 1000 allowing brain metabolites to be depicted on the spectrum.

As long as water is the main component of living beings and its concentration is much higher than that of metabolites, it becomes necessary to suppress the signal of resonance from the hydrogen of water[24].

The most commonly used technique for suppressing signal from water is chemical shift selective water suppression (CHESS) which pre-saturates water signal using frequency selective 90° pulses before the localizing pulse sequence. Because the signal from water is so large when compared with that of other metabolites, it needs to be reduced to allow optimal receiver amplifier gain settings to provide adequate signal to noise for detecting the lower concentration metabolites. This technique uses a series of selective 90-degree pulses to reduce the water signal by a factor of approximately 1000 [15].

Other techniques used are Variable Pulse power and Optimized Relaxation Delays (VAPOR) and Water suppression Enhanced Through T1 effects (WET).

MRS Artifacts

MRS is prone to artifacts. Motion, poor water or lipid suppressions, field inhomogeneity, eddy currents, and chemical shift displacement are some examples of factors that introduce artifacts into spectra)[25].

Spectra

H-MRS allows the detection of brain metabolites. The metabolite changes often precede structural abnormalities and MRS can demonstrate abnormalities before MRI does. 1H spectra of metabolites are plotted on x and y axes. The **x,** horizontal, axis displays the chemical shift of the metabolites in units of ppm. The ppm increases from right to left. The **y,** vertical, axis demonstrates arbitrary signal amplitude of the metabolites. The height of metabolic peak refers to a relative concentration and the area under the curve to metabolite concentration[26].

Each spectrum shows peaks corresponding to the different metabolite values: Myoinositol at 3.56 and 4.06 ppm; Choline at 3.23 ppm; Creatine at 3.03 and 3.94 ppm; N acetyl- aspartate at 2.02 ppm; Glx-glutamine and glutamate, 2.1-2.55 ppm and 3.8 ppm .Other peaks observed are lactate 1.33 (peak doublet) and 4.1(2nd peak) ppm; lipids at 0.8-1.3 ppm, alanine at 1.48 ppm, scylloinositol at 3.36 ppm, ethanol (triplet resonance) at 1.16 ppm, macromolecules at 0.5 to 1.8 ppm and acetate at 1.92 ppm[22].

Brain metabolites

N-acetylaspartate (NAA): The peak of NAA is the highest peak in normal brain. It resonates at 2.02 ppm. Glutamate and N-acetyl-aspartyl glutamate (NAAG) are co-localized with NAA in neurons. It is found exclusively in the nervous system (peripheral and central) and detected in both grey and white matter. It is a marker of neuronal and axonal viability and density.

It is also found in immature oligodendrocytes and astrocyte progenitor cells. It plays a role as a cerebral osmolyte. The absence or decreased concentration of NAA is a sign of neuronal loss or degradation. Decreased concentration of NAA results from neuronal destruction from malignant neoplasms and many white matter diseases. Increased NAA is specific for Canavan disease. It is absent in tissues with no neurons (i.e., metastasis, craniopharyngioma, meningioma). A typical meningioma is characterized by an absence of NAA, decrease of Cr, prominent peak of choline and a peak of alanine and glutamine[27].

Creatine (Cr): Cr peak is assigned at 3.02 ppm. An additional peak for Cr is visible at 3.94 ppm. The peak for creatine contains contributions from creatine, creatine phosphate, GABA, lysine, and glutathione. It serves as reserve for high-energy phosphates and as a buffer in ATP/ADP reservoirs. It remains stable in many disease processes. So it is may be used as a control, with levels of other metabolites expressed as a ratio to creatine (i.e., Cho/Cr, NAA/Cr)[28].It is a marker of energetic systems, intracellular metabolism and in the osmoregulation. Concentration of Cr is relatively constant and remains stable in many diseases and hence used as an internal reference for calculating metabolite ratios.

Gliosis causes minimal increase due to increased density of glial cells proliferation. Cr is increased in hypo-metabolic states and increased in hyper-metabolic states[28].

Choline (Cho): Its peak is assigned at 3.22 ppm. It is a constituent of the phospholipids of cell membranes. It is a precursor for acetylcholine and phosphatidylcholine. Its peak contains contributions from glycerophosphocholine, phosphocholine, and phosphatidylcholine and reflects total brain choline. Increased Cho reflects increased membrane synthesis or an increased number of cells.

In tumors, Cho levels correlate with degree of malignancy reflecting cellularity. Cho peak may help with treatment response, diagnosis and progression of tumor. Choline is also increased in chronic hypoxia, epilepsy, Alzheimer's disease, trauma, hyperosmolar states and diabetes mellitus. Increase Cho may be seen in infarction (from gliosis or ischemic damage to myelin) or inflammation (glial proliferation). Hence elevated Cho is nonspecific. Choline elevations are seen also in pseudotumoral forms of multiple sclerosis[27,29,30].

Lactate (Lac):-The peak of Lac is hardly visualized in the normal brain. It is a doublet at 1.32 ppm. The presence of lactate indicates disruption of normal cellular oxidative respiration, such as in hypoxia. Altering TE may provide confirmation that a peak at 1.32 ppm is lactate. It projects above the baseline on short TE acquisition and inverts below the baseline at TE of 135-144 ms.

It is a product of anaerobic glycolysis so its concentration increases under anaerobic metabolism such as cerebral hypoxia, ischemia, seizures and metabolic disorders (especially mitochondrial). Increased Lac signals also occur with macrophage accumulation (e.g. acute inflammation). It accumulates in tissues with poor washout such as cysts, normal pressure hydrocephalus, and necrotic and cystic tumors. The lactate peak indicates anaerobic glycolysis in tumours[31].

Lipids (Lip): Lipids are components of cell membranes not visualized on long TE because of their very short relaxation time. There are two peaks of lipids: methylene protons at 1.3 ppm and methyl protons at 0.9 ppm[31]. These peaks are absent in the normal brain. Lipid peak is seen when there is cellular membrane breakdown or necrosis such as in metastases or primary malignant tumors. Lipid peak indicates necrosis in malignant tumours either before or after treatment[18]. It is increased in high grade tumors reflecting necrosis, stroke, multiple sclerosis lesions and tuberculomas[16].

Alanine (Ala): Ala is an amino acid that has a doublet centered at 1.48 ppm. It is located above the baseline in spectra obtained with short/long TE and inverts below the baseline on acquisition using TE of 135-144 ms. Its peak may be obscured by Lac (at 1.33 ppm). The function of Ala is uncertain but it plays a role in the citric acid cycle[28].Increased concentration of Ala may occur in oxidative metabolism defects[31]. In tumors, elevated level of Ala is specific for meningiomas.[16] It is also reported that its peak is seen between 1.3 to 1.4 ppm, in the same area as lactate.

Myoinositol (MI): It is a simple sugar assigned at 3.56 ppm. It is a glial marker because it is primarily synthesized in glial cells, almost only in astrocytes and acts as an osmolyte. It may represent a product of myelin degradation. Elevated peak occurs with proliferation of glial cells or with increased glial-cell size as found in inflammation. It is a marker and is elevated in gliosis, astrocytosis and in Alzheimer's disease[28,31]. MI is involved in hormone sensitive neuroreception and is a precursor of glucuronic acid, which detoxifies xenobiotics by conjugation. Elevated MI, elevated choline and decreased NAA is seen in low-grade astrocytomas[15]. It is the dominant peak in newborns and decreases with age[16.]

Glutamate-Glutamine (Glx): Glx is a complex peaks from glutamate (Glu), Glutamine (Gln) and gamma-aminobutyric acid (GABA) assigned at 2.05-2.50 ppm. These metabolite peaks are difficult to separate at 1.5 T. Glu is an important excitatory neurotransmitter and also plays a role in the redox cycle. Elevated concentration of Gln is seen in hepatic encephalopathy[31,32]. Glutamate (Glu) and glutamine (Gln) resonate close together and are represented by their sum (Glx) as peaks at 2.1 to 2.5 ppm. Gln plays a role in detoxification and regulation of neurotransmitter activities[16].

Normal brain metabolites are summarized in Figure 15 and Table 1 : Normal brain metabolites

Table 1 : Normal brain metabolites

CHEMICAL COMPOUND	CHEMICAL SHIFT	COMMENTS
N-Acetylaspartate (NAA)	2.0	Neuronal marker.
Creatine/phosphocreatine	3.0,3.9	Energy metabolism. Supplier of phosphate to convert ADP to ATP.
Choline (cho)	3.2	Cell membrane marker.
Myo–inositol (ml)	3.6	Glial cell marker, osmolyte hormone receptor mechanisms
Glutamate (glu) Glutamine (Gln) (Glu+Gln=Glx)	2.1-2.5	An excitatory neuro transmitter and regulator
Lipid (lip)	0.9-1.4	Cell breakdown/ brain destruction indicator.
Lactate (Lac)	1.3	An end product of anaerobic glycolysis

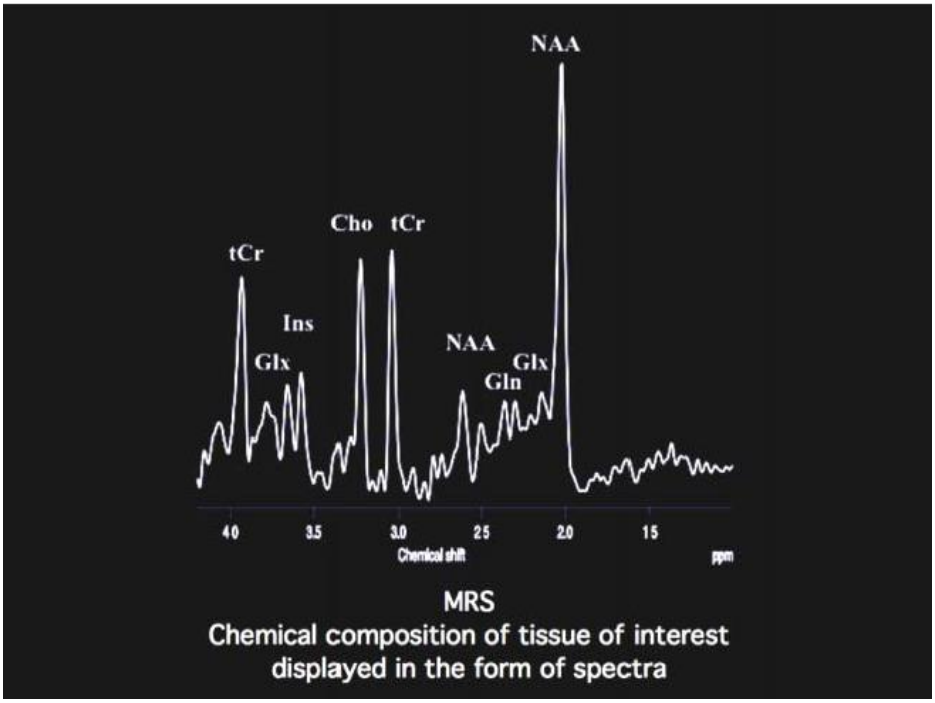

Figure 15:Normal single voxel MR spectrum.

MAGNETIC RESONANCE SPECTROSCOPY IN ICSOL

Infectious diseases

Focal lesions showing a ring-shape contrast enhancement could generate problems of differential diagnosis between tumors and abscesses. Elevation of lipids, lactates and elevations of several amino acids (leucine, isoleucine, valine, alanine) have been reported in bacterial abscesses and cysticercosis[33,34].In tuberculous abscesses only peaks of lactate and lipids are observed, without elevation of amino acids[35,36].

Neurocysticercosis

Cysticercosis is the most common parasitic infection of the human CNS worldwide. The causative agent in cysticercosis is the pork tape worm, Taenia solium. Each cyst measures 3-18 mm in diameter and contains a scolex. When alive , the cyst provokes minimal surrounding inflammation and remains viable for 2-6 years after infestation. As the cyst dies antigen and metabolic products leak from the wall into the surrounding brain, inciting an intense inflammatory reaction in the adjacent parenchyma with edema and mass effect. The patient may become symptomatic with seizures or focal neurological signs. The clear cyst fluid becomes turbid and gelatinous. The cyst then collapses , degenerates and often calcifies. The location of involvement can be meningo-basal, parenchymal, intraventricular or the combination of the sites[37].

Imagings finding in neurocysticercosis are quite often characteristic. Imaging findings in each stage reflect underlying changes in the disease process and host response. Parenchymal cysticercosis are classified into following four stages[37].

Vesicular Stage

After several weeks the larva develops into a cyst containing the scolex. In 3-12 months, a cysticercus is fully grown and contains clear fluid. Mature cysts are readily apparent on CT and MR images and measure 5-20 mm. Cysts are common at the gray white junction but are also seen in the basal ganglia, cerebellum, and brainstem. The cyst wall is thin and smooth, and a 2- to 4-mm scolex is identified within the cyst. Little or no edema surrounds the cyst[37].

CT shows a nonenhancing or mildly enhancing cyst wall containing a small scolex and CSF-density cystic fluid. A low-signal-intensity cyst cavity containing a nodule that is isointense or hyperintense relative to white matter is seen on Tl-weighted MR images. On T2-weighted MR images the scolex can be isointense or hyperintense and can be obscured by high signal intensity cystic fluid. The scolex is better seen on proton density-weighted images[37].

Colloidal Vesicular Stage

In this stage the larva begins to degenerate. As the larva dies the scolex disintegrates and the host's inflammatory response causes a fibrous capsule to form with surrounding parenchymal edema. The severity of this inflammatory response varies widely because it depends on the host's immune response to cysticerci infestation[37].

Diffuse encephalitis may occur, especially in children and after use of the oral anthelmintic agents praziquantel or albendazole, requiring large doses of corticosteroids to control brain edema6. CT depicts ring-enhancing cystic lesions with hyperdense fluid content and surrounding edema. T1 –weighted MR images show a cyst hyperintense to CSF because of proteinaceous fluid and accumulated debris within the cystic cavity. T2- weighted MR images show a hyperintense cyst surrounded by hyperintense parenchymal edema[37].

Granular Nodular Stage

In this stage, the cyst retracts and forms a granulomatous nodule that will later calcify. CT reveals an enhancing nodule with mild surrounding edema. MR images show a thick enhancing ring or nodule with or without surrounding edema simulating tuberculoma, granuloma, or metastatic nodule[37].

Nodular Calcified Stage

In this final stage, the granulomatous lesion is shrunken and completely calcified. On CT the lesion appears as single or multiple calcified nodules. These nodules are hypointense on all MR imaging sequences[37].

Cisternal Cysticercosis

In cisternal cysticercosis the subarachnoid spaces and adjacent meninges are involved. Cisternal cysticercosis and spinal cysticercosis are rare and are frequently associated with parenchymal cysticercosis. Cysts within the cisterns may manifest as space-occupying lesions that may cause obstructive hydrocephalus. Hydrocephalus may also be caused by basilar arachnoiditis. Larvae can have a racemose form that occurs in the subarachnoid spaces and may simulate a low-density tumor in the sellar region or cerebellopontine angle region. The subarachnoid cysts usually lack a scolex[38]

Intraventricular Cysticercosis

Intraventricular cysticercosis often leads to obstructive hydrocephalus and ventriculitis. On MR imaging, the scolex, subependymal reaction, and cyst wall are readily apparent, indicating the intraventricular larva. MRS findings of cysticercosis include a combination of elevated levels of lactate, alanine, succinate and choline and reduced levels of NAA and creatine[34].

In a study by Pretell et al, the Cho/Cr ratio was greater than 1 in all tuberculomas but in none of the cysticerci (n=6)[39]. MRS findings of cysticercosis include a combination of elevated levels of Lac,Ala,Suc and Cho and reduced levels of NAA and Cr[34].Recently MRS is a useful tool for the diagnosis of NCC[39,40,41,42.]. Pyruvate is the predominant metabolite in cysticercosis cysts[39].Tuberculomas had higher lipid peaks, more choline, less N-acetylaspartate, and less creatine than neurocysticercosis[39]. The combination of elevated lactate, alanine, succinate and choline levels and reduced NAA and creatine levels helps to characterize a cystic intra-axial lesion in the brain as NCC[34]. Pyruvate is the predominant metabolite in cysticercosis cysts. MRS showed a low NAA peak compatible with NCC[39]. MRS of NCC is elevated lactate, alanine, succinate, and choline levels and reduced levels of N -acetylaspartate and creatine[34].

In **cysticercosis,** resonances of lactate, succinate, alanine, acetate, and/or unassigned resonances were observed. Only lactate is commonly observed in a variety of intracranial cystic masses, except for abscess and cysticercosis, in which resonances of acetate, succinate, amino acids, and/or unassigned metabolites can be seen in addition to a lactate peak[43].

Tuberculomas

CNS tuberculosis may take a variety of forms, including tubercular meningitis, abscess, focal cerebritis and tuberculoma. Tuberculomas may be single or multiple, and can be seen anywhere in the brain parenchyma. The number of identified lesions per patient may range from one to 12 (or more), with the size varying from 1 mm to 8 cm. Its presence in the ventricular system is very rare. Although no precise patterns of localization have been observed according to race, age, or sex, children develop infratentorial tuberculomas more commonly than do adults. Symptoms are often limited to seizures and mass effect, resulting in an increased intracranial pressure.

Neurological deficit reflects the topographic location of the lesion. These lesions originate as a conglomerate of micro granulomata in an area of tuberculous cerebritis that join to form a noncaseating tuberculoma. In most cases, subsequent central caseous necrosis develops that is initially solid, but in some instances, may eventually liquefy[44].

Intracranial tuberculomas usually show hypo- or isointensity or central hyperintensity with a hypointense rim on T2W images and isointensity and/or hypointensity on T1W images[44]. Certain tuberculomas show a varied range of signal intensities on MRI. Depending on its stage of maturation, a tuberculomas appearance varies on MRI, i.e., whether noncaseating, caseating with a solid center, or caseating with a liquid center[44,45].A noncaseating tuberculoma usually appears hyperintense on T2W and slightly hypointense on T1W images[44].

These granulomas show homogenous enhancement after injection of paramagnetic contrast on T1W images. A solid caseating tuberculoma appears relatively iso- to hypointense on both T1W and T2W images with an iso- to hyperintense rim on T2W images. In the presence of edema, the rim appears inseparable on T2W images. It shows rim enhancement on postcontrast T1W images. The degree of hypointensity of the solid caseating tuberculoma on T2W images depends on the complex relationship between the solid caseation, associated fibrosis/gliosis, macrophage infiltration, and perilesional cellular infiltrate. When the solid center of the caseating lesion liquefies, the center appears hyperintense with a hypointense rim on T2W images.

The postcontrast T1W images show rim enhancement. MRI features of tuberculomas are known to overlap with those of other intracranial focal lesions, like the healing stage of neurocysticercosis, fungal granulomas, chronic pyogenic brain abscess, and lymphomas. Some gliomas and metastases may also have features similar to those of tuberculomas and should be considered in their differential diagnoses[44]. Sometimes, large tuberculomas mimic neoplastic lesions on MRI as they appear predominantly hyperintense on T2W images, with mixed intensity on T1W images, and may show heterogeneous enhancement on postcontrast studies . Quantitative MT imaging and in vivo proton MRS may help in the differential diagnosis of tuberculomas[45].

MRS increases specificity of diagnosis by identifying lipids within the lesions that are characteristic for TB. In vivo and in vitro MRS has shown elevated lipid peaks within the TB lesions[46].Gliomas, metastases, abscesses and demyelinating disease are the differential diagnosis to be considered. In vivo spectra are found to be specific for intracranial tuberculoma and demonstrate the biochemical fingerprints of tubercle bacilli in a granuloma.

Gupte et al. have performed in vivo, ex vivo, and in vitro MRS to fingerprint the metabolites of Tuberculosis in tuberculomas[36].There is slight decrease in NAA/Cho[35].The Cho/Cr ratio is greater than 1 in tuberculomas[39]. Prominent lipid resonances are seen in intracranial tuberculomas, with particularly important signals at the 1.3 and 0.9 ppm, corresponding to the methylene and terminal methyl groups of fatty acids, respectively[47]. MRS revealed a lipid peak at 0.9–1.3 ppm in all of the 14 lesions evaluated by Batra and Tripathi[48,49].MR spectroscopy of tuberculomas shows a decrease in NAA/Cr, slight decrease in NAA/Cho and lipid-lactate peaks are usually elevated (86%)[39].

Tuberculous abscess*:-* Tuberculous abscesses typically have high lipid and lactate peaks. These abscesses have no peaks for amino acids (leucine, isoleucine, and valine) at 0.9 ppm, succinate at 2.41 ppm, acetate at 1.92 ppm, and alanine at 1.48 ppm, in contrast to pyogenic abscesses, which have peaks for all these metabolites. Elevated lipid peaks within the tuberculous lesions can be used to discriminate between tuberculous and non-tuberculous brain lesions. The cell wall of mycobacteria is predominantly composed of lipids in contrast to that of other bacteria[50,51.]

The methylene and terminal methyl groups generate the lipid resonances at 0.9 and 1.3 ppm, respectively, of fatty acids contained in the caseous material[35,52,53] .There is a relative lack of proteolytic enzymes in the tuberculous inflammatory exudates as compared with pyogenic inflammation. The absence of amino acids at 0.9 ppm in tuberculous abscesses is due to the presence of large numbers of tubercle bacilli and the lack of proteolytic enzymes, resulting in poor degradation of proteins into amino acids[54].Acetate and succinate are the end products of fermentation in pyogenic abscesses[35].Thus, 1H-MRS exhibiting lipid peaks is highly indicative for tuberculous lesions.

Brain Abscesses

Pyogenic brain abscesses may, at times, be multiple. Multiple brain abscesses are often caused by hematological spread of bacteria from a primary source and are frequently found in middle cerebral artery territory. The likely sources of primary infection in patients with multiple brain abscesses include cyanotic heart disease, endocarditis, suppurative lung diseases, skin infection and abdominal and pelvic infections. Multiple pyogenic brain abscesses are common in patients with human immunodeficiency virus infection, organ transplant recipients, intravenous drug abuse, chemotherapy for lymphoma, congenital cardiac defects or prosthetic cardiac valves and diabetes[55].

STAGES OF ABSCESS FORMATION

1) *Early (3-5days) and late (5-14 days) cerebritis stage*

They are differentiated on the basis of mass effect present in the latter. On T1-weighted images, cerebritis may be visible as an ill-defined, isointense to hypointense area relative to adjacent normal brain parenchyma, On FLAIR and T2-weighted images, early cerebritis demonstrates as an area of increased signal intensity with mass effect 10. Cerebritis shows patchy restricted diffusion on DWI[55].

2) *EARLY (2-4weeks) AND LATE(weeks to months) CAPSULE STAGE*

They are differentiated on the basis of peripheral edema which is present in the former and absent in the latter stage. In a typical abscess with central liquefy active necrosis, the center of the cavity is slightly hyperintense to CSF, whereas the surrounding edematous brain is slightly hypointense to normal brain parenchyma on T1-weighted images. On unenhanced MR images, the mature, surgically drainable abscess often has a rim with distinctive features[56].

The rim is isointense to slightly hyperintense to white matter on T1-weighted images and is hypointense on T2-weighted images. The abscess ring is most commonly very smooth, regular in thickness, and thin walled (approximately 5 mm in thickness), although it may be thinner along its medial margin, possibly due to variations in perfusion of gray and white matter..

Abscesses tend to demonstrate high signal intensity on DWI, with a corresponding reduction in the apparent diffusion coefficient values[57,58]. This is directly related to the cellularity and viscosity of the pus contained within an abscess cavity[57]. In contrast, high-grade gliomas and metastases with central necrosis have a low signal on DWI and high apparent diffusion coefficient values[57]. These lesions include metastases, rarely glioblastoma multiforme, and even residual diffusion change persisting into the early stages of enhancement of an evolving recent cerebral infarction

Typical MR spectroscopic features of brain abscesses include elevated peaks of amino acid, lactate, alanine, acetate, pyruvate and succinate and absent signals of NAA, creatine and choline. Abscesses have a distinct spectroscopic pattern that allows differentiation from other entities[59,60]. Elevation of Cho and absence of signal from a variety of amino acids, acetate and succinate are features that would favor a neoplastic process, whereas alanine, acetate, pyruvate and succinate−favor abscesses. MRS may shed light on which organism is responsible for the abscess, because the presence of anaerobic bacteria tends to cause elevated acetate and succinate peaks[61].Absence of acetate and succinate signals are more likely with obligate aerobes or facultative anaerobes[62,63].

Brain Tumors: Brain tumors are currently the main application of H-MRS. H-MRS may help with differential diagnosis, histologic grading, degree of infiltration, tumor recurrence, and response to treatment mainly when radionecrosis develops and is indistinguishable from tumor by conventional MRI[16].

Primary Neoplasms

The most common primary brain neoplasms are of glial origin. Low-grade glial neoplasms occur most often in patients aged 20–40 years. High-grade glial lesions occur in older adults. High-grade glial neoplasms are differentiated from low-grade ones by pathologic evidence of increasing cellular atypia, nuclear pleomorphism, neovascular proliferation, and necrosis. The typical H-MRS features for primary neoplasms are elevated peaks of Cho, Lip, Lac, MI and reduced NAA. The anaerobic environment of many neoplasms and derangements in glucose metabolism result in incomplete glucose breakdown and accounts for the elevated lactate signal[64].

Published MR spectroscopic results showed a sensitivity of 79% and a specificity of 77% for a Choline/NAA ratio of greater than 1 as an indicator of a neoplastic process[65]. A Cho/NAA cutoff ratio of 2.2 reliably separates high-grade neoplasms from low grade neoplasms and nonneoplastic conditions[66]. High-grade neoplasms tend to have elevated Lip, which is often absent in low-grade neoplasms[67]

Astrocytomas

They are classified into low grade (grade I and II) and high grade gliomas (anaplastic gliomas or grade III, and glioblastoma multiforme or grade IV). High grade gliomas have higher Cho and lower NAA than low grade ones. Elevation of MI, decrease of NAA and mild elevation of Cho characterize low-grade[68].High-grade gliomas (malignant) present with marked increase of Choline, decrease of NAA and the presence of lactate and lipids peak[69].

Cho/Cr is the most frequently used ratio. Some institutions use a threshold value of 2.0 for Cho/Cr to differentiate low grade from high grade gliomas while some use a cutoff value of 2.5[16].Cho/Cr ratios are greater than 2.0 in gliomas, between 1.3 and 2.0 in hamartomas, and less than 1.3 in normal brain tissue. A Ch/Cr ratio equal or higher than 1.56 and lactate peak in gliomas and metastases predict malignancy at 88.9% sensitivity and 91.7% specificity[70].

NAA is usually reduced to 40% to 70%of normal. Several MRS findings are correlated with histologic grade of malignancy. Presence of lactate and lipid resonances correlates with a higher degree of malignancy, as seen in GBM, and reflects tumor hypoxia, and necrosis. A threshold value of 1.56 for the Cho/Cr ratio produced a 75.8 per cent sensitivity and 47.5 per cent specificity for differentiating high- from low-grade gliomas[71].

Oligodendroglioma:

MRS of oligodendroglioma demonstrates significantly higher Cho, Cho/Cr ratio, and a higher incidence of Lac and Lip in high grade than in low-grade tumors. Low grade oligodendroglioma may show highly elevated Cho, mimicking high grade tumors, because, these low grade tumors can have high cellular density but absent endothelial proliferation and necrosis[72].The level of Glx is significantly higher in low grade than in low grade astrocytomas and may help to distinguish these tumors from each other[73].

Brainstem lesions represent a special clinical challenge, because of the danger of biopsy in this area, in most cases patients are treated based on clinical and imaging findings. MRS is also challenging in this area, because of the need for small voxels, and the magnetic susceptibility changes around the skull base. The authors have found that MRS is useful in this area and that if changes in all metabolites are taken into consideration neoplastic and nonneoplastic processes can be distinguished in many cases(Table 2)[74].

Table 2:H-MRS changes in tumor characteristics and differential diagnosis

	Cho	NAA	Lac	Lip	Myo	Glu	Suc	Acet	Ala	Aa
Low grade tumor	↑	↓			↑					
High grade tumor	↑	↓	↑	↑						
Metastasis	↑	absent[1]	↑	↑						
Oligodendroglioma	↑	↓	↑[2]							
Meningioma	↑	absent							↑	
Gliomatosis cerebri	↑	↓								
Lymphoma	↑	absent[1]		↑						
Radionecrosis	↓	↓	↑	↑						
Abscess	N	↓	↑	↑			↑	↑	↑	↑
Demyelination	↑	↓	↑[3]	↑	↑	↑[3]				

↑- increased peak; ↓ - reduced peak; N- normal peak; Cho – choline; NAA – N-acetylaspartate; Lac– lactate; Lip – lipids; Myo – Myoinositol; Glu – glutamine; Suc – succinate; Acet –acetate; Ala –alanine; Aa- amino acids. 1 NAA is absent in the core of the tumor, but may be present where it infiltrates brain parenchyma or with voxel bleeding.2 The presence of lactate depends on the grade of the tumor. 3 Lac and Glu are increased only in the early stage of the disease.

Metastatic Neoplasms

Almost 80% to 85% of metastases are located in the supratentorial compartment. These lesions may be the direct result of microscopic foci of neoplastic cells transported into the brain via the hematogenous route with subsequent growth in situ, or the metastatic deposit may be primarily to the surrounding calvarium or dural membranes and impinge on the brain secondarily. Intraparenchymal metastases are the most common type of metastatic disease to affect the intracranial space. Most common, in decreasing incidence, are lung cancer, breast cancer, melanoma, gastrointestinal cancers, renal cell carcinoma, and tumors of unknown primary[75].

Most intracerebral metastases are multiple, regardless of the site of origin; however, there is a high incidence of solitary metastasis, estimated to range from 30% to 50% and especially common in melanoma, lung, and breast carcinoma[76]. Surgical intervention is often indicated for solitary metastases whereas radiotherapy or radiosurgery without surgery is generally the therapy for multiple lesions, the detection of intracerebral metastases is critical to patient management.

Early metastatic foci are commonly found at gray matter–white matter interfaces, a feature shared by all hematogenously disseminated embolic disease. Metastases are notoriously surrounded by massive amounts of edema. The edema accompanying metastases usually does not cross the corpus callosum nor does it involve cortex, features that often help to distinguish these lesions from primary infiltrative brain malignancies

Although many intracerebral metastases are apparent on noncontrast scans, it has been well documented that intravenous contrast increases the sensitivity for the detection of intracerebral metastases. The ring enhancement of a neoplastic lesion characteristically differs from the enhancement of benign conditions, such as abscess, resolving hematoma, and demyelinating disease, by its wall characteristics[77].

Malignant neoplasms, but not all neoplasms, demonstrate thick, irregular, or nodular enhancement, as opposed to the regular, thin, even, and smooth enhancing wall of the aforementioned benign conditions[78]. It should be stressed that in any patient with a primary extracranial neoplasm and intracranial enhancement in a nonvascular distribution, metastases should be considered the diagnosis until proven otherwise. The major differential diagnosis of a solitary, thick-walled, ring-enhancing lesion in the supratentorial brain of an adult, in the absence of a history of prior irradiation, resides in primary glioblastoma versus singular metastasis, a distinction that generally cannot be made on the basis of imaging studies alone[79].

Typical MR spectroscopic features for secondary neoplasms include elevated signals of Lip, Lac, Cho and reduced/ absent NAA signal. The metastatic lesion has a sharp margin with no spectroscopic abnormality in the immediately adjacent tissue. In contrast, primary neoplasm shows spectroscopic abnormalities extending beyond the enhancing margin of tumor[15].So interrogation of areas outside the enhancing portion of the lesion is more promising[80].Various metabolite signal ratios have been suggested for this purpose. In one study, a Cho/NAA ratio of greater than 1 had an accuracy of 100%[81].

Differential diagnosis between brain abscess and neoplasms (primary and secondary):-

If the VOI is positioned in the enhancing area, presence of Cho favors a neoplasm and if positioned in the cystic area of a lesion, abscess and tumor both demonstrate high peak of lactate. The presence of acetate, succinate, and amino acids (AAs) such as valine, alanine and leucine in the core of the lesion has high sensitivity for pyogenic abscess. These peaks are not seen in tumors and in pyogenic brain abscess that are under antibiotic therapy. These are believed to be from protein degradation by proteolytic enzymes[82].

Meningioma:-Meningioma can usually be distinguished from intra-axial glial neoplasms on routine imaging studies by their extra-axial locations. A typical meningioma is characterized by an absence of NAA, decrease of Cr, prominent peak of Cho and a peak of Ala and Glx. Marked elevation of Cho levels up to three times that of normal brain parenchyma has been reported, particularly in recurrent meningiomas. The Cho/Cr ratio has been reported to be higher in malignant meningioma than in benign meningioma[83].

Theoretically, NAA is not present in meningioma, which arise from arachnoid structures and not from within the central nervous system (CNS); however, in clinical experience it is not uncommon to detect NAA in these extra-axial tumors, particularly in atypical and malignant varieties[83].

Mobile lipids have been reported in meningioma, and this may be due to fatty degeneration or contamination of the MRS voxel from subcutaneous tissues or fat at the skull base. Detection of alanine, although not invariably present, is considered characteristic of meningioma. Lac levels may be elevated in some meningiomas. With MR spectroscopy, meningioma characteristically shows the presence of an alanine peak at 1.5 ppm[83].

Schwannoma: An extraaxial lesion that lacks the alanine peak and instead shows the presence of MI at 3.55 ppm.MR spectra of acoustic schwannomas show absence of Cr, marked reduction in NAA, and increased lipids[83].

MR spectroscopy for treatment monitoring

Radiation necrosis and gliosis may be indistinguishable from residual or recurrent neoplasm particularly when new contrast-enhancing lesions are seen. In patients with tumor recurrence, MRS shows elevated Cho or NAA, Cho or Cr, and lactate. Patients with radiation necrosis show low NAA, Cho, and Cr and a broad peak at 0 to 2.0 ppm (Figure 16).Cho/Cr and/or Cho/NAA ratios are significantly higher in recurrent tumor than in radiation injury[84].

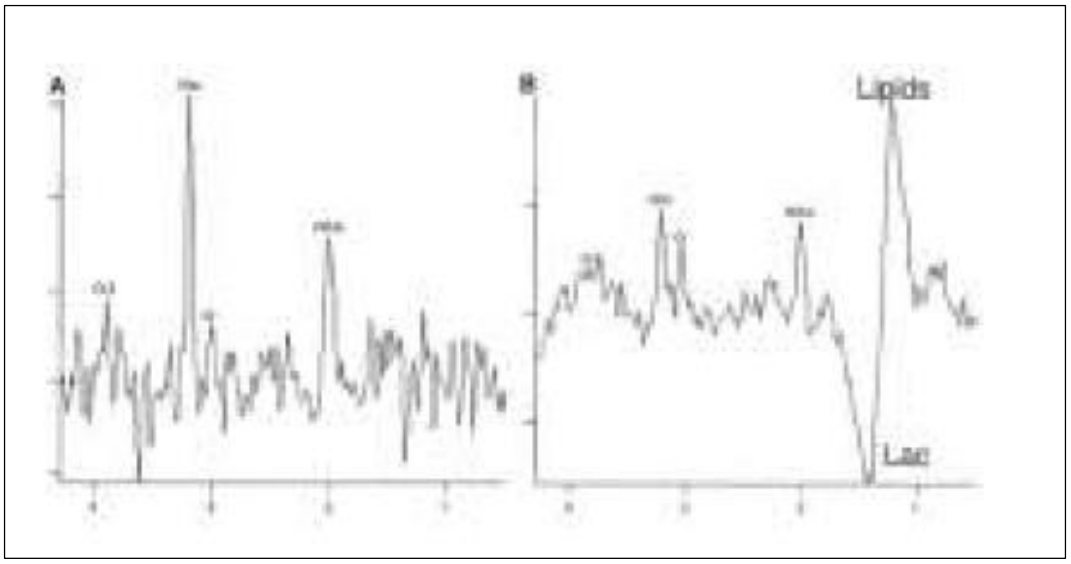

Figure 16: MRS for treatment monitoring Pre-treatment (A) and post-treatment (B) MR spectroscopy with a long echo time (TE = 135) from a metastatic brain lesion. Notice post-treatment shows reduced relative level of choline, higher relative NAA, and a broad peak around 1.0–1.5 ppm, representing lipids. Post treatment spectrum also shows inverted doublet peak of lactate (Lac) at 1.3 ppm.

Radionecrosis: After chemotherapy and/or radiotherapy spectroscopic findings should be interpreted with caution during the first 6 months because radiotherapy elevates choline levels and there may be still tumoral cells. After 6 months, Cho elevation suggests tumoral receive or therapy failure. If no metabolites are found and lactate and lipids are present, it suggests radionecrosis. Post radiotherapy demyelination appears after six to eight months of treatment and may progress for two years and its spectrum contains increases of Cho compounds and MI due to gliosis and decreases of NAA[85].

Pituitary adenomas:-They show only a choline peak or no metabolites at all in the case of intratumoral hemorrhage (as hemosiderin worsens the magnetic field homogeneity)[86]. In another study of various brain lesions by Kinoshita Y et al, they found that that the concentration of glycine was high in neuroectodermal tumors, whereas that of taurine was high in medulloblastoma and pituitary adenoma. Alanine was increased in meningioma, glioma, and pituitary adenoma[87].

Epidermoid Cyst:-Epidermoid cysts are occasionally difficult to differentiate from other nonenhancing nonneoplastic cysts, such as arachnoid cysts, with MR imaging or CT. Proton MR Spectroscopy may assist in distinguishing these cysts, as elevation of lactate is seen in the former but not in the latter. In three cases of epidermoid cysts studied by Ping ‑Hong et al, lactate was observed and could be differentiated from 3 cases of arachnoid cysts, which showed only minimal lactate[88].

MATERIALS AND METHODS

Source of data:

This study was carried out on 52 patients (with intracranial space occupying lesions), serially collected, diagnosed by conventional MRI at department of Radio-Diagnosis for MRI Brain (plain and contrast study), R. L. Jalappa Hospital and Research Centre, Tamaka, Kolar from January 2016 to June 2017, over a period of 18 months. An informed consent was taken from individuals for their willingness to participate in the study.

Inclusion Criteria:

All patients with space occupying lesions detected in routine MRI Brain study

Exclusion Criteria:

Lesions close to the skull base or calvarium where it may not be technically feasible to acquire MRS data

Patients in whom MRI is contraindicated.

Method of collection of data:

This study was approved by the institutional review board and informed consent was taken from all the individuals prior to inclusion in the study. Patients in whom ICSOL was detected on conventional MR imaging were included in the study.

Study design: Hospital based descriptive observational study.

Sampling and sample size: The study is time bound study with sample size of 52 cases.

MRI technique: - MRI was performed on SIEMENS Magnetom Avanto® 1.5 Tesla scanner using head coil. Conventional spin echo sequences, axial T1, T2 and FLAIR: Coronal T2; Sagittal T1; Post contrast axial, coronal and sagittal; CSI at TE of 135ms and/or SVS at TE of 135ms. The TR used was 1500 ms and number of averages was 4.Automatic water suppression was done, as provided by the vendor of MRI. Various peaks obtained in MRS were evaluated for integral values and ratios of Cho/Cr and Cho/NAA. Gadobenate dimeglumine contrast was used with dosage being 0.1 mmol/kg bodyweight.

No specific patient preparation was necessary. It was ensured that no contraindication to MRI existed such as pacemakers, ferromagnetic implants, implanted drug infusion device, shrapnel, ferromagnetic prosthetic valves, and aneurysm clips etc.

Baseline data were collected from patients along with pertinent clinical history. Any previous studies, if available was requested and reviewed.

Imaging diagnosis was confirmed by one or more of the following:

- Response to treatment on follow up CT scan.
- CSF analysis.
- Surgery and histopathological findings.
- PET CT/PET MRI for evaluation of metastases.

Image Assessment

Images obtained by conventional MRI pulse sequences and MRS spectra were reviewed by the radiologist. The reviewers were not blinded to clinical history and conventional MRI findings for spectroscopy interpretation, however were blinded to final diagnosis.

Statistical Analysis

Data was recorded into Microsoft® Excel® and was analyzed using OpenEpi® software. All the data were presented as percentages and proportions.

Siemens Magnetom Avanto® 1.5 T MR Scanner used in the study

RESULTS

The study included a total of 52 patients with a slight male preponderance (n = 30, 57.6%). The age group of patients ranged from 1-80 years (mean age 40 years). The most commonly involved age group was 31 to 50 years (n = 18; 34.6%) followed by 51 to 70 years (n = 13; 25 %) and < 18 years (n = 11; 21.1%). The least number of patients belonged to age group of >70 years (n = 3; 5.7 %). The age group from 31 to 70 years constituted more than 59.6 % of the patients (Figure 17).

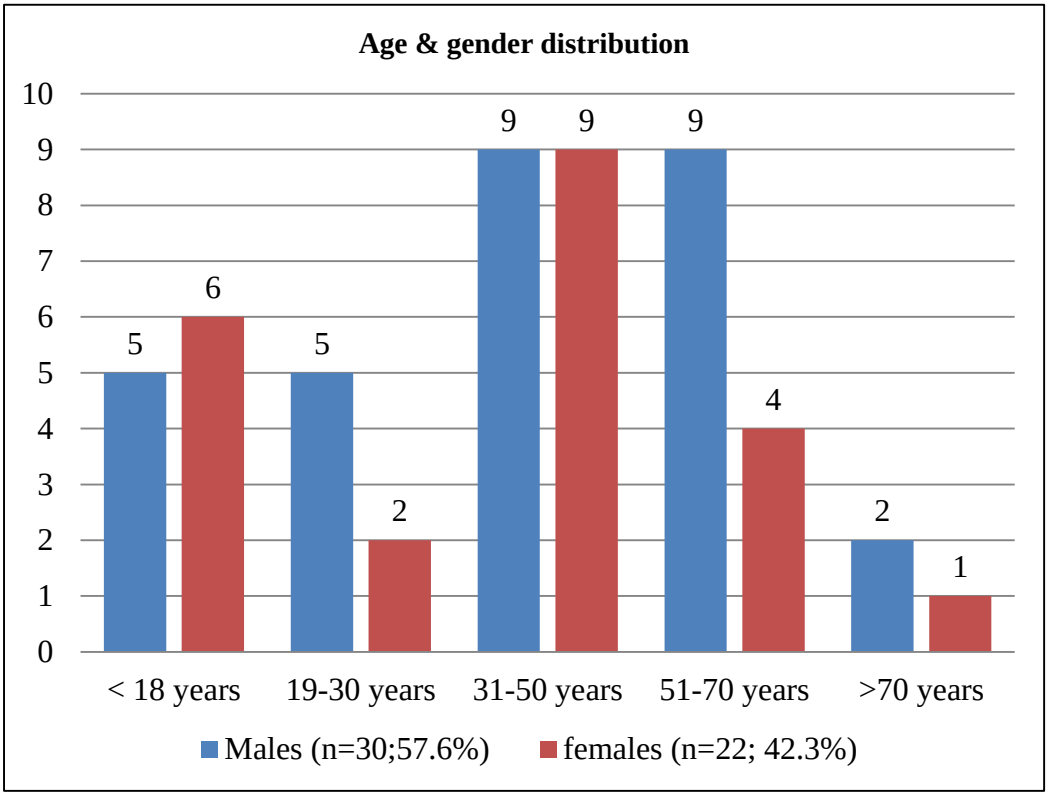

Figure 17. Age and gender distribution

Chief clinical symptom associated with ICSOL was seizures (n = 27, 41.9%), closely followed by headache (n = 24, 46.1%), blurring of vision (n = 11, 21.1%) and fever (n = 8, 15.3%). Fever was commonly reported in patients with infective etiology, among whom it was common in patients with tuberculoma. Few patients presented with cough (n = 3, 5.7 %) and tinnitus (n = 2, 3.8%). Nausea, tremors, dizziness were seen in one case each (1.9%), in whom ICSOL was incidentally detected. A total of 18 patients presented with more than clinical symptom, as depicted in Figure 18.

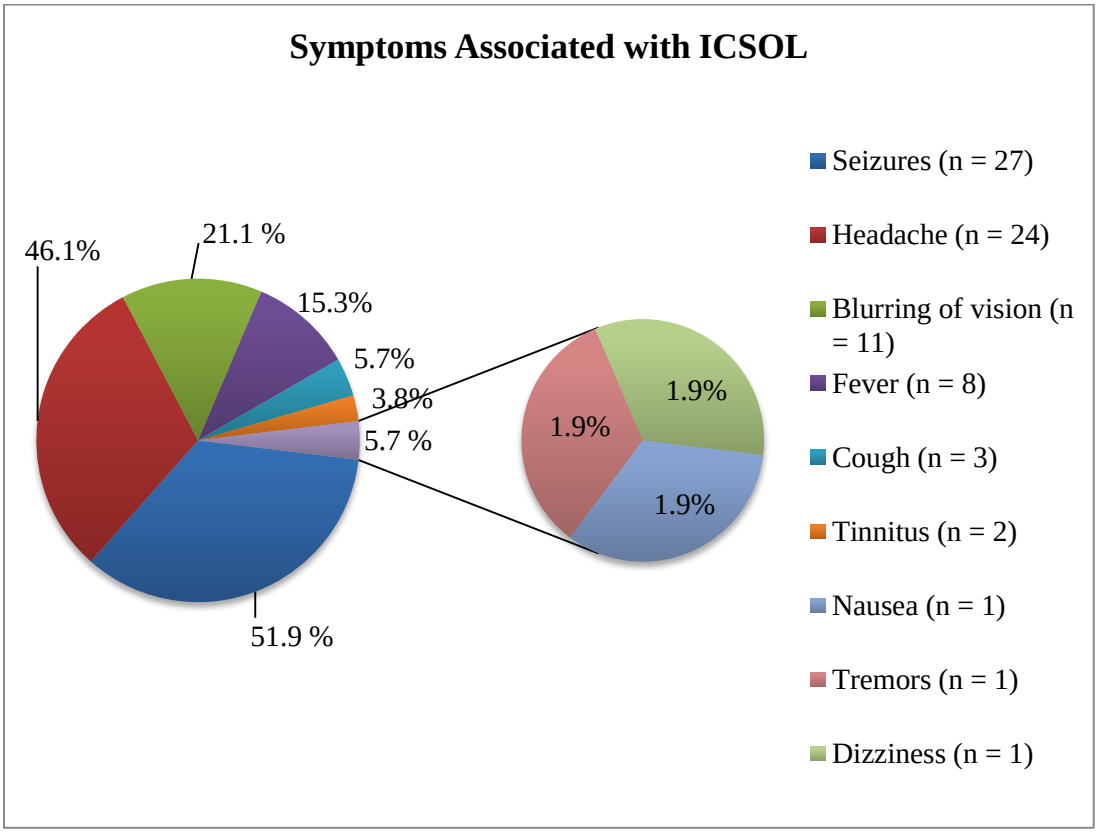

Figure 18: Symptoms associated with ICSOL.

Majority of the patients had intra-axial lesions (n = 43; 82.6%) and remaining nine patients (17.3%) presented with extra-axial lesions (Figure 19). Intraxial lesions included neurocysticercosis (n=15; 28.8%), tuberculoma (n=10; 19.2 %), high grade glioma (n=6; 11.5%), metastases (n=3; 5.7 %) and low grade glioma (n=2; 3.8%). Radiation necrosis, developmental venous anomaly, pilocytic astrocytoma, pineocytoma, subependymoma, choroid plexus carcinoma and pyogenic abscess were seen in one patient each (1.9% each).

Among extraaxial lesions, there were two cases of meningioma (3.8%) and one case each of epidermoid cyst, arachnoid cyst, pituitary macroadenoma, craniopharyngioma, acoustic schwannoma and glomus jugalare tumor (n = 1.9% each).

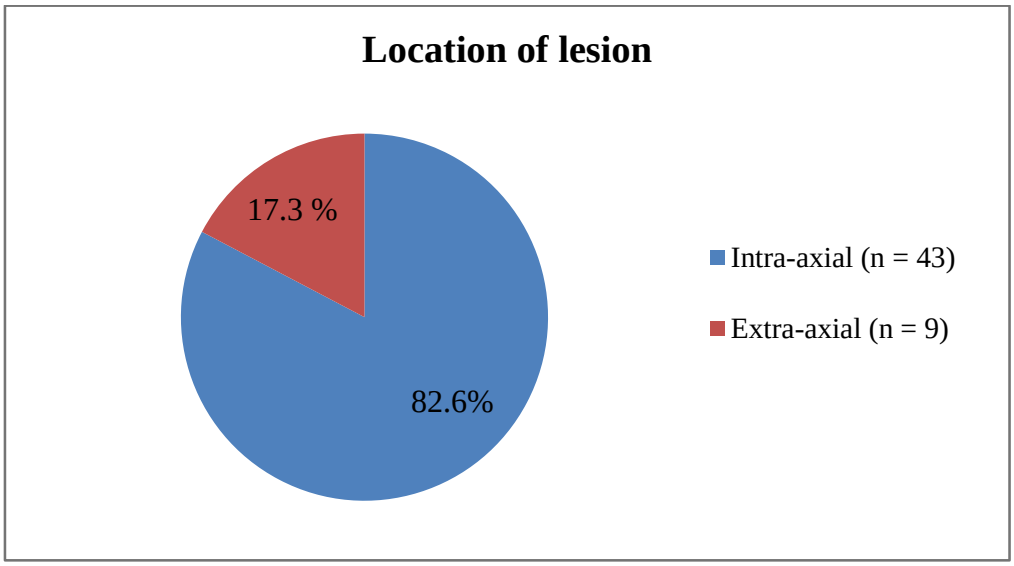

Figure 19: Location of ICSOL

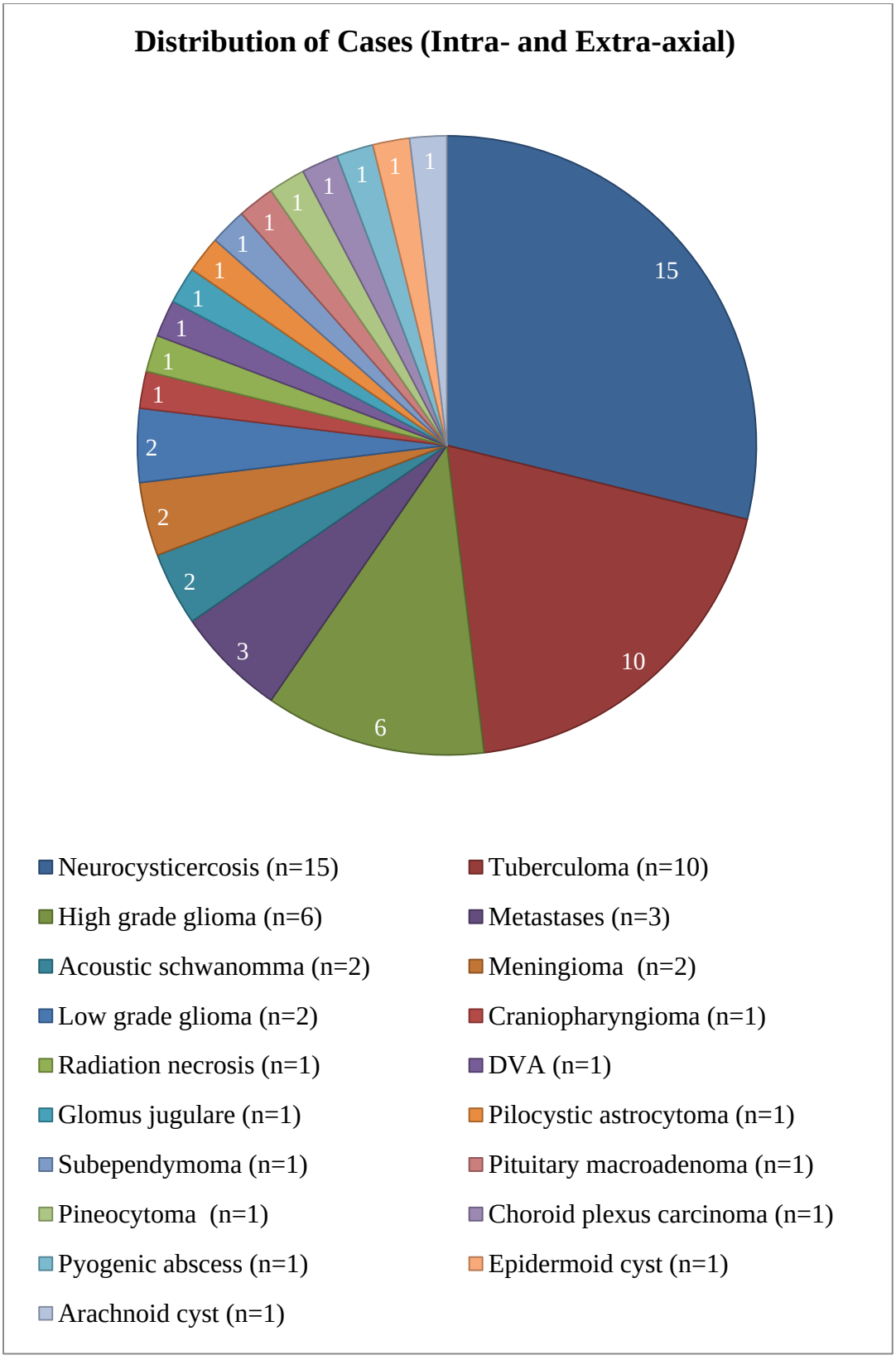

Figure 20. Distribution of cases.

In our study, there were 25 patients with lesions on right side and 15 patients with lesions on left side (48.1 % and 28.8 % respectively). Bilateral involvement and midline lesions were seen in six patients each (11.5%). Midline lesions included one case of arachnoid cyst, epidermoid cyst, craniopharyngioma, pituitary macroadenoma, pineocytoma and high-grade glioma involving basifrontal cortex (Figure 21).

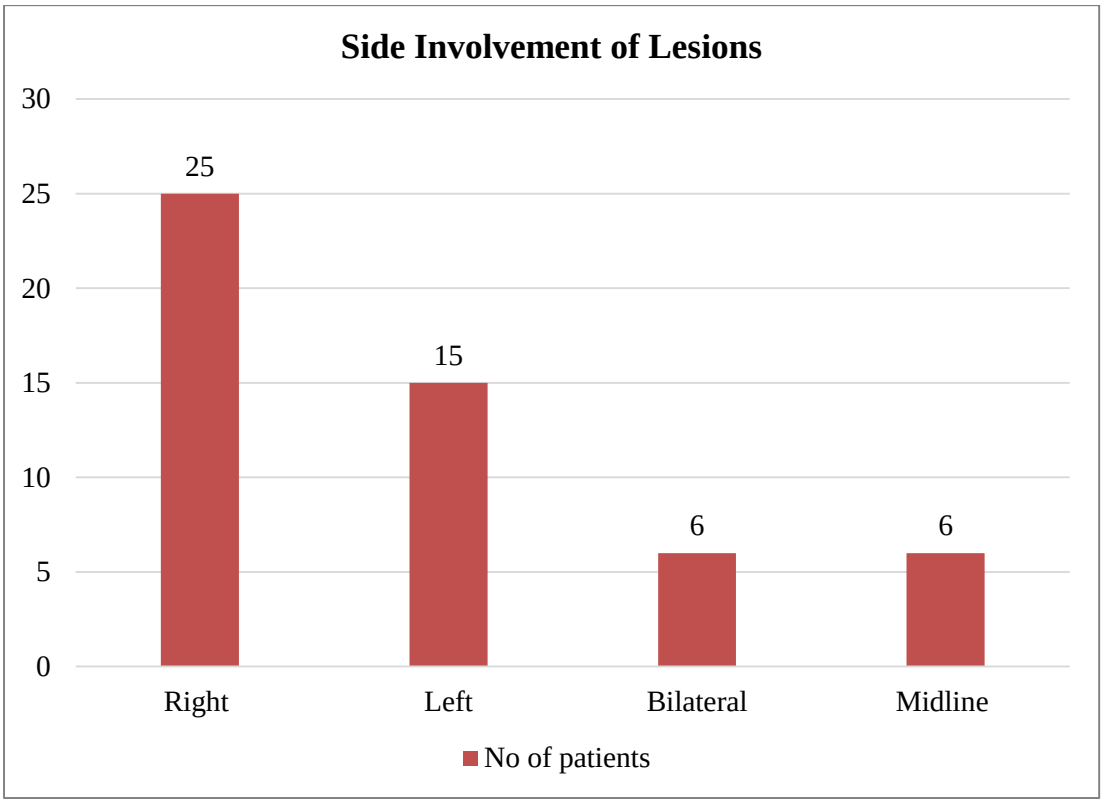

Figure 21. Side involvement of lesions.

Most of the lesions were seen in cerebral parenchyma, predominantly in frontal lobe, which was the commonest site involved (n = 20; 30.03 %) followed by occipital lobe (n = 14; 21.2%) and parietal lobe (n = 12; 18.1 %). Temporal lobe was the least affected region with only three cases (4.5%) reported.

There were three lesionsm each involving sella/ suprasellar region (craniopharyngioma, pituitary macroadenoma and pilocytic astrocytoma of optic chiasma) and cerebellopontine angle (two cases of schwannoma and one case of epidermoid cyst). There were two lesions (3.03%) located within the ventricles and basal ganglia. Lastly, there was one lesion involving thalamocapsular region, pons, right cerebellar hemisphere, right hippocampus, medulla, midbrain and pineal region each (1.9%). Ten patients had lesions in more than location (Figure 22).

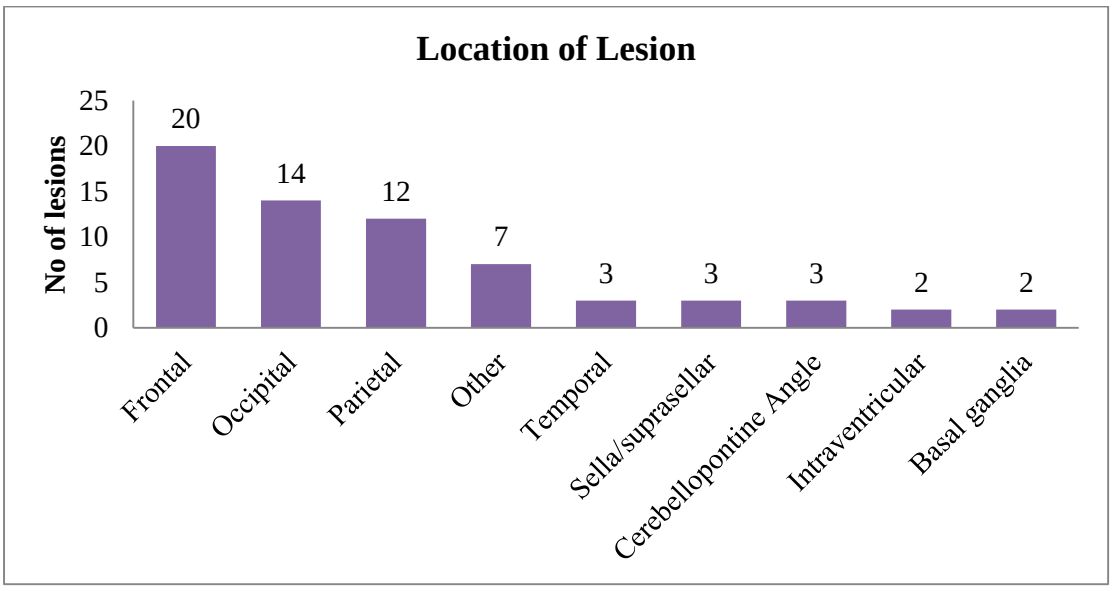

Figure 22. Location of lesions.

Majority of the patients presented with solitary ICSOL (n = 38, 57.5 %). Rest of the patients presented with multiple lesions (n = 14; 26.9%). There were two lesions in four patients, three lesions in five patients and more than three lesions in five patients.

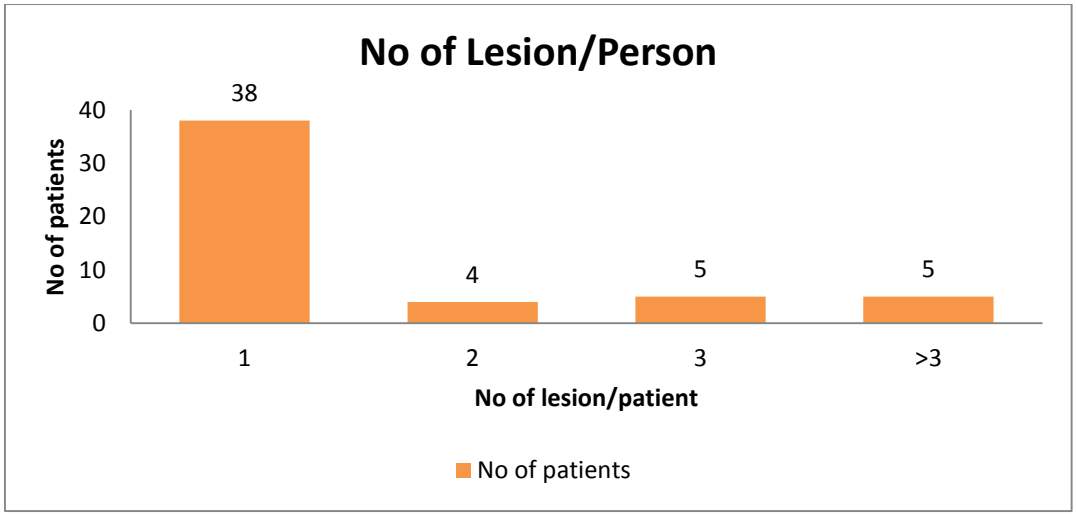

Figure 23. Distribution of lesions per patient.

Majority of the lesions encountered in the present study were of infective etiology (n = 26, 50%), followed by malignant lesions and benign lesions (n = 13 each; 25%).

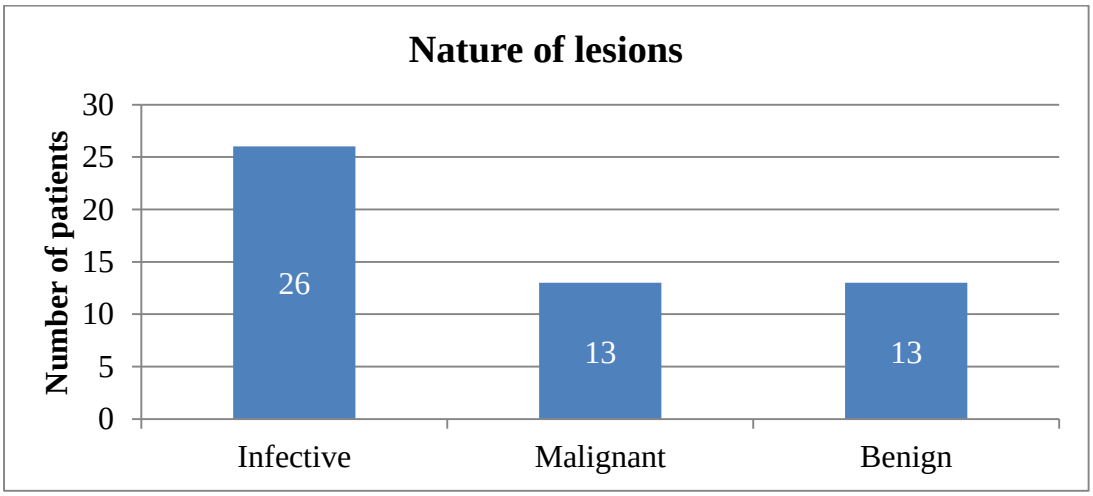

Figure 24. Nature of lesions.

Among patients presenting with NCC (n = 15), MRS findings reported were reduced NAA levels, elevated choline level and a Cho/Cr <1 (n = 10, 66.6 %). In remaining five cases (33.3%), MRS was inconclusive as their walls were partly calcified. All cases with tuberculomas (n = 5) showed Cho/Cr>1 and elevated lipid peak. There was one case with pyogenic abscess, which showed acetate, reduced NAA and increased choline peaks (Cho/NAA ratio <2.3).

Among the patients who had benign lesions (n=13, 25%), MRS findings were helpful in characterization of five lesions accurately. In radiation necrosis, MRS showed reduced NAA, Cho and other metabolites that was consistent with gliosis. In two cases of meningioma, though both cases showed absence of NAA, indicative of its non-neuronal origin, only one case showed characteristic Alanine peak. There was one case of epidermoid cyst, which on MRS, showed absent NAA with lactate peak. A case of craniopharyngioma showed broad lipid peak on MRS along with reduced NAA. In other cases, though the findings were not specific for the various benign entities, MRS was able to ascertain the non-neuronal nature (n-5, 38.4%) or benignity (n=1, 7.6%) of the lesions.

In all malignant lesions, MRS is effective in grading it as high grade lesions as MRS showed Cho/NAA >2.3.

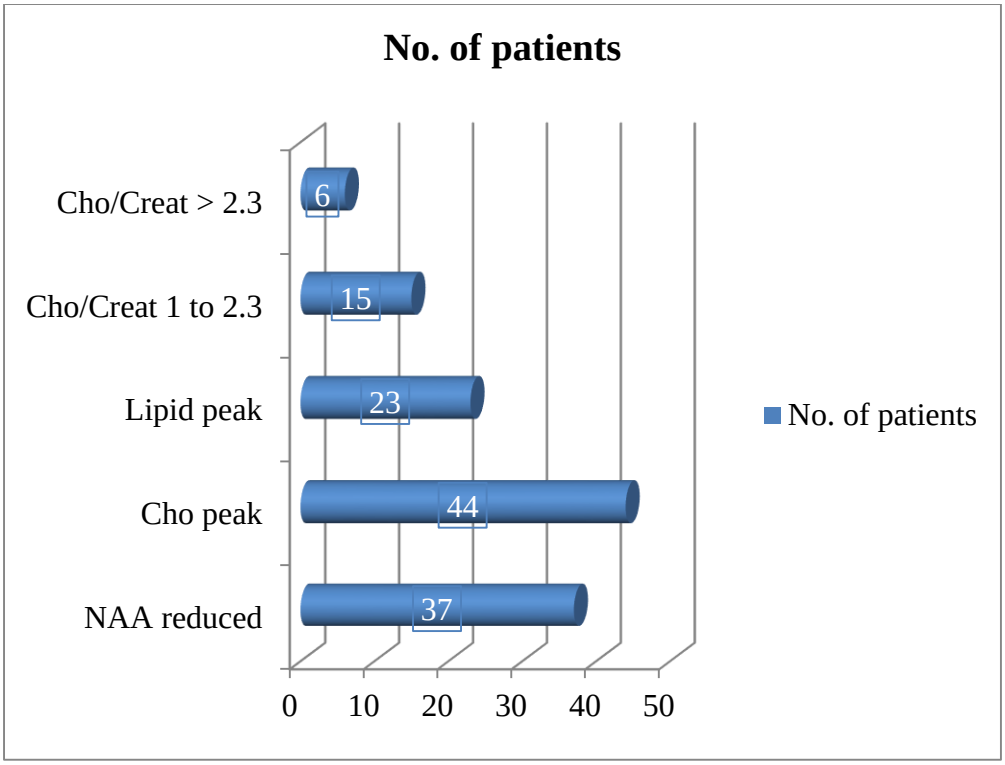

Figure 25. Demonstrating various metabolite activity in ICSOL

In this study, MRS helped in arriving at a definitive diagnosis in 40 patients (76.9%), narrowed differential diagnoses in seven patients (13.4%) and was not contributory in five patients (9.6%) as seen in Table 3 and Figure 26

Among infective lesions, MRS contributed to narrow down the conventional MRI diagnosis in 80.7% of patients (21 of 26 patients). MRS was not contributory in five patients with infective causes, as the lesions showed calcifications.

MRS helped in narrowing down the diagnosis by differentiating benign from malignant lesions, however was useful in categorizing the benign lesions in five patients (38%). In rest of the eight cases, MRS did not provide any additional information to narrow the diagnosis.

In the remaining 13 cases, MRS was helpful in diagnosing the lesion as malignant in 12 cases (one case was a known case of GBM with recurrence). MRS was also helpful in grading the aggressiveness of the lesion in the cases, which was determined based on Cho/Cr ratio >2.3 or <2.3, suggestive of high-grade or low-grade tumour respectively. The patient with GBM was included in the study, as the patient was already operated for the same and the study was performed to rule out recurrence of the lesion.

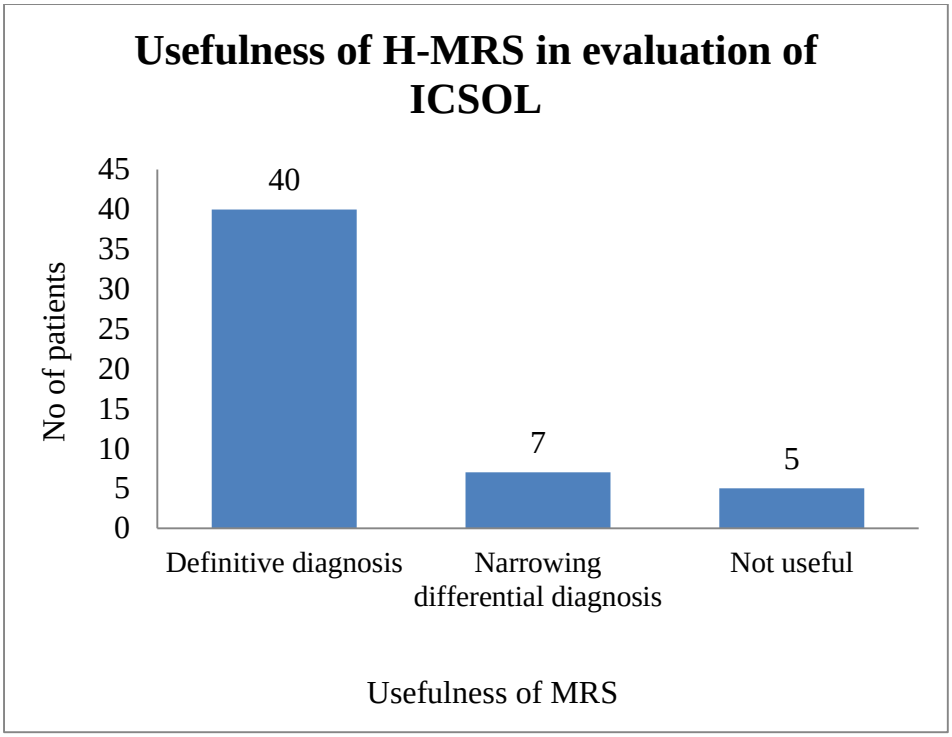

Figure 26. Usefulness of MRS in evaluation of ICSOL

Table 3. Contribution of MRS in final diagnosis of ICSOL

	MRS Contributory	MRS non contributory	Total
Infective	21 (80.7%)	5	26
Malignant	12 (92%)	1	13
Benign	5 (38%)	8	13

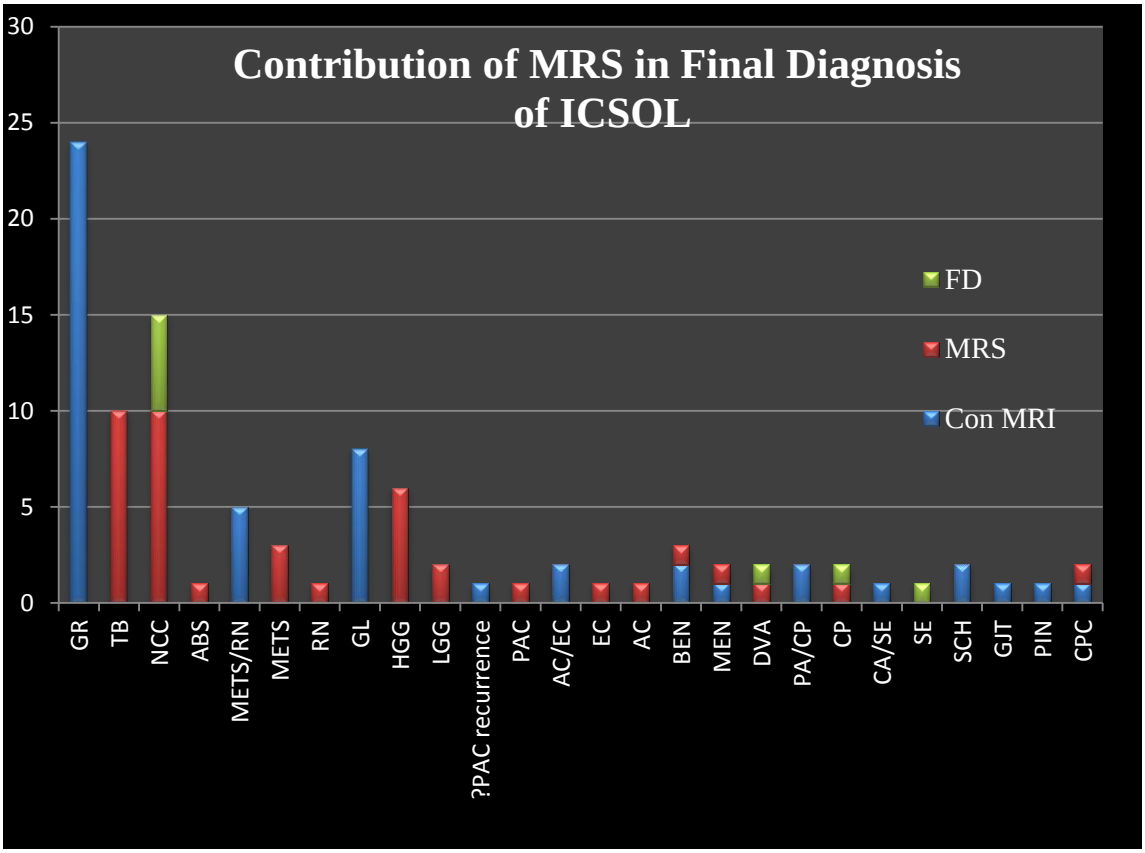

Figure 27. Contribution of MRS in final diagnosis

Conventional MRI may not provide specific diagnosis in granulomatous lesions, which was seen in 24 patients. Addition of MRS helped to narrow the diagnosis as NCC (n = 10 of 15) or tuberculoma (n = 9 of 9) in majority of the cases. In remaining 5 cases MRS was not contributory as the lesions showed calcification. There was one case of abscesses, which although showed features of abscess, could not be distinguished from pyogenic or fungal abscess. However, addition of MRS showed features suggestive of pyogenic abscess. Additionally, there was one case with MRI diagnosis suggestive of metastases in a patient with known case of carcinoma esophagus, post chemo-radiotherapy status. MRS findings showed features suggestive of tuberculoma. The patient was treated with anti-tubercular drugs and the condition improved. No further follow-up was done after 4 weeks.

There were five cases, which were suspicious of metastasis/radiation necrosis. MRS showed features of metastasis in three patients and one patient showed features suggestive of radiation necrosis and one case showed features suggestive of tuberculoma (discussed above).

There were eight cases, which were diagnosed with glioma on MRI. MRS findings were helpful in grading the lesions into high-grade and low-grade based on Cho/Cr ratio >2.3 or <2.3 respectively.

There was one case of suspected pilocytic astrocytoma recurrence, who presented for follow-up. MRI features were suggestive of pilocytic astrocytoma. MRS helped to confirm the diagnosis of anaplastic pilocytic astrocytoma involving optic chiasma.

There were two cases in which conventional MRI provided the differential diagnoses of arachnoid cyst versus epidermoid cyst. MRS was helpful in differentiating the two lesions based on presence of lactate peak in epidermoid cyst, which is not seen in arachnoid cyst. Based on MRS findings one case was diagnosed with arachnoid cyst and another case as epidermoid cyst.

There were two cases, which did not have any specific findings and were classified as benign tumours on conventional MRI. MRS additionally picked up one more lesion, which was benign in morphology; however, MRI was not helpful in differentiating these lesions. These three cases were meningioma (n = 2) and developmental venous anomaly (n = 1). Conventional MRI was able to pick up on case of meningioma successfully; however, it missed one more case, which was diagnosed based on MRS findings (absence of NAA and alanine peak). One case of DVA was classified as benign intraxial tumor on conventional MRI; however it was diagnosed based on MRS finding (absence of NAA, suggestive of non-neuronal origin). Further evaluation with MR venogram (T1 WI postcontrast) was done for confirmation in this case.

There were two cases, which features suggestive of a locally aggressive sellar/parasellar lesion. On conventional MRI, a differential diagnosis of aggressive pituitary macroadenoma versus craniopharyngioma was given. MRS showed reduced NAA, predominant Cho peak and broad lipid peak in one of the lesions, which was suggestive of craniopharyngioma, hence contributing to final diagnosis. The other case did not show any specific MRS features to differentiate. On dynamic contrast imaging the lesion showed delayed homogenous enhancement of the lesion which was suggestive of pituitary adenoma, which was given as final diagnosis and the patient's hematological reports were also in concurrence with pituitary adenoma.

MRS yielded nonspecific data in other benign entities such as subependymoma, glomus jugalare tumor, acoustic schwannoma and pineocytoma; thus not providing additional information to conventional MRI for arriving at a definitive diagnosis.

IMAGES

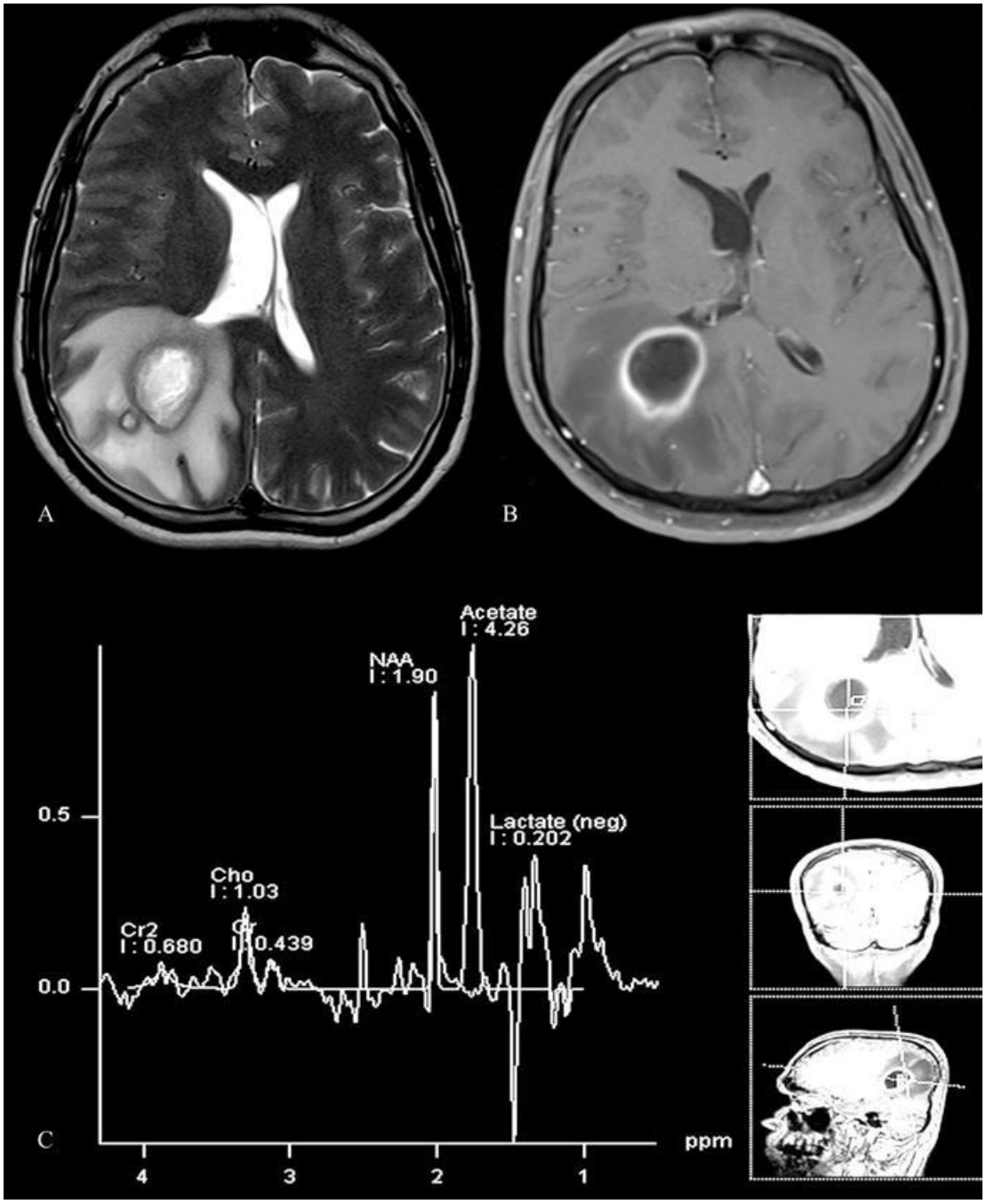

Figure 28: A 42 year old male patient with fever and seizures. (A) T2 axial (B) T1 FS axial post contrast, shows ring enhancing rounded cystic lesion in parieto-occipital region with perilesional edema (C) On MRS, there is acetate peak suggestive of pyogenic abscess.

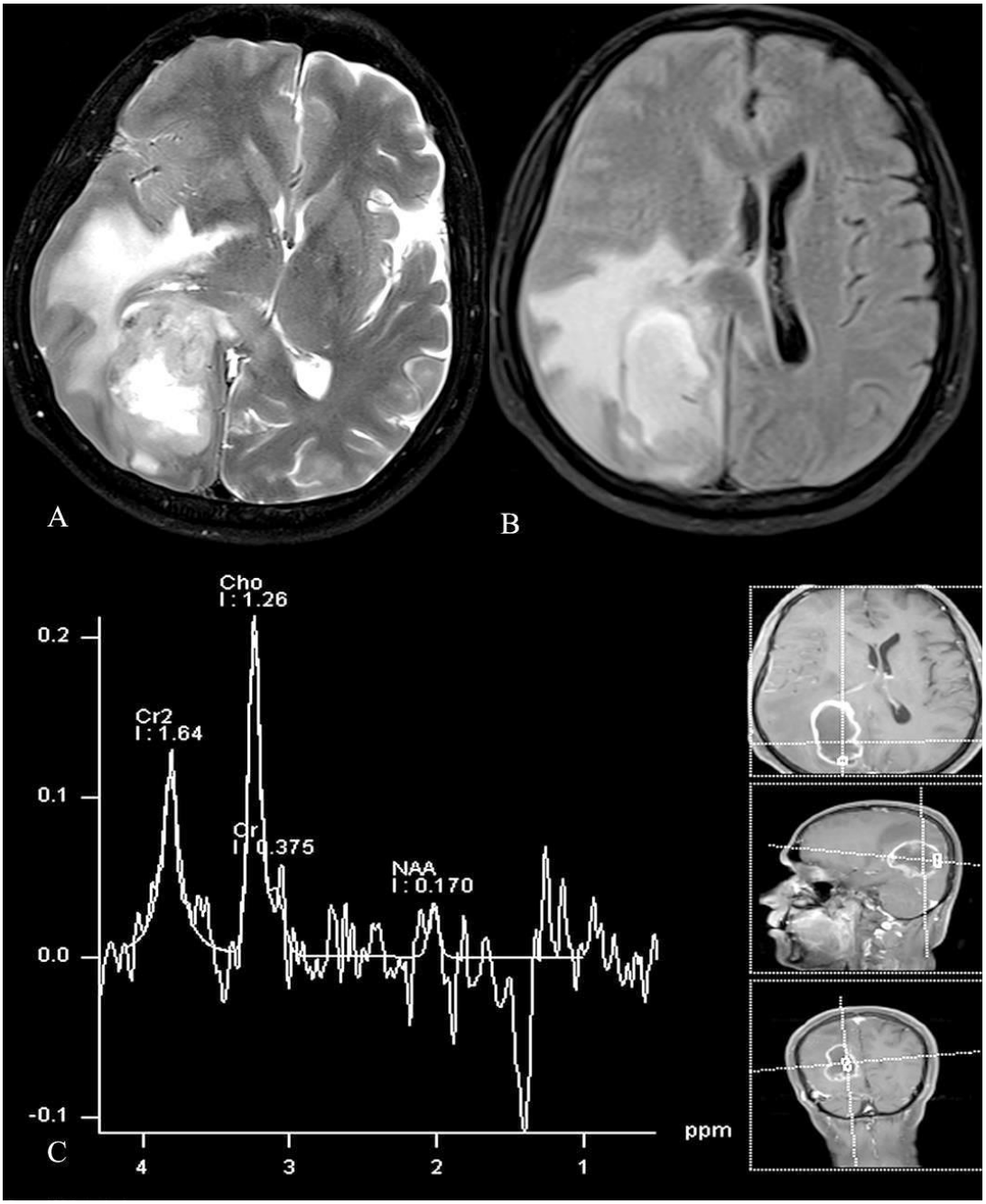

Figure 29: A 61 year old male patient presented with headache (A) T2 axial (B) FLAIR axial images showing heterogeneously hyperintense mass lesion in right parieto-occipital region with significant perilesional subcortical white matter edema (C) On MRS, there is reduced NAA, increased Cho and Cho/Cr ratio>2.3, suggestive of high grade glioma

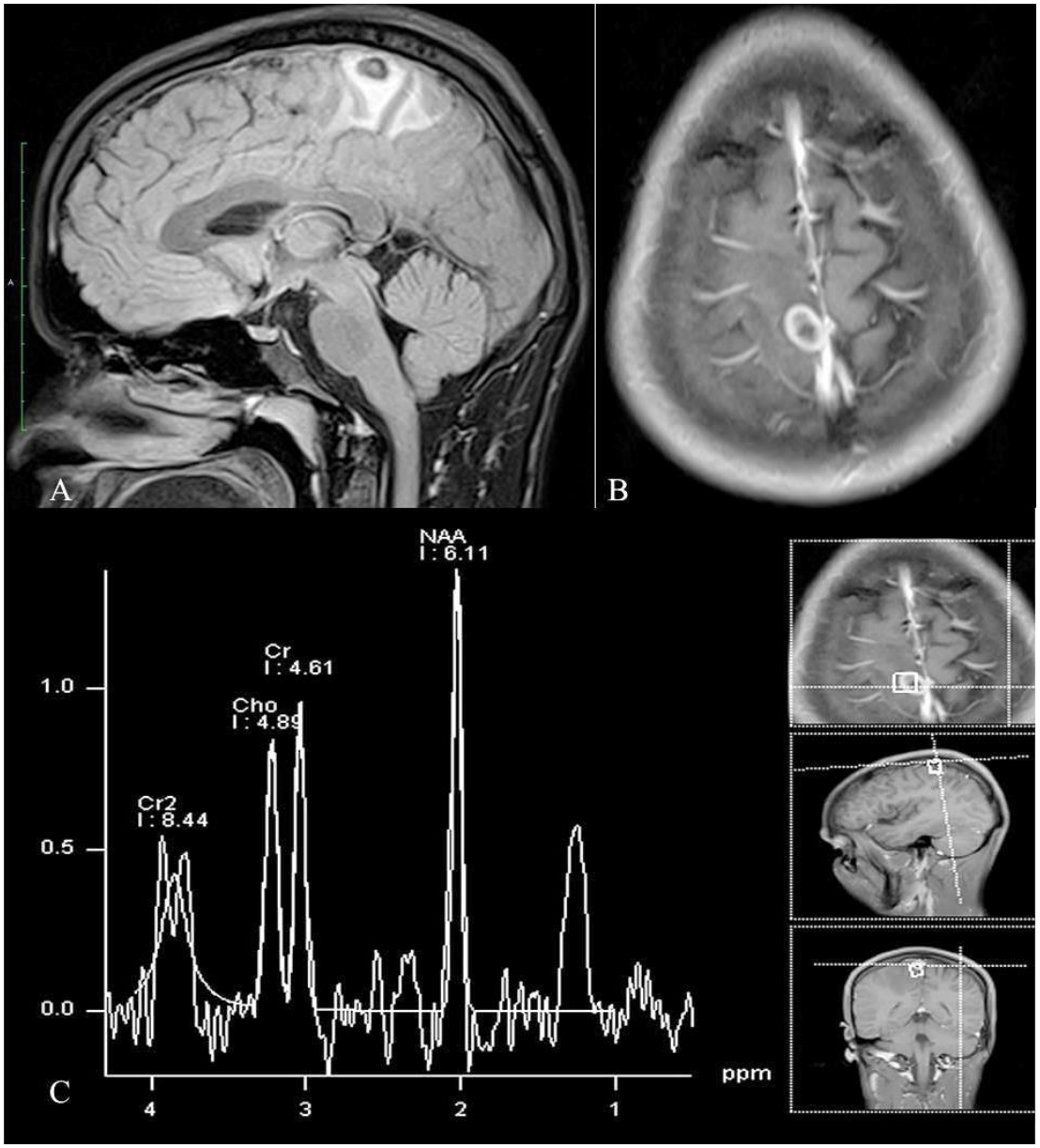

Figure 30: A 22 year old male patient who presented with seizures (A) FLAIR sagittal (B) T1 postcontrast FS axial, shows subcentimetric ring enhancing lesion in left high parietal region and (C) MRS demonstrates mildly reduced Cho, absent lipid peak and Cho/ Cr ≤ 1, suggestive of neurocysticercosis

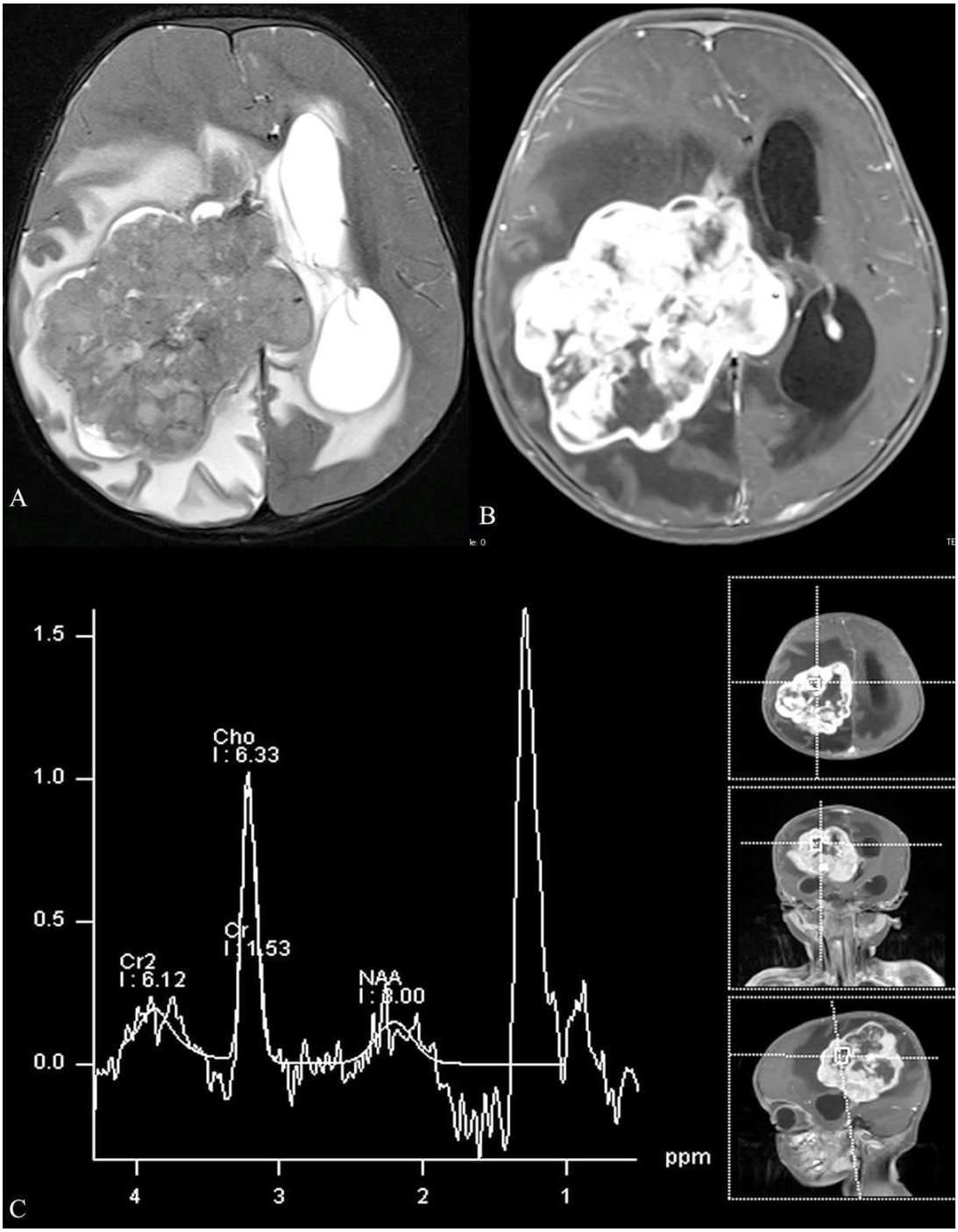

Figure 31: A 1 year old male child presented with seizures. (A) T2WI axial (B) T1 FS post contrast axial sections show heterogeneously enhancing T2 hyperintense intraventricular mass lesion (C) MRS demonstrating decreased NAA, increased choline, Cho/ Cr >2.3, suggestive of high grade neoplasm.

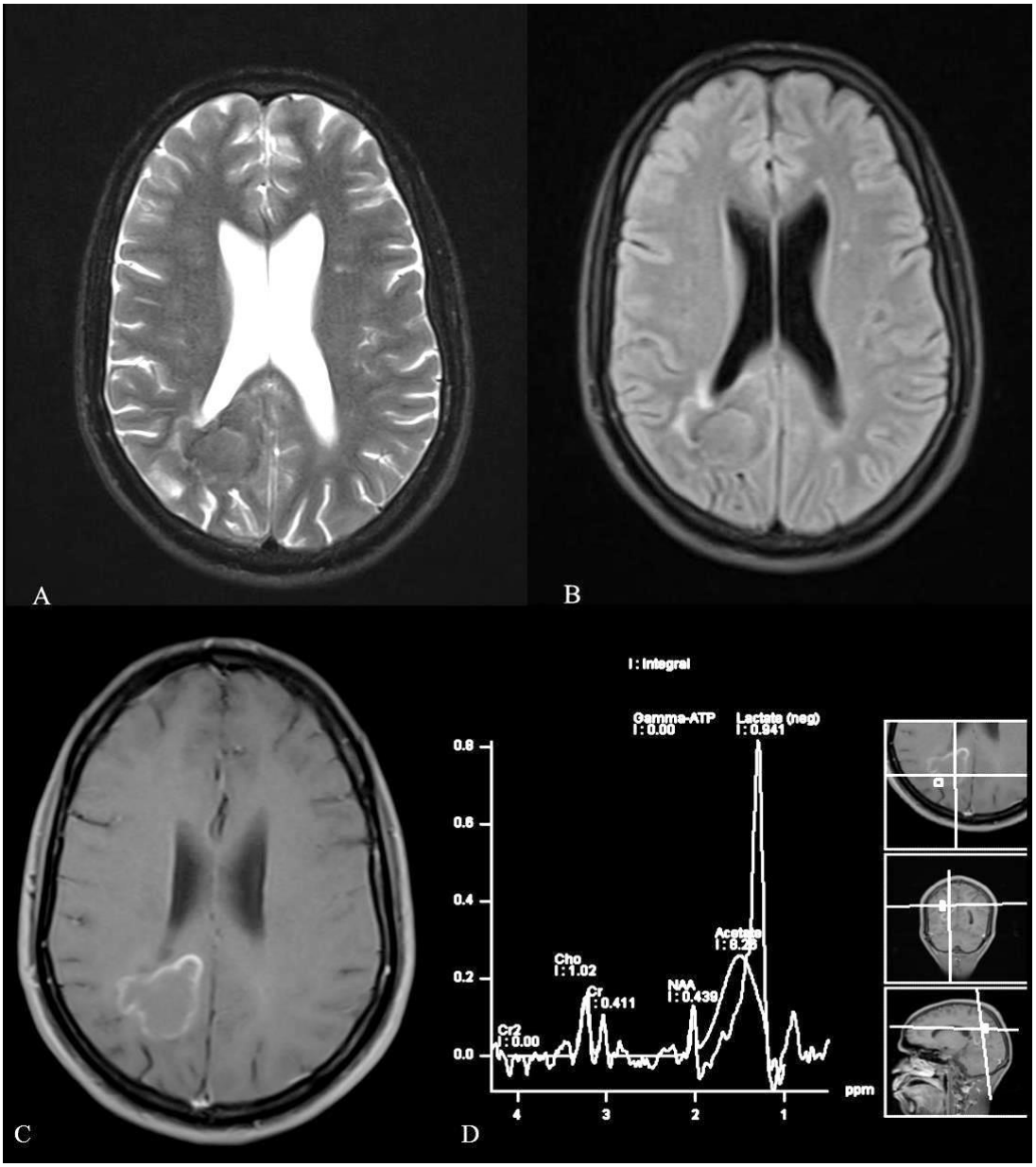

Figure 32: A 32 year old male presented with new onset seizures (A) T2WI axial (B) FLAIR axial (C) T1FS post contrast shows a ring enhancing lesion in right periventricular occipital white matter region with T2 hypointense signal intensity (D) MRS demonstrating reduced NAA, and large lipid/lactate peak and Cho/ Cr > 1, suggesting a tuberculoma.

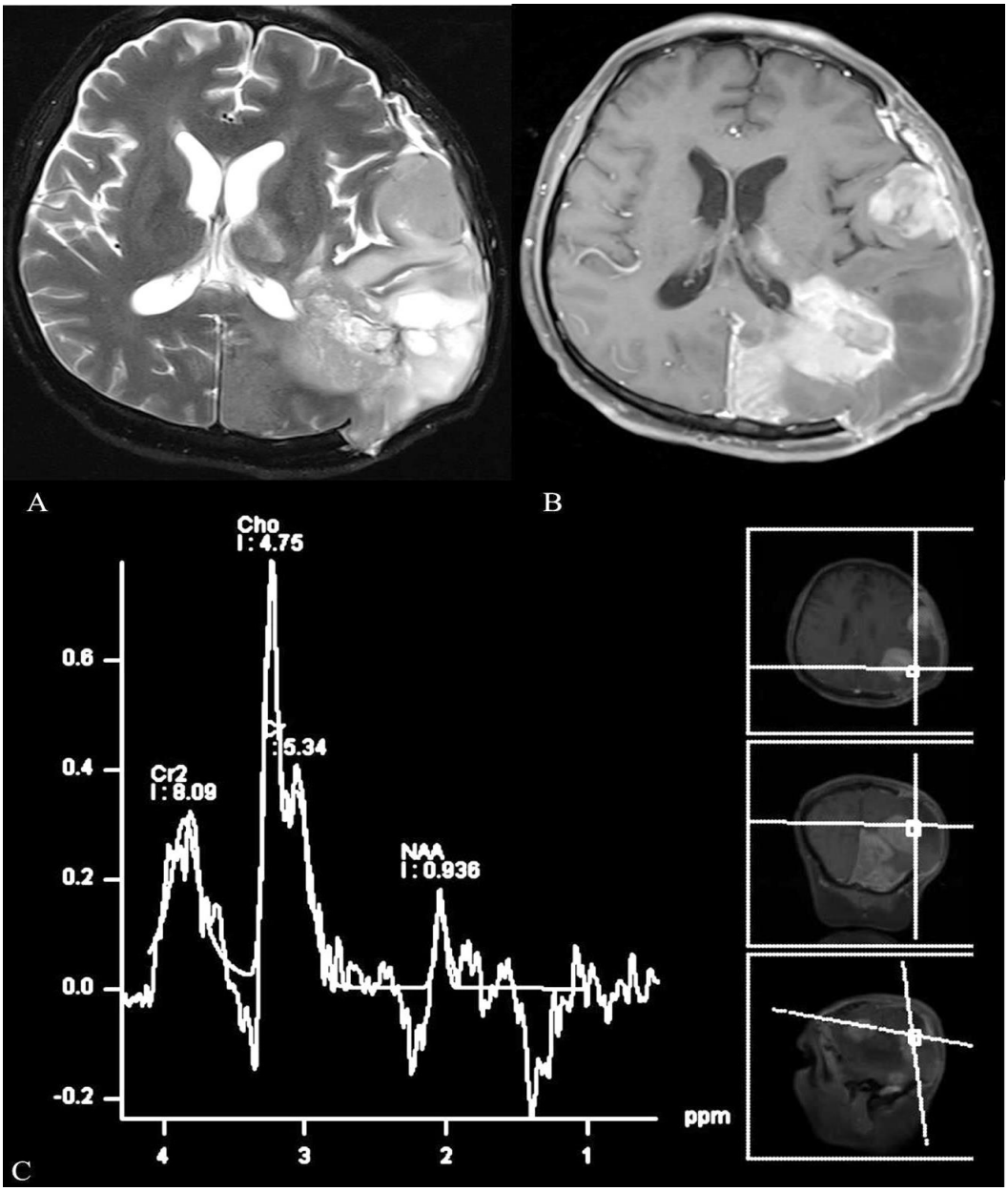

Figure 33: A 39-year-old male patient K/c/o GBM, post craniectomy, neoadjuvant chemo and radiotherapy present with headache (A) T2WI axial (B) T1FS post contrast demonstarting heretogeneously enhacing T2 hyperintense lesion invovling left parieto-occipital region. (C) MRS shows reduced NAA with predominnet choline peak suggesting a recurrent lesion.

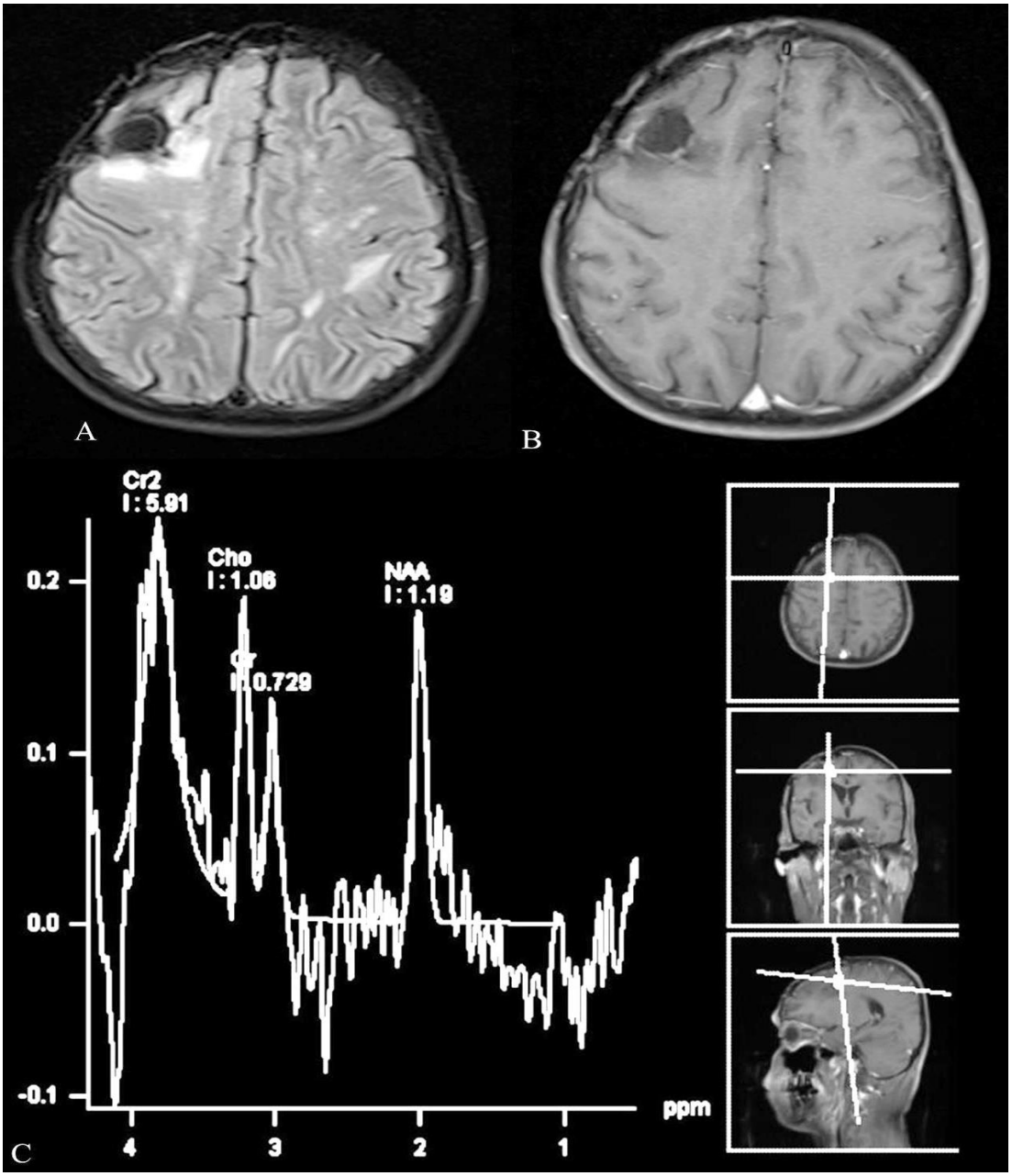

Figure 34: A 37 year old male patient Follow up c/o anaplastic oligodendroglioma, post-surgical and radiotherapy status (A) FLAIR axial (B) T1FS post contrast axial sections showing mild peripherally enhancing hypointense lesion in right frontal region with mild perilesional edema (C) MRS demonstrating normal NAA and Cho/ Cr ratio within the lesion and in perilesional edema, suggestive of radiation necrosis.

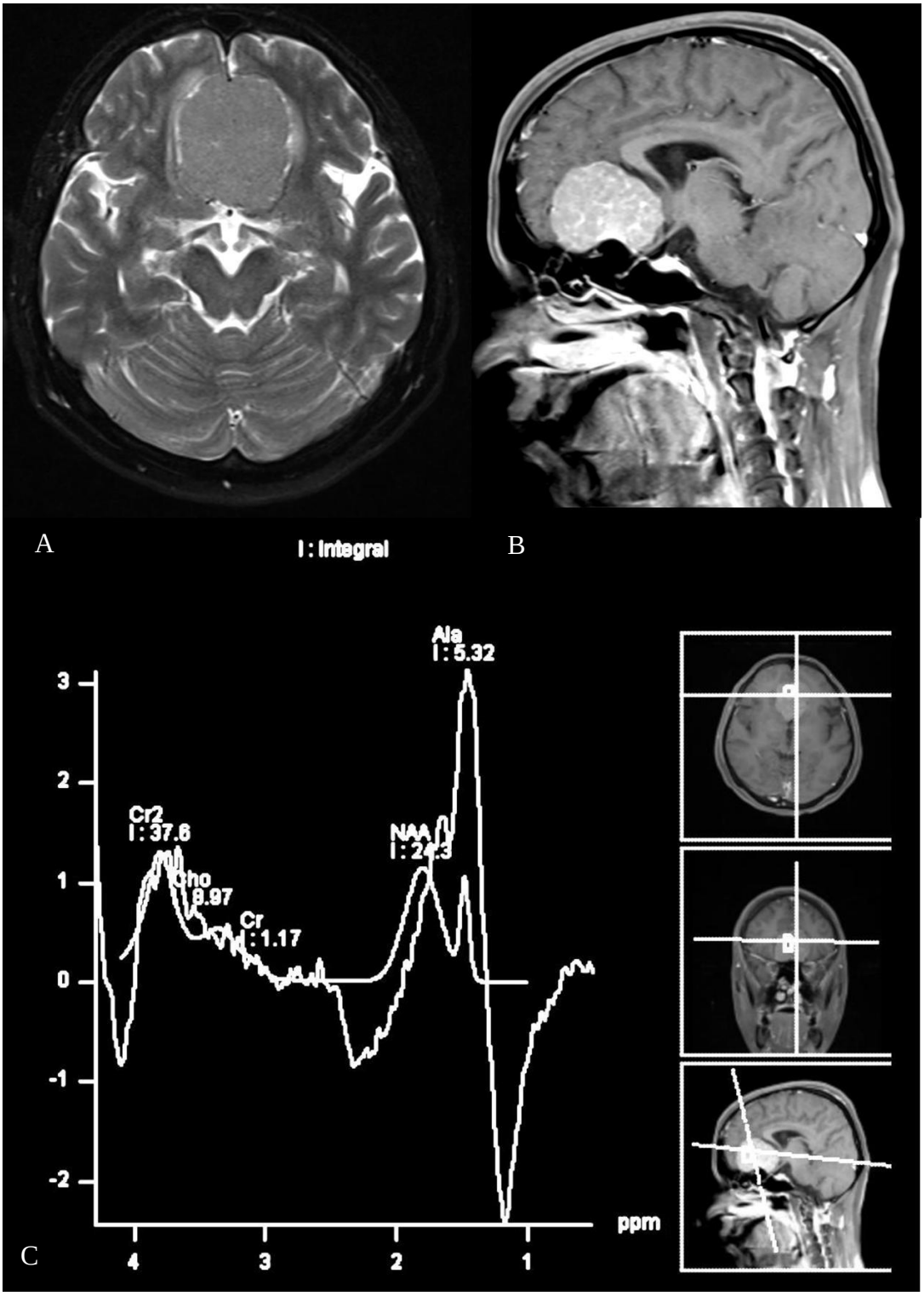

Figure 35: A 45 year old female patient presented with headache (A) T2 Axial (B) T1 FS post contrast sagittal images showing a large extra-axial homogenously enhancing mass lesion in midline frontal region (C) MRS shows reduced NAA and Alanine peak, suggestive of meningioma

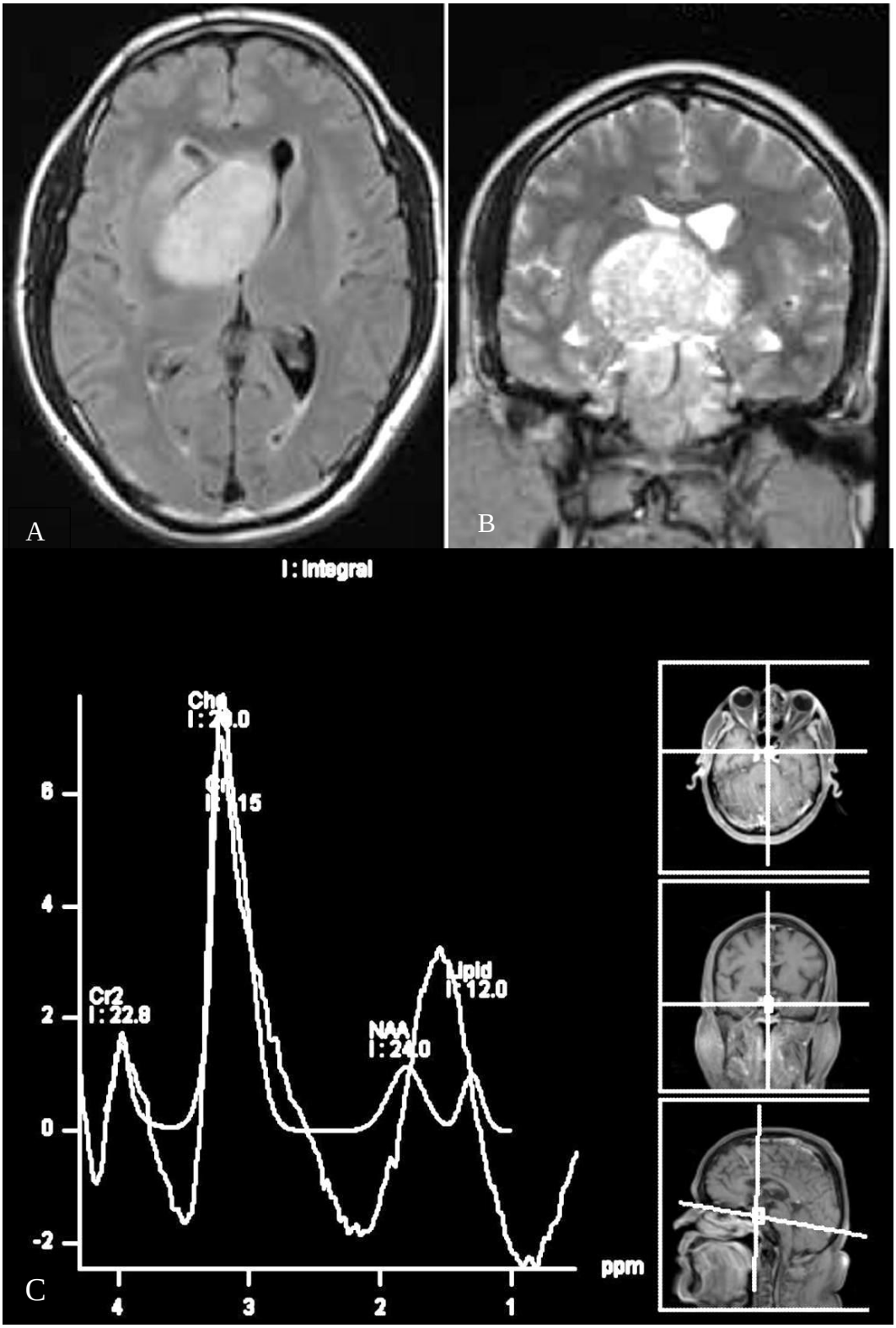

Figure 36: A 50 year old male patient presented with blurring of vision (A) FLAIR axial (B) T2 coronal image showing revealed relatively hyperintense sellar SOL with supra-sellar extension (C) MRS shows predominant peak of Cho, reduced NAA and broad Lip peak, suggestive of craniopharyngioma

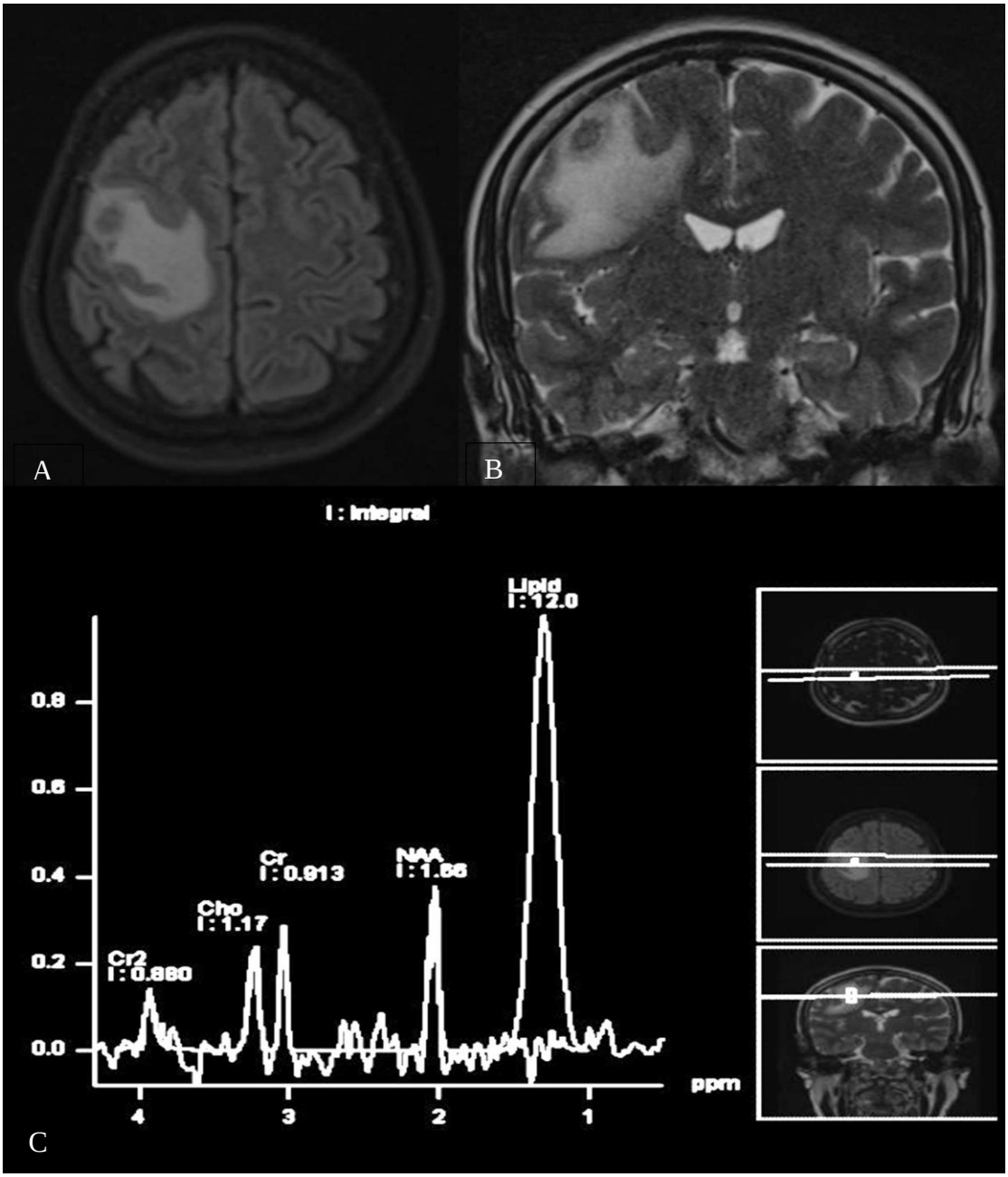

Figure 37: A 50 year old female patient, K/c/o oesophageal carcinoma post chemo radiotherapy status presented with seizures (A) FLAIR axial (B) T2WI coronal showing a hypointense mass lesion in high right fronto-parietal region with perilesional edema (C) mildly reduced NAA, lipid peak with Cho/ Cr =1.3, suggesting tubercular etiology.

DISCUSSION

This study included a total of 52 patients. The most commonly involved age group were patients belonging to age group of 31 to 50 years (n = 18; 34.6%) followed by 51 to 70 years (n = 13; 25 %) and < 18 years (n = 11; 21.1%). The least commonly presenting patients belonged to age group of >70 years (n = 3; 5.7 %). The age group from 31 to 70 years constituted more than 59.6 % of the patients.

Our findings are consistent with a cross-sectional observational study by Butt et al who studied the incidence of ICSOL in all age groups and found that it occurs more commonly in 4th and 5th decade[89].

In our study, we observed slight male preponderance (57.6 %). This is in agreement with retrospective study done by Soomro et al, who also reported a similar male preponderance in their study[90].

Chief clinical symptom associated with ICSOL is seizures (n = 27, 41.9%), closely followed by headache (n = 24, 46.1%). Our results are in contrast to the clinical symptoms observed by other studies. A review by Ramamurthi et al on prevalence of ICSOL on 200 patients, found that majority of the patients presented with headache[91].

The difference in clinical presentation in our study is probably because we have included patients who were diagnosed as ICSOL by conventional MRI. Not all patients with smaller / asymptomatic ICSOL or mild headache may have undergone MRI in our setup, and this may have resulted in more patients with seizures as chief clinical complaint in our study

In our study, we observed that solitary lesions (n=38, 57.5 %) are more common than multiple lesions. Our findings are similar to findings reported in Indian populations where nearly half of the patients with ICSOL had solitary lesions (n = 49; 48.5%)[92].

In our study, frontal lobe was the commonest location (n = 20; 30.03 %). Similar finding was reported by Pandey et al, who observed that more than 31% were seen in the frontal lobe[93].

In our study, neurocysticercosis (n=15, 28.8%) was the most common pathology followed by tuberculoma (n=10, 19.2 %), high grade glioma (n=6, 11.5%), metastases (n=3, 5.7 %) and low grade glioma (n=2, 3.8%). Radiation necrosis, developmental venous anomaly, pilocytic astrocytoma, pineocytoma, subependymoma, choroid plexus carcinoma and pyogenic abscess were seen in one patient each. Extraaxial lesions included two cases of meningioma, epidermoid cyst, arachnoid cyst, pituitary macro adenoma, craniopharyngioma, acoustic schwannoma and glomus jugalare tumor.

Our results are in agreement with Yashodhara et al who in their study of 40 patients found 24 patients (60%) had NCC, followed by tuberculoma (n = 8; 20%), neoplasms in 12.5% (n = 5), and calcified granuloma, arachnoid cyst and brain abscess were found in one patient each (2.5%)[94].

In the present study, majority of the lesions were to be infective in nature (n=26, 50%). Malignant (n=13) and benign (n=13) lesions constituted remaining 25% each.

NCC

Out of the 26 infective lesions encountered in the study, NCC (n = 15, 57%) were the commonest. All the cases showed intraparenchymal forms of NCC and scolex was identified in 8 cases. All the lesions were hypo- to isointense on T1 weighted images and 12 cases were hyperintense on T2 WI. Out of these 12 lesions, nine lesions showed inversion on FLAIR suggesting that the contents are similar to that of CSF. Intense ring enhancement with surrounding perilesional edema was seen in 10 cases, suggestive of active lesions.

Most of NCC lesions (n=10) showed reduced NAA, increased choline and Cho/ **Cr** <1. Features of parenchymal forms of NCC in our study are similar to the study done by do Amaral et al[95]

.Cho / Cr ratio was less than 1.1 in all active lesions in our study. This finding is in agreement with data reported from other studies[96,97,98]. MRS was inconclusive in remaining 5 cases as their walls were partly calcified.

Tuberculoma

Out of fifty two patients evaluated, tuberculomas were seen in 10 (23.8%) of cases. Solitary lesion was noted in eight patients and multiple lesions were seen in two cases. The multiple lesions were seen as conglomerate lesions hypointense on both T1 and T2 WI. On T1 WI the lesions showed iso- to hyperintense ring which was seen in 60% cases in our study. Follow up scan (CT/MRI) was performed in six patients, who showed resolution of the lesion as well as perilesional oedema.

Tuberculomas may show a nodular or irregular ring like enhancement. All our cases presented with presented with ring enhancement. Additionally, nodular enhancement was also seen in two cases. MRS showed a lipid peak in nine cases and Cho/Cr>1 in all cases. Lipid peak is important as it helps in differentiation of tuberculomas from other infective granulomas. T2 WI helps to identify the stage of tuberculomas (caseous or non caseous stage). Post contrast images are helpful in identifying size of tuberculomas and help differentiate granuloma from surrounding edema.

Kim et al demonstrated that tubercular granulomas have a slightly hyperintense rim on T1 WI. On T2 WI, tubercular granulomas have slightly heterogeneous isointense or hypointense signal with small markedly hypointense foci. On postcontrast T1 WI, tuberculomas showed single or multiple conglomerate ring enhancements[99].

Additionally, Jayasundar et al reported that presence of lipid could be used for differentiating tuberculomas from both non-specific infectious granulomas and NCC[96].

Gliomas

In our study, glioma cases were reported as low grade or high grade, according to the MR characterization of tumors. Both conventional sequences and different parameters of MR spectroscopy was optimized for better results. Glioma constituted 15% of cases (n = 8) and was the commonest brain neoplasm in our study. Conventional MRI showed heterogeneous lesions with both solid and necrotic components in all the cases. Additionally, 7 out of 8 (87.5%) cases demonstrated perilesional edema. Of 8 cases of gliomas, 6 were classified as high grade and 2 cases as low grade glioma based on the MRS findings. All cases showed moderate to intense enhancement.

High grade gliomas exhibited decreased levels of NAA & creatine, elevated choline peak with Cho/ Cr ratio > 2.3. Four cases also showed a lipid peak. All low grade gliomas showed similar findings, however the Cho/Cr ratio was <2.3.

MRI findings were correlated with histopathology of the tumor in 7 out of 8 cases. Histopathology was not done in one case of brainstem glioma.

Our findings are in agreement with findings reported by Felix et al, who demonstrated that gliomas show heterogeneously hyperintense signal intensity on T2 WI, cystic/necrotic core and perilesional edema[100].

The MRS findings seen in our study are in agreement with findings reported by Spampinato et al who evaluated MRS in high- and low-grade gliomas. They reported that a significantly higher Cho/Cr ratio (p =0.002) in high-grade than in low-grade tumors. A Cho/Cr ratio cut off value of 2.33 had the highest accuracy in identification of high-grade tumors, which was also taken as cutoff in our study. Thus, MRS is helpful in differentiating low-grade from anaplastic oligodendroglial tumors[101].

Metastasis

There were three patients with metastasis in our study, which were observed in 4th and 7th decade. On conventional MR, the lesions appeared heterogeneous-to-hypointense on T1 WI and heterogeneously hyperintense on T2 WI, with perilesional edema. The lesions were ill-defined, and showed intense ring enhancement on post contrast T1 WI.

On MRS, there was strong Cho peak without elevation in surrounding peritumoral edema, reduced NAA and Cr with increased lipid/lac peak in one of the tumors. There was increased Cho/ Cr ratio > 2.3, increased Cho/NAA ratio of 3.5 and reduced NAA/Cr peak at 0.8. Cho/cr ratio was not elevated in peritumoral edema.

Our findings are in agreement with study by Law et al who reported elevated choline levels (choline-to-creatine ratio was 2.28 ± 1.24) in the peritumoral region of gliomas but not in metastases (choline-to-creatine ratio was 0.76 ± 0.23)[102]. This finding was considered as key differentiating factor for diagnosis of gliomas and metastasis.

Abscess

In our study there was one case of cerebral abscess in middle aged male patient who presented with fever and seizures. On conventional MRI, T1 hypointense and T2/ FLAIR hyperintense ring enhancing lesion was seen in right frontal lobe. MRS showed presence of acetate peak, which was suggestive of pyogenic abscess. There was resolution of symptoms following conservative medical management and no further imaging studies were warranted.

Our results were in agreement with study done by Pal et al who reported that presence of amino acids is a sensitive marker of pyogenic abscess, but its absence does not rule out a pyogenic etiology[103].

The presence of acetate ± succinate favors an anaerobic bacterial origin of the abscess; however, this may also be seen in some of the abscesses secondary to facultative anaerobes[103].

Radiation necrosis

In our study, there was one case of radiation necrosis in middle aged male patient who underwent surgery and radiotherapy for anaplastic oligodendroglioma and presented with seizures. There was a T1 hypointense and T2 mildly hyperintense lesion with no peritumoral edema. On MRS there was slight reduction in NAA with absent Cho peak was observed. FDG PET CT showed low uptake and confirmed the diagnosis of radiation necrosis.

Our results are in agreement with findings reported by Smith et al. who reported that Cho/NAA ratio has sensitivity of 85%, a specificity of 69% for differentiating between recurrent tumor and radiation necrosis. They reported that an elevated Cho/NAA ratio correlated with evidence of tumor recurrence and allowed creation of a prediction rule to aid in lesion classification, whereas unchanged Cho/NAA ratio was suggestive of radiation necrosis. The authors concluded that MR spectroscopy is a useful tool in assigning patients with nonspecific enhancing lesions to either invasive biopsy or conservative management[104].

Craniopharyngioma

In our study, there was one case of craniopharyngioma, who was 50 year old male patient who presented with headache and visual disturbances. On conventional MRI, there was heterogenous T1 hypo and T2/ FLAIR hyperintense lesion in sella. On MRS, there was absent NAA, moderate Cho peak and broad lipid peak.

Our result was similar to prospective study done by Mohammad et al who reported significant reduction of the NAA peak, predominant Cho peak and broad lipid peak[105].

Meningioma

In our study, we had two patients with meningioma. On conventional MRI, the lesions were T1 isointense and T2 hyperintense with dural tail sign seen on post contrast images. MRS showed absent NAA in both the cases. However, only one of these cases showed characteristic alanine peak on MRS. This may be probably due to extensive calcifications present within the mass resulting in inconclusive MRS findings.

Our findings are in agreement with data by Kinoshita et al, who found that though alanine was not invariably present in meningioma, alanine was present in meningioma, glioma, and pituitary adenoma. NAA is absent in meningioma confirming its extra-axial origin.[106].

Epidermoid Cyst and Arachnoid cyst

In our patients we had two patients who presented with extra-axial non neoplastic cysts. On conventional MRI, probable diagnosis was given as epidermoid or arachnoid cyst. On MRS, one of the lesions showed the presence of lactate peak with absent NAA, thus providing the final diagnosis of epidermoid cyst in one patient and the other case was diagnosed with arachnoid cyst.

Ping –Hong et al demonstrated that lactate was observed in epidermoid cyst and could be differentiated from arachnoid cysts[107], which formed the basis of differentiating epidermoid and arachnoid cyst in our study.

Others

In our study, we had two cases of acoustic schwannoma, one case of each of glomus jugalare tumor, pineocytoma and craniopharyngioma. The MRS graph obtained in these patients did not contribute to conventional MRI in the final diagnosis.

This may be due to spectroscopy data obtained at constant TE and TR Perhaps modifying TE and TR values could have yielded better results, thus contributing to the final diagnoses.

Ideally, both long TE and short TE sequences are required to be done as the short TE sequence can pick up metabolites such as myoinositol, glutamate complex, lipid, for confirming alanine peak at around 1.48 ppm which lies below the baseline at long TE and above the baseline at short TE and for confirmation of lactate peak at 1.32 ppm which lies below the baseline at long TE and above the baseline at low TE[108]. Acoustic schwanomma has been shown to have myoinositol peak.

Glomus jugulare tumor, pineocytoma and pituitary adenoma do not have any specific MRS findings. However, MRS may be employed in the evaluation as it helps to rule out other causes.

Our study had certain limitations. MRS could not be performed in four lesions due to presence of lesion close to the bone. MRS is not sensitive especially for evaluating lesions which are close to bone. Additionally for the diagnosis only conventional sequences were used. Use of advanced sequences like DWI and MR perfusion were not included in the study. These techniques are also useful in differentiation of neoplastic and non-neoplastic lesions. For example, a case of epidermoid can be diagnosed by presence of restricted diffusion on DWI.

CONCLUSION

In our study, MRS was helpful in evaluation of infective lesions and malignant lesions. It also helped to differentiate low-grade and high-grade gliomas. It could demonstrate the presence of intra- and extra-axial lesions. MRS provided additional information about the biochemical components of the tissue evaluated.

This information provided additional support to the imaging diagnosis and also grade tumours whenever possible. It thus a valuable adjunct to structural imaging with MRI, and helps increase the confidence level of giving the imaging diagnosis of a lesion in the brain. We conclude that MRS be employed in evaluation of ICSOL as in addition to helping in arriving at correct diagnosis, it may also help in ruling out potentially severe lesions such as metastasis and high-grade tumours, thus guiding appropriate treatment and management.

SUMMARY

The "gold standard" for diagnosis of any lesion is by histopathology. Obtaining tissue sample of intracranial lesions requires craniotomy / burr hole and has a definite risk of morbidity and even mortality. H-MRS is an advanced MR imaging technique that gives us information of the biochemical characteristic of a lesion. Additional information obtained by MRS may help in preoperatively establishing the diagnosis or narrowing the differential diagnosis.

In this study out of 52 cases, 43 were intra-axial lesions and 9 were extraaxial. In the present study, majority of the lesions were to be infective in nature (n=26, 50%). followed by malignant (n=13) and benign (n=13) lesions constituting 25% each.

Chief clinical symptom associated with ICSOL was seizures (n = 27, 41.9%), closely followed by headache. Most of them were solitary lesions located within the cerebral parenchyma, predominantly in frontal lobe.

In this study, MRS helped in arriving at a definitive diagnosis in 40 patients (76.9%), narrowed the diagnosis in seven patients (13.4%) and was not contributory in five patients (9.6%).

MRS helped in differentiating among the granulomatous lesions. NCC, showed reduced NAA levels, elevated choline level and a Cho/Cr<1 and tuberculomas showed Cho/Cr>1 and elevated lipid peak. It helped in establishing the etiology of intracranial abscess as pyogenic abscess, as it showed acetate peak.

Among benign lesions (n=13), MRS findings were helpful in definitive characterization of five lesions, which included radiation necrosis (reduced NAA, Cho and other metabolites, consistent with gliosis), meningioma (absent NAA and characteristic Alanine peak), epidermoid cyst, (absent NAA with lactate peak) and craniopharyngioma (broad lipid peak along with reduced NAA).

Among malignant lesions, MRS was very helpful in grading the aggressiveness of the lesion, which was determined based on Cho/Cr ratio >2.3 or <2.3, suggestive of high-grade or low-grade tumour respectively.

We conclude that in patients undergoing MRI brain for diagnosis of intracranial space occupying lesions, MRS sequence can be a significant adjunct to conventional MR imaging and plays an additive role in effective diagnosis of such lesions.

BIBLIOGRAPHY

1. Kaki RR, Anuradha B, Rani BS, et al. Imaging of intracranial space occupying lesions- A prospective study in a tertiary care centre, A.P. J. Evid. Based Med. Healthc. 2017; 4(11), 617-623

2. Buckner JC, Brown PD, O'Neill BP, et al. "Central Nervous System Tumors." Mayo Clin Proc. 2007; 12(10):1271-86

3.Sachdeva V, Kataria S, Singh VJ, Kukkar V, Bilandi A. Magnetic Resonance Imaging [MRI]: A boon to biomedical diagnostic imaging technology International Journal of Universal Pharmacy and Life Sciences. 2012;2, 382-393

4.Bulakbasi N. Clinical applications of proton MR spectroscopy in the diagnosis of brain tumors. Spectroscopy 2004; 18(2): 143-145

5.BB Yeole. Trends in the Brain Cancer Incidence in India. Asian Pacific J Cancer Prev,2008; 9, 267-270

6.Moore K, Persaud T, Torchia M. The developing human. 10th ed. Philadelphia, PA: Elsevier; 2016.

7.Standring S, Gray H. Gray's anatomy. 41st ed. [Edinburgh]: Churchill Livingstone/Elsevier; 2016.

8.Butler P. The skull and brain. In: Butler P, Mitchell A, Harold E, editors. Applied radiological anatomy for medical students. 1st edition. Cambridge University Press, NY. 2007;64-80.

9. Moeller TB, Reif E. Pocket Atlas of Sectional Anatomy Volume I: Head and Neck. 3rd edition. Thieme. Stuggart. Pg. 2-43

10. McCulloch ML. MRI Historical Background. Methodist Debakey Cardiovasc J 2009;5:13-4.

11. Hoeffner EG, Mukherji SK, Srinivasan A, Quint DJ. Neuroradiology Back to the Future: Brain Imaging. AJNR Am J Neuroradiol 2012;33:999–1006.

12. Nakamura T, Yabe Y, Horiuchi Y, Takayama S. Magnetic resonance imaging In brain. J Bone Joint Surg Br 1997;79:764-9.

13. Bottomley PA. Spatial localization in NMR spectroscopy in vivo. Ann N Y Acad Sci 1987;508:333–348

14. Castillo M, Kwock L, Mukherji S. Clinical applications of MR spectroscopy. AJNR 1996;17:1–15.

15. Keith Smith, Mauricio Castillo, Lester Kwock. MR Spectroscopy of brain tumours. MRI clinics of North America 2003; 11:415-429.

16. Debora Bertholdo, Arvemas Watcharakorn and Mauricio Castillo. Brain Proton MR Spectroscopy. AJNR 2010; 1:1-21

17. Maheshwari, Fatterpeaker, M. Castillo and Mukherji SK, Proton MR Spectroscopy of the brain. Seminars in Ultrasound, CT, MR 2000; 21: 434-451.

18. Nicolas Fayed, Salvador Olmos, Umberto Morales, Pedro J. Physical basis of MRS and its application to CNS diseases. American Journal of Applied Sciences 2006; 3(5):1836-1845.

19. Smith JK, Kwock L, Castillo M. Effects of contrast material on single-volume proton MR spectroscopy. AJNR 2000; 21(6):1084–9.

20. Hsu YY, Chen MC, Lim KE and Chang C. Reproducibility of hippocampal single-Voxel proton MR spectroscopy and chemical shift imaging. AJNR 2001; 176: 529-36.

21. Law M. MR spectroscopy of brain tumors. Top Magn. Reson. Imaging 2004; 15: 291-313.

22. Nicolas Fayed, Salvador Olmos, Umberto Morales, Pedro J. Physical basis of MRS and its application to CNS diseases. American Journal of Applied Sciences 2006; 3(5):1836-45

23. Majós , Juliá-Sapé, Alonso and Serrallonga. Brain tumor classification by proton MR spectroscopy: Comparison of diagnostic accuracy at short and long TE. AJNR 2004; 25: 1696-1704.

24. Bonavita, Di Salle and G. Tedeschi. Proton MRS in neurological disorders. European Journal of Radiology1999; 30: 125-131.

25. Mansfield, PK Grannell. Solid State Physics. Journal of Physics 1973; 6:422-426.

26. Hancu I, Zimmerman EA , Sailasuta N, Hurd RE. MR spectroscopy using TE averaged PRESS: A more sensitive technique to detect neurodegeneration associated with Alzheimer's disease. Magnetic Resonance 2005; 53: 777-782.

27. Shimizu H, Kumabe T, Tominaga T, Kayama T, Hara, Ono Y et al. Noninvasive evaluation of malignancy of brain tumors with proton MR spectroscopy. AJNR 1996; 17:737-747

28. Soares DP, Law M. Magnetic resonance spectroscopy of the brain: review of metabolites and clinical applications. Clinical Radiology 2009; 64:12-21.

29. Law M, Meltzer DE and Cha S. Spectroscopic magnetic resonance imaging of a tumefactive demyelinating lesion. Neuroradiology 2002; 44: 986-989.

30. Saindane AM, Cha S, Law M, Xue X, Knopp EA and Zagzag D. Proton MR spectroscopy of tumefactive demyelinating lesions. AJNR 2002; 23: 1378-1386.

31. Van der Graaf. In vivo magnetic resonance spectroscopy: basic methodology and clinical applications. European Biophysics Journal 2010; 39:527-540.

32. Hancu I, Zimmerman EA , Sailasuta N, Hurd RE. MR spectroscopy using TE averaged PRESS: A more sensitive technique to detect neurodegeneration associated with Alzheimer's disease. Magnetic Resonance 2005; 53: 777-782.

33 Dev R, Gupta RK, Poptani H , Roy R, Sharma S and Husain M. Role of in vivo proton magnetic resonance spectroscopy in the diagnosis and management of brain abscesses.Neurosurgery 1998; 42: 37-43.

34 Pandit S, Lin A , Gahbauer H , Libertin CR and Erdogan B. MR spectroscopy in neurocysticercosis. J Comput Assist Tomogr 2001; 25:950-952.

35 Gupta RK, Vatsal DK ,Husain N , Chawla S , Prasad KN and Roy R. Differentiation of tuberculous from pyogenic brain abscesses with in vivo proton MR spectroscopy and magnetization transfer MR imaging. AJNR 2001; 22: 1503-1509.

36. Gupta RK, Roy R, Dev R, Husain M , Poptani H and Pandey R .Finger printing of Mycobacterium tuberculosis in patients with intracranial tuberculomas by using in vivo, ex vivo,and in vitro magnetic resonance spectroscopy.Magn. Reson. Med 1996; 36: 829-33

37. Zee CS, Segall HD, Boswell W, et al.MR imaging of neurocysticercosis. J Comput Assist Tomogr 1988:12:927-934

38. Martinez HR. Rangel-Guerra R, Elizondo G, et al. MR imaging in neurocysticercosis: a study of 56 cases. AJNR 1989:10:1011-1019

39. Pretell EJ, Martinot C Jr, Garcia HH, Alvarado M, Bustos JA, Martinot C. Differential diagnosis between cerebral tuberculosis and neurocysticercosis by magnetic resonance spectroscopy. J Comput Assist Tomogr 2005; 29: 112-114

40. Jayakumar P N ,Chandrashekar HS, Srikanth SG, Guruprasad AS, Devi BI, Shankar SK.MRI and in vivo proton MR spectroscopy in a racemose cysticercal cyst of the brain.Neuroradiology 2004; 46:72-74.

41. Jayakumar P N , Srikanth SG , Chandrashekar H S, Kovoor JM, Shankar SK, Anandh B.Pyruvate: an invivo marker of cestodal infestation of the brain on proton MR spectroscopy.Journal of Magnetic Resonance Imaging 2003;18:675-680,2003.

42. Grodd W, Krageloh-Mann I, Klose U, Sauter R. Metabolic and destructive brain disorders in children: findings with localized proton MR spectroscopy. Radiology 1991;181:173-181

43 Daniel B, Three-dimensional Proton MR Spectroscopic Imaging of Premature and Term Neonates. AJNR 2001;22:1424–1433.

44. Gupta RK, Husain N, Kathuria MK, Datta S, Rathore RK, Husain M. Magnetization transfer MR imaging correlation with histopathology in intracranial tuberculomas. Clin Radiol. 2001;56:656–63.

45. Gupta RK, Lufkin RB. In Tuberculosis and other non-tuberculous bacterial granulomatous infection. New York: Kluwer Academic/Plenum Publishers; 2001. MR imaging and spectroscopy of central nervous system infection; pp. 95–145

46. Santy K, Nan P, Chantana Y. The diagnosis of brain tuberculoma by (1)H-magnetic resonance spectroscopy. European Journal of Pediatrics 2011;379–87.

47. Cecil KM, Lenkinski RE. Proton MR Spectroscopy in inflammatory and infectious brain disorders. Neuroimaging Clinics of North America 1998; 8:863-880.

48. Gupta RK, Pandey R, Khan EM, Mittal P, Gujral RB, Chhabra DK. Intracranial tuberculomas: MRI signal intensity correlation with histopathology and localised proton spectroscopy. Magnetic Resonance Imaging 1993; 11(3):443–449.

49. Batra A, Tripathi RP. Diffusion-weighted magnetic resonance imaging and magnetic resonance spectroscopy in the evaluation of focal cerebral tubercular lesions. Acta Radiol 2004;45:679-88.

50. Russell DG, Who puts the tubercle in tuberculosis? Nat Rev Microbiol 2007; 5:39–47

51. Karakousis PC, Bishai WR, Dorman SE ,Mycobacterium tuberculosis cell envelope lipids and the host immune response.Cell Microbiology 2004; 6:105–116

52. Luthra G, Parihar A, Nath K, Jaiswal S, Prasad KN, Husain N et al. Comparative evaluation of fungal, tubercular, and pyogenic brain abscesses with conventional and diffusion MR imaging and proton MR spectroscopy. AJNR 2007; 28:1332–1338

53. Mishra AM, Gupta RK, Jaggi RS, Reddy JS, Jha DK, Husain N et al. Role of diffusion weighted imaging and in vivo proton magnetic resonance spectroscopy in the differential diagnosis of ring-enhancing intracranial cystic mass lesions. J Comput Assist Tomogr 2004;28:540–547

54. Karakousis PC, Bishai WR, Dorman SE ,Mycobacterium tuberculosis cell envelope lipids and the host immune response.Cell Microbiology 2004; 6:105–116

55. Sze G, Zimmerman RD. The magnetic resonance imaging of infections and inflammatory diseases. Radiol Clin North Am 1988;26:839–859

56. Haimes AB, Zimmerman RD, Morgello S, et al. MR imaging of brain abscesses. AJR Am J Roentgenol 1989;152:1073-85

57. Desprechins B, Stadnik T, Koerts G, et al. Use of diffusion-weighted MR imaging in differential diagnosis between intracranial necrotic tumors and cerebral abscesses. AJNR Am J Neuroradiol 1999;20:1252-57.

58. Kim YJ, Chang KH, Song IC, et al. Brain abscess and necrotic or cystic brain tumor: discrimination with signal intensity on diffusion-weighted MR imaging. AJR Am J Roentgenol 1998;171:1487-90

59. Yamagata NT, Miller BL, McBride D . In vivo proton spectroscopy of intracranial infections and neoplasms. J Neuroimaging 1994; 4(1):23–28.

60. Remy C, Lebars E, Ibarrola D, Lai ES, Grand S, Decorps M. In-vivo imaging of metabolites using nuclear-magnetic-resonance spectroscopy. J Trace Microprobe Tech 1995; 13(3):293–301.

61. Burtscher IM, Holtas S. In vivo proton MR spectroscopy of untreated and treated brain abscesses. AJNR 1999; 20(6):1049–1053.

62. Sener RN. Rasmussen's encephalitis: proton MR spectroscopy and diffusion MR findings. J Neuroradiol 2000; 27(3):179–184.

63. Lai PH, Li KT, Hsu SS. Pyogenic brain abscess: findings from in vivo 1.5-T and 11.7-T in vitro proton MR spectroscopy. AJNR 2005; 26(2):279–288

64. RiyadhN, Al Okaili, Jaroslaw Krejza, Sumei Wang, John H Woo, Elias R Melhem.Advanced MR Imaging Techniques in diagnosis of intraaxial brain tumours in adults.Radiographics 2006; 26:S173-S189

65. Butzen J, Prost R, Chetty V. Discrimination between neoplastic and nonneoplastic brain lesions by use of proton MR spectroscopy: the limits of accuracy with a logistic regression model. AJNR 2000; 21(7):1213–1219

66. RiyadhN, Al Okaili, Jaroslaw Krejza, Sumei Wang, John H Woo, Elias R Melhem.Advanced MR Imaging Techniques in diagnosis of intraaxial brain tumours in adults.Radiographics 2006; 26:S173-S189

67. Howe FA, Barton SJ, Cudlip SA. Metabolic profiles of human brain tumors using quantitative in vivo H-1 magnetic resonance spectroscopy. Magnetic Resonance Med 2003;49(2):223–232.

68. Butzen J, Prost R, Chetty V. Discrimination between neoplastic and nonneoplastic brain lesions by use of proton MR spectroscopy: the limits of accuracy with a logistic regression model. AJNR 2000; 21(7):1213–1219

69. Fan G, Sun B, Wu Z, Guo Q and Guo Y. In vivo single-voxel proton MR spectroscopy in thedifferentiation of high-grade gliomas and solitary metastases. Clinics of Radiology 2004, 59:77-85

70. Fayed N, Morales H, Modrego PJ and Pina MA. Contrast/Noise ratio on conventional MRI and Choline/Creatine ratio on proton MR spectroscopy discriminate low-grade from high-grade cerebral gliomas. Academy of Radiology 2006;13:728-737

71. Law M. MR spectroscopy of brain tumors. Top Magn. Reson. Imaging 2004; 15:291-313

72. Rijpkema M, Schuuring J, van der Meulen Y, van der Graaf M, Bernsen H, Boerman R.Characterization of oligodendrogliomas using short echo time 1H MR spectroscopic imaging.NMR Biomed 2003; 16(1):12-21.

73. Xu M, See SJ, Ng WH, Arul E, Back MF, Yeo TT, Lim CC. Comparison of magnetic resonance spectroscopy and perfusion-weighted imaging in presurgical grading of oligodendroglial tumors. Neurosurgery 2005; 56(5):919-26

74. Smith JK, Londono A, Castillo M, Kwock L.Proton Magnetic Resonance Spectroscopy of Brain-Stem Lesions. Neuroradiology 2002; 44:825–9

75. Posner JB, Chernik NL. Intracranial metastases from systemic cancer. Adv Neurol 1978;19:579–592

76. Meyer PC, Reah TG. Secondary neoplasms of the central nervous system and meninges. Br J Cancer 1953;7:438

77. Vieth RG, Odom GL. Intracranial metastases and their neurosurgical treatment. J Neurosurg 1965;23:375–383

78. Smirniotopoulos JG, Murphy FM, Rushing EJ, Rees JH, Schroeder JW. Patterns of contrast enhancement in the brain and meninges. Radiographics 2007;27:525-50.

79. Maarouf M, Kuchta J, Miletic H, Ebel H, Hesselmann V, Hilker R, et al. Acute demyelination: diagnostic difficulties and the need for brain biopsy. Acta Neurochir 2003;145:961-90

80. Burtscher IM, Skagerberg G, Geijer B, Englund E, Stahlberg F, Holtas S. Proton MR spectroscopy and preoperative diagnostic accuracy: an evaluation of intracranial mass lesions characterized by stereotactic biopsy findings. AJNR 2000; 21(1):84–93.

81. Simone IL, Federico F, Tortorella C. Localised H-1-MR spectroscopy for metabolic characterization of diffuse and focal brain lesions in patients infected with HIV. J Neurol Neurosurg Psychiatry 1998;64(4):516–523

82. Lai PH, Weng HH, Chen CY, Hsu SS, Ding S, Ko CW, Fu JH, Liang HL, Chen KH. In vivo differentiation of aerobic brain abscesses and necrotic glioblastomas multiforme using proton MR spectroscopic imaging. AJNR 2008; 29(8):1511-8.

83. Gill SS, Thomas DGT, Van Bruggen N. Proton MR spectroscopy of intracranial tumors: In vivo and in vitro studies. J Comput Assist Tomogr 1990; 14:497-504

84. Zeng QS, Li CF, Liu H, Zhen JH, Feng DC. Distinction between recurrent glioma and radiation injury using magnetic resonance spectroscopy in combination with diffusion-weighted imaging. Int J Radiat Oncol Biol Phys. 2007;68(1):151-8

85. Burlina, A., T. Aureli, F. Bracco and F. Conti, MR spectroscopy: a powerful tool for investigating brain function and neurological diseases. Neurochem, Res 2000; 25:1365-72

86. Stadlbauer A, Buchfelder M, Nimsky C, Saeger W, Salomonowitz E, Pinker K. Proton magnetic resonance spectroscopy in pituitary macroadenomas: Preliminary results. J. Neurosurg 2008;109:306–12

87 Kinoshita Y . Proton magnetic resonance spectroscopy of brain tumors: an in vitro study. J. Neurosurg 1994; 35(4):606-13

88. Ping-Hong Lai. Proton magnetic resonance spectroscopy and diffusion-weighted imaging in intracranial cystic mass lesion. Surg. Neurol. Int 2007; 68:S25-36

89. Butt ME, Khan SA, et al. Intra-cranial Space Occupying Lesions: A Morphological Analysis.Biomedica 2005;21(6):1-10.

90. Soomro BA, Khalid S, Alvi S. Analytic study of clinical presentation of intracranial space-occupying lesions in adult patients. Pakistan J Neurol Sci 2014;9:1-5.

91. Ramamurthi B."Intra-cranial tumors in India: Incidence and variations."International Surgery.1973;58 (8):542-47.

92. Garg RK, Nag D. Brain lesions in Indian patients with seizures: clinical and radiological evaluation and follow-up. J Trop Pediatr. 1998;44:204-10.

93. Pandey J, Gujral RB. Role of computerized tomography scan in seizure disorders. West Afr J Radiol 2014;21:26-30.

94. Yashodhara P, Thirupathi Reddy Et al. Prospective Study of Intracranial Space Occupying Lesions in Children in Correlation with C.T. Scan. Int J Sci Res 2015;4:2-7.

95. Amaral L, Maschietto M, Maschietto R, Cury R, Ferreira NF, Mendonça R, Lima SS. Ununsual manifestations of neurocysticercosis in MR imaging: analysis of 172 cases. Arq Neuropsiquiatr 2003;61:533-41.

96. Jayasundar R, Singh VP, Raghunathan P, Jain K, Banerji AK Inflammatory granulomas: evaluation with proton MRS. NMR Biomed. 1999;12(3):139-44.

97. Suss RA, Maravilla KR, Thompson J MR imaging of intracranial cysticercosis: comparison with CT and anatomopathologic features. AJNR Am J Neuroradiol1986;7(2):235-42.

98 Kumar A, Kaushik S, Tripathi RP, Kaur P, Khushu S. Role of in vivo proton MR spectroscopy in the evaluation of adult brain lesions: Our preliminary experience. Neurol India 2003;51:474-78

99.Tae Kyoung Kim et al Intracranial Tuberculoma: Comparison of MR with Pathologic Findings AJNR 2008;16:1903-8.

100 Felix R, Schörner W, Laniado M, Niendorf HP, Claussen C, Fiegler W, et al. Brain tumors: MR imaging with gadolinium-DTPA. Radiology. 1985;156:681-8.

101. Spampinato MV, Smith JK, Kwock L, Ewend M, Grimme JD, Camacho DL,Castillo M. Cerebral blood volume measurements and proton MR spectroscopy in grading of oligodendroglial tumors. AJR Am J Roentgenol 2007;8(1):204-12.

102. Meyer PC, Reah TG. Secondary neoplasms of the central nervous system and meninges. Br J Cancer 1993;7:438.

103. D. Pal , A. Bhattacharyya ,M. Husain ,K.N. Prasad ,C.M. Pandey ,R.K. Gupta. In Vivo Proton MR Spectroscopy Evaluation of Pyogenic Brain Abscesses: A Report of 194 Cases.AJNR Am J Neuroradiol 2010;31:360–66.

104. Smith EA, Carlos RC, Junck LR, et al. Developing a clinical decision model:MR spectroscopy to differentiate between recurrent tumor and radiation change in patients with new contrastenhancing lesions. AJR Am J Roentgenol 2009;192(2):45–52.

105. Mohammad F, Hasan D, Ammar M. MR spectroscopy and diffusion MR imaging in characterization of common sellar and supra-sellar neoplastic lesions. Egypt J Radiol Nucl Med.2014;45(3):859-867.

106. Kinoshita Y . Proton magnetic resonance spectroscopy of brain tumors: an in vitro study.Neurosurgery 1994;35(4):606-13.

107. Ping-Hong Lai. Proton magnetic resonance spectroscopy and diffusion-weighted imaging in intracranial cystic mass lesion. Surgical neurology 2007; 68:25-36

108. Majos , Julia-Sape, Alonso and Serrallonga. Brain tumor classification by proton MR spectroscopy: comparison of diagnostic accuracy at short and long TE. AJNR 2004; 25: 1696-1704.

PROFORMA

ROLE OF MAGNETIC RESONANCE SPECTROSCOPY (MRS) IN THE EVALUATION OF INTRACRANIAL SPACE OCCUPYING LESIONS DIAGNOSED BY CONVENTIONAL MAGNETIC RESONANCE IMAGING (MRI)

Demographic details:

Name:

Age: **Sex:**

Clinical History:

Provisional Diagnosis:

Previous CT/ MRI findings if available:

Conventional MRI Findings:

Sequence	**Findings**
T1 WI	
T2 WI	
FLAIR	

MRS Findings

SNo	CaseNo	NAA	Cr	Cho	Cho/Cr	NAA/Cr	Cho/NAA	Others

Impression:

Conventional MRI diagnosis:

Conventional MRI +MRS diagnosis:

Final diagnosis:

INFORMED CONSENT FORM

Name of the subject:

Age :

Gender :

a. I have been informed in my own language that this study involves MRI and use of contrast material as part of procedure. I have been explained thoroughly and understand its complication and possible side effects.
b. I understand that the medical information produced by this study will become part of institutional record and will be kept confidential by the said institute.
c. I understand that my participation is voluntary and may refuse to participate or may withdraw my consent and discontinue participation at any time without prejudice to my present or future care at this institution.
d. I agree not to restrict the use of any data or results that arise from this study provided such a use is only for scientific purpose(s).
e. I confirm that _____ (chief researcher/ name of PG guide) has explained to me the purpose of research and the study procedure that I will undergo and the possible risks and discomforts that i may experience, in my own language. I hereby agree to give valid consent to participate as a subject in this research project.

Participant's signature/thumb impression

Signature of the witness: Date:

1)

2)

I have explained to _____ (subject) the purpose of the research, the possible risk and benefits to the best of my ability.

Chief Researcher/ Guide signature Date:

PATIENT INFORMATION SHEET

Principal Investigator: Dr. KEERTHI M/ Dr. AHANTHEM NABA KUMAR SINGH

I, Dr. Keerthi M, post-graduate student in Department of Radio-Diagnosis at Sri Devaraj Urs Medical College. I will be conducting a study titled "Role of Magnetic Resonance Spectroscopy in the evaluation of intracranial space occupying lesions diagnosed by conventional Magnetic Resonance Imaging" for my dissertation under the guidance of Dr. Ahanthem Nabakumar Singh, Associate Prof., Department of Radio-Diagnosis. In this study, we will assess the diagnostic value of MRS for evaluation of intracranial space occupying lesions. You would have undergone MRI brain before entering the study. There will be no additional expenses incurred by you for the additional MRS sequence as it is part of routine scan procedure. You will not be paid any financial compensation for participating in this research project.

All of your personal data will be kept confidential and will be used only for research purpose by this institution. You are free to participate in the study. You can also withdraw from the study at any point of time without giving any reasons whatsoever. Your refusal to participate will not prejudice you to any present or future care at this institution

Name and Signature of the Principal Investigator

Date

ಸಮ್ಮತಿ ಪತ್ರ

ಈ ಕೆಳಗೆ ಸಹಿ ಮಾಡಿರುವ ---------- ಆದ ನಾನು ಈ ಅಧ್ಯಯನದಲ್ಲಿ ಪಾಲ್ಗೊಳ್ಳುವ ಸಲುವಾಗಿ ವೈದ್ಯಕೀಯ ಪ್ರಯೋಗ ಪರೀಕ್ಷೆಗೆ ಒಳಪಡಲು ನನ್ನ ವೈಯ್ಯಕ್ತಿಕ ವಿವರಗಳನ್ನು ನೀಡಲು ಸಮ್ಮತಿಸಿರುತ್ತೇನೆ.

ಈ ಅಧ್ಯಯನದ ಉದ್ದೇಶ, ಅಧ್ಯಯನದ ಸಂದರ್ಭದಲ್ಲಿ ನೀಡುವ ಮತ್ತು ಸಂಗ್ರಹಿಸುವ ಮಾಹಿತಿಯ ಗೋಪ್ಯತೆಯ ಬಗ್ಗೆ ನನಗೆ ನನ್ನ ಸ್ಥಳೀಯ ಭಾಷೆಯಲ್ಲಿ ಓದಿ ಹೇಳಲಾಗಿದೆ/ವಿವರಿಸಲಾಗಿದೆ ಮತ್ತು ನಾನು ಇದನ್ನು ಅರ್ಥ ಮಾಡಿಕೊಂಡಿರುತೇನೆ. ಈ ಅಧ್ಯಯನದ ವಿವಿಧ ಅಂಶಗಳ ಬಗ್ಗೆ ಪ್ರಶ್ನೆಗಳನ್ನು ಕೇಳುವ ಅವಕಾಶವನ್ನು ನನಗೆ ನೀಡಲಾಗಿದೆ ಮತ್ತು ನನ್ನ ಪ್ರಶ್ನೆಗಳಿಗೆ ತೃಪ್ತಿಕರವಾದ ಉತ್ತರಗಳು ದೊರೆತಿರುತ್ತೆವೆ. ಈ ಅಧ್ಯಯನದ ಮೂಲಕ ಸಂಗ್ರಹಿಸಿರುವ ಮಾಹಿತಿಯನ್ನು ಸಂಶೋಧನೆಯ ಉದ್ದೇಶಕ್ಕೆ ಮಾತ್ರ ಬಳಸತಕ್ಕದ್ದು.

ಈ ಅಧ್ಯಯನದಿಂದ ಯಾವುದೇ ಸಂದರ್ಭದಲ್ಲಿ ಹಿಂದೆ ಸರಿಯುವ ಸ್ವಾತಂತ್ರ್ಯ ನನಗಿದೆ ಎಂಬುದನ್ನು, ಈ ಅಧ್ಯಯನದಲ್ಲಿ ಪಾಲ್ಗೊಳ್ಳುವುದರಿಂದ ನನಗೆ ಯಾವುದೇ ಹೆಚ್ಚುವರಿ ವೆಚ್ಚ ತಗಲುವುದಿಲ್ಲವೆಂಬುದನ್ನು ತಿಳಿದಿರುತ್ತೇನೆ.

ಪರೀಕ್ಷಾರ್ಥಿಯ ಹೆಸರು ಮತ್ತು ಸಹಿ/ಹೆಬ್ಬೆಟ್ಟಿನ ಗುರುತು

ಸಾಕ್ಷಿಗಳ ಹೆಸರು ಮತ್ತು ಸಹಿ

1. ದಿನಾಂಕ:

2. ದಿನಾಂಕ:

ಸಂದರ್ಶಕರ ಹೆಸರು ಮತ್ತು ಸಹಿ

ದಿನಾಂಕ:

ಪ್ರಧಾನ ಪರೀಕ್ಷಕರ ಹೆಸರು ಮತ್ತು ಸಹಿ

ದಿನಾಂಕ:

Key to Master Chart

↑	Hyperintense
↓	Hypointense
↔	Isointense
↕	Heterogenous
®	Right
Ш	Midline
A	Absent
ABS	Abscess
AC	Arachnoid cyst
APA	Aggressive pituitary adenoma
B	Bilateral
BEN	Benign
BLP	Broad lipid peak
CP	Craniopharyngioma
CPC	Choroid plexus carcinoma
DVA	Developmental venous anomaly
E	Elevated
EA	Extra-axial
EC	Epidermoid cyst
F	Female
GJT	Glomus jugulare tumor
GLI	Glioma
GR	Granulomatous lesion
HG	High grade glioma

Homo	Homogeneous enhancement
IA	Intra-axial
L	Left
LG	Low grade glioma
M	Male
MaE	Markedly Elevated
MaR	Markedly Reduced
ME	Mildly Elevated
MEN	Meningioma
MET	Metastases
MoE	Moderately elevated
MR	Mildly reduced
N	No
Ñ	Normal
N/A	Not Applicable
NCC	Neurocysticercosis
PCA	Pilocytic Astrocytoma
PIN	Pineoblastoma
PM	Pitutary macroadenoma
R	Reduced
RN	Radiation necrosis
SCH	Schwannoma
SE	Subependymoma
TB	Tuberculoma/Tuberculosis
Y	Yes

Master Chart

Sl No.	Trial ID	Age (in years)	Sex	CS-Headache	CS-Seizures	CS-BV	CS-Others	CS-Non specific	Location	Size (in cm)	No of lesions in patient	Side	Frontal	Parietal	Temporal	Occipital	BG	IV	S/S	CPA	Other	MRI- T1	MRI- T2	MRI- Flair	MRI- T1 post contrast	MRI diagnosis	MRS_CHO	MRS_LACTATE	MRS_LIPID	MRS_NAA	MRS_CREAT	MRS_ACETATE	MRS_ALANINE	MRI+MRS DIAGNOSIS	Final diagnosis	MRS contributory to Conventinal MRI
1	81402	39	M	Y	N	N	N	N	IA	>4	2	L		Y	Y	Y						↑	↕	↕	↕	GLI	MaE	MaE	ME	A	MR			HG	HG	Y
2	26282	37	M	Y	N	N	N	N	IA	<2	1	®	Y									↓	↑	↑	NE	MET/ RN	Ñ	A	A	MR	Ñ			RN	RN	Y
3	82895	58	M	N	Y	Y	N	N	IA	2 to 4	2	B	Y	Y	Y	Y					Y	↓	↑	↑	Ring	GR	Ñ	MaE	MaE	Ñ	MR			TB	TB	Y
4	45769	50	M	Y	N	Y	N	N	EA	>4	1	Ш							Y			↑	↔	↔	Homo	APA/ CP	ME	A	BLP	A	Ñ			BEN	CP	Y
5	53904	45	F	Y	Y	N	N	N	IA	<2	1	®	Y									↓	↕	↑	Ring	GLI	ME	ME	A	MR	MR			LG	LG	Y
6	96525	50	M		Y	Y	N	N	IA	2 to 4	>3	B									Y	↓	↑	↑	Ring	GR	ME	MaE	MaE	Ñ	MR			TB	TB	Y
7	60354	18	F	N	Y	Y	N	N	IA	<2	>3	®	Y									↓	↑	↑	Ring	GR	ME	MaE	MaE	MR	Ñ			TB	TB	Y
8	61456	58	F	Y	Y	N	N	N	IA	>4	1	Ш	Y									↓	↕	↑	↕	GLI	ME	MaE	MaE	MaR	MaR			HG	HG	Y
9	32853	50	F	Y	N	N	Nau	T	EA	<2	1	L								Y		↔	↔- ↑	↕	Avid	SCH	Ñ	Ñ	Ñ	A	A			SCH	SCH	N
10	65601	9	M	N	Y	N	N	N	IA	2 to 4	>3	®		Y								↔	↓	↓	Ring	GR	ME	ME	A	MR	MR		ME	NCC	NCC	Y
11	21699	50	F	N	Y	N	N	N	IA	< 2	1	®	Y									↓	↓	↓	Ring	?MET	ME	MaE	MaE	MR	MR			TB	TB	Y
12	69523	80	M	Y	N	N	N	N	EA	2 to 4	1	L			Y							↔	↔	↔	Homo	MEN	ME	A	ME	A	A			MEN	MEN	N
13	25728	54	F	N	N	N	N	T	EA	<2	1	L					Y					↓	↑	↑	Avid	GJT	ME	A	A	A	Ñ			GJT	GJT	N
14	97524	16	M	Y	N	Y	N	N	IA	>4	1	®							Y			↓	↑	↑	Avid	PCA	MaE	MaR	ME	MR	MR			PCA	PCA	Y
15	57893	55	M	Y	N	N	N	N	IA	>4	1	L						Y				↔	↑	↑	↕	CA/SE	ME	A	A	ME	Ñ			BEN	SE	N
16	24800	40	M	N	Y	N	N	C	IA	2 to 4	1	®	Y									↔	↓	↓	Ring	GR	ME	MaE	MaE	MR	MR			TB	TB	Y
17	60503	18	F	Y	Y	N	N	N	IA	<2	>3	B									Y	↓	↓	↑	Ring	GR	ME	MaE	MaE	MR	MR			TB	TB	Y
18	64728	41	F	Y	N	N	N	N	IA	>4	2	®	Y								Y	↓	↑	↓	NE	?MET	MAE	A	MaE	MR	ME			MET	MET	Y
19	61807	5	F	N	Y	N	F	N	IA	<2	1	L		Y		Y						↓	↓	↑	Ring	GR	ME	ME	A	MR	Ñ		ME	NCC	NCC	Y
20	3410	62	F	N	Y	N	N	N	IA	<2	>3	B									Y	↓	↓	↑	Ring	GR	ME	ME	A	MR	MR			NCC	NCC	Y

↑ = Hyperintense; ↓ = Hypointense; ↔ = Isointense; ↕ = Heterogenous; Ш = Midline; ®=Right; A = Absent; ABS = Abscess; AC = Arachnoid cyst; APA = Aggressive pituitary adenoma; B=Bilateral; BEN = Benign; BLP = Broad lipid peak; BV= blurring of vision CP = Craniopharyngioma; CPC = Choroid plexus carcinoma; DVA = Developmental venous anomaly; E = Elevated; EA = Extra-axial; EC = Epidermoid cyst; F = Female; GJT = Glomus jugalare tumor; GLI = Glioma; GR = Granulomatous lesion; HG =High grade glioma; Homo = Homogeneous enhancement; IA = Intra-axial; L=Left; LG = Low grade glioma; M = Male; MaE = Markedly elevated; MaR = Markedly reduced; ME = Mildly elevated; MEN = Meningioma; MET = Metastases; MoE = Moderately elevated; MR = Mildly reduced;N = No; Ñ = Normal; Nau = Nausea; N/A = Not Applicable; NCC = Neurocysticercosis; NE = necrotic core; PCA = Pilocytic astrocytoma; PIN = Pineoblastoma; PM = Pitutary macroadenoma; R = Reduced; RN = Radiation necrosis; SCH = Schwannoma; SE = Subependymoma; TB = Tuberculoma; Y = Yes

Master Chart

Sl No.	Trial ID	Age (in years)	Sex	CS-Headache	CS-Seizures	CS-BV	CS-Others	CS-Non specific	Location	Size (in cm)	No of lesions in patient	Side	Frontal	Parietal	Temporal	Occipital	BG	IV	S/S	CPA	Other	MRI- T1	MRI- T2	MRI- Flair	MRI- T1 post contrast	MRI diagnosis	MRS_CHO	MRS_LACTATE	MRS_LIPID	MRS_NAA	MRS_CREAT	MRS_ACETATE	MRS_ALANINE	MRI+MRS DIAGNOSIS	Final diagnosis	MRS contributory to Conventinal MRI
21	25463	23	F	N	N	N	N	D	IA	< 2	1	L	Y									↓	↓	↑	Ring	GR	MaE	A	A	MR	MR		ME	NCC	NCC	Y
22	54131	10	M	N	Y	Y	F	N	IA	<2	1	®					Y					↓	↓	↑	Ring	GR	ME	ME	MaE	MR	MR			TB	TB	Y
23	91245	38	F	Y	N	Y	N	N	IA	<2	1	Ш									Y	↔	↓	↓	↕	PIN	Ñ	A	A	MR	Ñ			PIN	PIN	N
24	7145	1	M	N	Y	N	N	N	IA	>4	1	®						Y				↔ -↓	↑	↑	NE	CPC	MaE	ME	MaE	MR	ME			CPC	CPC	N
25	76946	52	F	Y	N	N	N	N	IA	<2	1	L				Y						↓	↑	↑	Ring	GR	ME	ME	A	MR	Ñ		ME	NCC	NCC	Y
26	77223	76	F	Y	N	N	N	TRE	IA	<2	1	®	Y									↔	↑	↑	Ring	GR	ME	ME	A	MR	MR		ME	NCC	NCC	Y
27	70768	22	M	N	Y	N	N	F	IA	<2	3	®	Y									↔	↑	↑	Ring	GR	ME	ME	A	MR	Ñ			NCC	NCC	Y
28	93276	28	M	N	Y	N	N	N	IA	<2	1	®		Y		Y						↔	↑	↑	Ring	GR	ME	ME	Ñ	MR	Ñ			NCC	NCC	Y
29	63173	61	M	Y	N	N	N	N	IA	>4	1	®				Y						↔ -↑	↕	↕	↕	GLI	ME	MaE	MaE	MaR	MaR			HG	HG	Y
30	18671	60	M	Y	N	N	N	N	IA	>4	1	®		Y		Y						↔ -↑	↕	↕	↕	GLI	ME	MaE	MaE	MaR	MaR			HG	HG	Y
31	41211	11	F	N	Y	N	N	F	IA	<2	1	L		Y								↓	↔	↔	Ring	GR	ME	ME	A	MR	MR			NCC	NCC	Y
32	9896	55	M	Y	N	N	N	N	EA	>4	1	®								Y		↓	↑	↑	↕	SCH	Ñ	ME	A	MaR	A			SCH	SCH	N
33	28633	32	M	N	Y	Y	N	F	IA	>4	1	®				Y						↑	I-↓	I-↓	Ring	GR	ME	ME	MaE	MR	Ñ			TB	TB	Y
34	88555	42	M	Y	N	Y	N	F	IA	>4	1	®		Y		Y						↔	↑	↕	Ring	ABS	MaE	ME	Ñ	MR	Ñ	MaE		ABS	ABS	Y
35	94315	38	M	Ñ	Y	Y	Ñ	C	IA	2 to 4	3	®	Y									↔ -↓	↓	↓	Ring	GR	ME	MaE	MaE	MR	Ñ			TB	TB	Y
36	99146	62	M	Y	Ñ	Ñ	Ñ	Ñ	IA	>4	1	®		Y		Y						↕	↕	↕	↕	GLI	ME	MaE	MaE	MaR	MaR			HG	HG	Y
45	75218	45	F	Y	Y	Ñ	Ñ	Ñ	EA	>4	1	Ш	Y									↔	↑	↑	Homo	BEN	ME	A	A	A	Ñ		MaE	MEN	MEN	Y
38	96187	17	F	Ñ	Ñ	Ñ	Ñ	Y	IA	<2	1	®		Y								↓	↑	↑	↕	GR	ME	A	A	MR	MR			GR	NCC	N
39	21066	29	M	Y	Ñ	Ñ	Ñ	Ñ	IA	>4	1	L	Y									↓	↑	↑	↕	GLI	ME	MaE	MaE	MaR	MaR			HG	HG	Y

↑ = Hyperintense; ↓ = Hypointense; ↔ = Isointense; ↕ = Heterogenous; Ш = Midline; ®=Right; A = Absent; ABS = Abscess; AC = Arachnoid cyst; APA = Aggressive pituitary adenoma; B=Bilateral; BEN = Benign; BLP = Broad lipid peak; BV= blurring of vision CP = Craniopharyngioma; CPC = Choroid plexus carcinoma; DVA = Developmental venous anomaly; E = Elevated; EA = Extra-axial; EC = Epidermoid cyst; F = Female; GJT = Glomus jugalare tumor; GLI = Glioma; GR = Granulomatous lesion; HG =High grade glioma; Homo = Homogeneous enhancement; IA = Intra-axial; L=Left; LG = Low grade glioma; M = Male; MaE = Markedly elevated; MaR = Markedly reduced; ME = Mildly elevated; MEN = Meningioma; MET = Metastases; MoE = Moderately elevated; MR = Mildly reduced;N = No; Ñ = Normal; Nau = Nausea; N/A = Not Applicable; NCC = Neurocysticercosis; NE = necrotic core; PCA = Pilocytic astrocytoma; PIN = Pineoblastoma; PM = Pitutary macroadenoma; R = Reduced; RN = Radiation necrosis; SCH = Schwannoma; SE = Subependymoma; TB = Tuberculoma; Y = Yes

Master Chart

Sl No.	Trial ID	Age (in years)	Sex	CS-Headache	CS-Seizures	CS-BV	CS-Others	CS-Non specific	Location	Size (in cm)	No of lesions in patient	Side	Frontal	Parietal	Temporal	Occipital	BG	IV	S/S	CPA	Other	MRI- T1	MRI- T2	MRI- Flair	MRI- T1 post contrast	MRI diagnosis	MRS_CHO	MRS_LACTATE	MRS_LIPID	MRS_NAA	MRS_CREAT	MRS_ACETATE	MRS_ALANINE	MRI+MRS DIAGNOSIS	Final diagnosis	MRS contributory to Conventinal MRI
40	90941	65	M	Ñ	Ñ	Ñ	F	Ñ	IA	2 to 4	3	B		Y		Y						↑	↑	↓	↕	?MET	ME	MaE	MaE	MaR	MaR			MET	MET	Y
41	76976	30	F	Y	Ñ	Ñ	Ñ	Ñ	IA	2 to 4	1	®									Y	↔	↑	↑	NE	BEN	A	A	A	A	A			BEN	DVA	Y
42	38620	76	M	Ñ	Ñ	Ñ	Ñ	Y	IA	2 to 4	3	B		Y		Y						↑	↑	↓	↕	?MET	ME	MaE	MaE	MaR	MaR			MET	MET	Y
43	8198	7	M	Ñ	Y	Ñ	Ñ	Ñ	EA	2 to 4	1	Ш				Y						↓	↑	↑	↕	AC/EC	A	A	A	A	A			AC	AC	Y
44	46964	29	M	Ñ	Y	Ñ	Ñ	C	IA	2 to 4	3	®	Y									I-↓	↑	↓	Ring	GR	ME	MaE	ME	MR	MR			TB	TB	Y
45	24010	6	F	Ñ	Y	Ñ	Ñ	Ñ	IA	<2	1	®	Y									↓	↔	↔	Ring	GR	ME	ME	A	MR	MR		ME	NCC	NCC	Y
46	47766	70	M	Y	Ñ	Ñ	F	Ñ	IA	>4	1	L				Y						↓	↑	↑	↕	GLI	ME	A	A	MR	MR			LG	LG	Y
47	78289	50	F	Ñ	Y	Ñ	Ñ	Ñ	IA	<2	1	L	Y									↓	↑	↑	Ring	GR	ME	A	A	A	Ñ			GR	NCC	N
48	15535	62	M	Y	Ñ	Y	Ñ	Ñ	EA	>4	1	Ш							Y			↓	↔	↔	Homo	APA/ CP	ME	A	A	MR	Ñ			BEN	PM	N
49	16094	26	M	Ñ	Y	Ñ	Ñ	Ñ	IA	<2	1	L	Y									↓	↑	↑	Ring	GR	ME	ME	A	MR	Ñ			GR	NCC	N
50	86957	38	M	Ñ	Y	Ñ	Ñ	Ñ	IA	<2	1	L	Y									↓	↑	↑	Ring	GR	ME	ME	A	A	Ñ			GR	NCC	N
51	98258	44	F	Ñ	Y	Ñ	Ñ	Ñ	EA	2 to 4	1	L								Y		↓	↑	↑	NE	AC/EC	A	MaE	ME	A	A			EC	EC	Y
52	74266	40	F	Ñ	Y	Ñ	Ñ	Ñ	IA	<2	2	®	Y									↓	↑	↑	Ring	GR	ME	ME	A	Ñ	Ñ			GR	NCC	N

↑ = Hyperintense; ↓ = Hypointense; ↔ = Isointense; ↕ = Heterogenous; Ш = Midline; ®=Right; A = Absent; ABS = Abscess; AC = Arachnoid cyst; APA = Aggressive pituitary adenoma; B=Bilateral; BEN = Benign; BLP = Broad lipid peak; BV= blurring of vision CP = Craniopharyngioma; CPC = Choroid plexus carcinoma; DVA = Developmental venous anomaly; E = Elevated; EA = Extra-axial; EC = Epidermoid cyst; F = Female; GJT = Glomus jugalare tumor; GLI = Glioma; GR = Granulomatous lesion; HG =High grade glioma; Homo = Homogeneous enhancement; IA = Intra-axial; L=Left; LG = Low grade glioma; M = Male; MaE = Markedly elevated; MaR = Markedly reduced; ME = Mildly elevated; MEN = Meningioma; MET = Metastases; MoE = Moderately elevated; MR = Mildly reduced;N = No; Ñ = Normal; Nau = Nausea; N/A = Not Applicable; NCC = Neurocysticercosis; NE = necrotic core; PCA = Pilocytic astrocytoma; PIN = Pineoblastoma; PM = Pitutary macroadenoma; R = Reduced; RN = Radiation necrosis; SCH = Schwannoma; SE = Subependymoma; TB = Tuberculoma; Y = Yes